Title	Pt/Ir ナノ粒子を修飾したデュアル機能剥離アセチレンブラックのリチウム空気電池への応用
Author(s)	周, 立航
Citation	
Issue Date	2024-03
Type	Thesis or Dissertation
Text version	ETD
URL	http://hdl.handle.net/10119/19078
Rights	
Description	supervisor: 松見 紀佳, 先端科学技術研究科, 博士

博士論文

Bifunctional Pt/Ir nano-particles decorated functionalized acetylene black and

its application in Li-air batteries

Pt/Ir ナノ粒子を修飾したデュアル機能剥離アセチレンブラックのリチウム空気電池への応用

ZHOU Lihang

主任研究指導教員　松見 紀佳

北陸先端科学技術大学院大学 金沢大学

融合科学共同専攻

融合科学

令和6年3月

Abstract

Bifunctional Pt/Ir nano-particles decorated functionalized acetylene black and its application in Li-air batteries

(Pt/Ir ナノ粒子を修飾したデュアル機能剥離アセチレンブラックのリチウム空気電池への応用)

Li-air batteries offer superior energy density compared to traditional Li-ion batteries , aligning with the global shift toward sustainable electric vehicles. The cathodic efficiency crucially hinges on the oxygen reduction reaction (ORR), for which platinum supported on carbon (Pt/C) has been a prevalent catalyst. However, the challenge in Li-air batteries lies in the simultaneous requirement for oxygen evolution reaction (OER) alongside ORR. This predicament has spurred investigations into amalgamating Pt with high OER activity metals like Ir, Co, and Fe. Despite their promising performance, the stability and potential leaching of these catalysts remain significant challenges [1].

This study exploits a carbon substrate demonstrating strong metal substrate interaction (SMSI) for heightened electrocatalytic durability. Building upon prior work [2], a novel functionalized acetylene black (Pt-FAB) was introduced, exhibiting remarkable catalytic activity due to efficient interfacial interactions with nanoparticles and electrolyte. The current study augments OER activity by incorporating Ir into the Pt-FAB catalyst. This unique Pt-Ir/FAB combination is anticipated to offer both high activity and durability, owing to efficient interfacial properties [3].

Acetylene Black (AB) is treated with a mixed strong acids to improve dispersion in water or organic solutions, enabling the formation of a catalyst with multiple functions. ORR and OER experiments are performed in an organic electrolyte, using TEGDME with 0.1 M LiFSI or LiTFSI. The next step involves constructing a Li-air battery, where a cathode slurry with active materials is coated on a carbon cloth. The electrolyte, consisting of 0.1 M LiI and 1 M LiTFSI in TEGDME, is used, and the battery operates under a 99.9% oxygen atmosphere at 0.1 MPa. The capacity is limited to 1000 mAh/gPt-Ir at charge-discharge rates of 125 mA/g and 250 mA/g to evaluate the material's long cycle life.

Acetylene Black (AB) treated with mixed strong acids enhances dispersion, which is crucial for forming a catalyst with controlled size and distribution. This work introduces a pioneering bimetallic Pt-Ir catalyst on functionalized acetylene black (FAB) for Li-air batteries. FAB, modified with -COOH functional groups, serves as a stable substrate for metal nanoparticle deposition. X-ray photoelectron spectroscopy (XPS) confirms successful Pt^0 and Ir^{4+} deposition on FAB. Electrochemical measurements reveal satistactory activities in ORR and OER, sustaining over 250 cycles in organic electrolytes. Cyclic voltammetry underscores its potential for Li-air battery. FAB180-Pt/Ir 1:1 with a 1000 mAh/g charge-discharge capacity maintained constant performance over 70 cycles, showcasing outstanding OER and ORR activity.

Bibliography

< References >
[1] Girishkumar, G., McCloskey, B., Luntz, A. C., Swanson, S., & Wilcke, W. The Journal of Physical Chemistry Letters, 1(14), 2193-2203 (2010).
[2] Badam, R., Vedarajan, R., & Matsumi, N. Chemical Communications, 51(48), 9841-9844 (2015).
[3] da Silva, G. C., Fernandes, M. R., Ticianelli, E. A., ACS Catal, 8, 2081e92 (2018).

Keywords: Oxygen reduction reaction, Oxygen evolution reaction, Dual electrocatalysts, Li air batteries, Rechargeable battery

Acknowledgements

Firstly, in completing this dissertation, I express my gratitude to all members of Matsumi Lab. I am especially thankful to Professor Matsumi for his invaluable guidance as my supervisor, offering both expertise and encouragement throughout this work. His patience, motivation, and extensive knowledge were instrumental in both my research and thesis writing.

I extend my appreciation to Professor Badam, an assistant professor, for the support and advice provided during laboratory experiments.

I would also like to thank Professors HORITA Susumu (JAIST), TAIMA Tetsuya (Kanazawa University), MIZUNO Motohiro (Kanazawa University), and Dr. HIGASHIMINE Koichi (JAIST) for their substantial contributions to my research.

Furthermore, I am sincerely grateful to everyone who supported me during my doctoral studies at JAIST. My thanks go to the members of Matsumi Lab and all professors who shared their knowledge during lectures and research.

I am deeply indebted to my family and friends for their support and extend my best wishes to all.

Lastly, I express my gratitude to JAIST. The doctoral period has been a profoundly significant experience in my life.

ZHOU Lihang
January 2024

Bifunctional Pt/Ir nano-particles decorated functionalized acetylene black and its application in Li-air batteries

ZHOU LIHANG (MATSUMI LAB.)

Contents

1. Chapter 1

Introduction

1.1. Background

Recently, global warming and alternative energy are becoming the exploratory aspects in the scientific world. Since the 1800s, as a result of the Industrial Revolution, fossil energy was a major source of power. With consumption of fossil energy, global CO_2 (Carbon Dioxide) emissions had grown up quickly (Fig. 1-1). At the same time, the concentration of CO_2 in the atmosphere under continuous monitoring has reached an alarming level (Fig. 1-2). [1]

How to control and reduce Global Warming is a challenge around the world. For this reason, we need to choose alternative energy sources. In the near future, wind power and solar power will be typical resources where from we would derive the electricity.

Since 1800s, the electric battery is an important source of electric power. In a narrow sense, a battery is a device that converts its stored chemical energy into electrical energy; battery could become a device that converts "pre-stored" energy into electrical energy for external use. Batteries are key to deal the problems in smooth and efficient use of stored energy for a number of cycles. Then, clean energy system will be set up and will work in a more desirable manner.
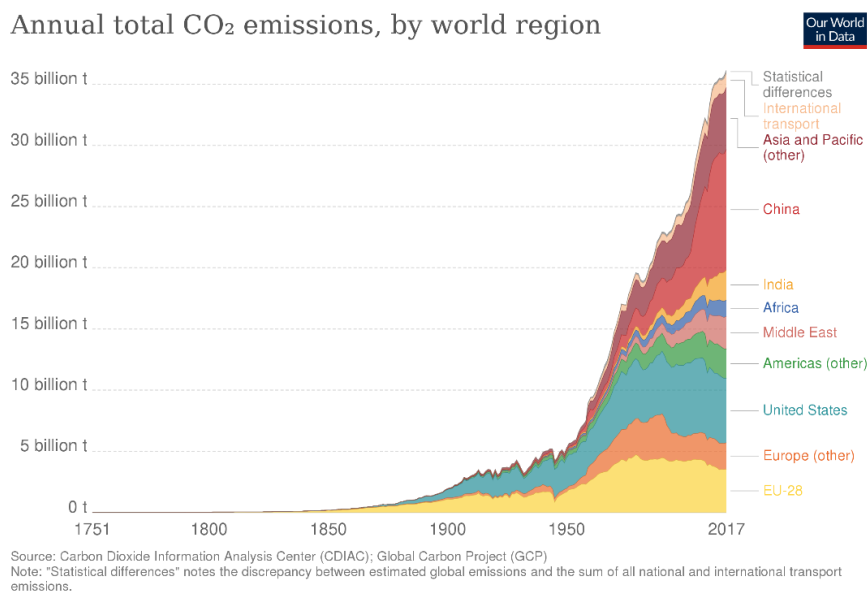
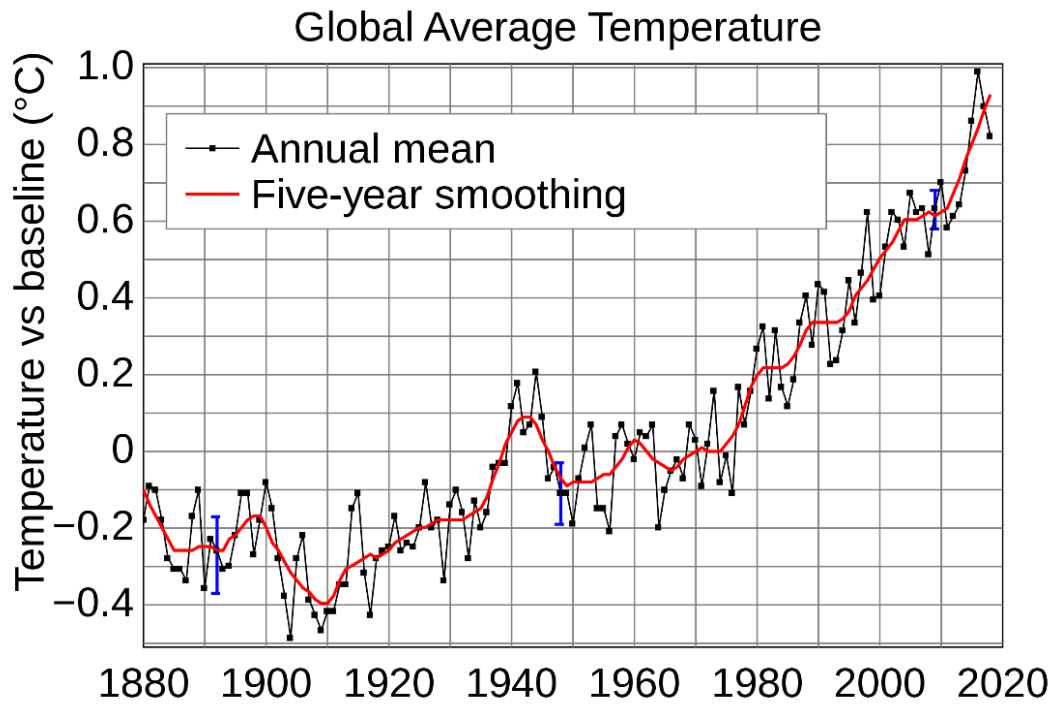Fig. 1-1 Global CO_2 emissions by world region since 1750

Fig. 1-2 The average annual temperature at the earth's surface has risen since the late 1800s, with year-to-year variations (shown in black) being smoothed out (shown in red) to show the general warming trend. [2]

1.2. Secondary Batteries and Lithium Air Batteries

Secondary battery (or rechargeable battery) is a type of electrical battery which can be charge-discharged. Secondary battery is one of energy storage device that can be used in all type of electrical equipment. As typical secondary batteries Lead–acid battery (Pb), Nickel-cadmium battery (Ni-Cd), nickel metal hydride battery (Ni-MH) and Lithium-ion battery (Li-ion) are widely available in our daily use. [3] Especially, Li-ion is most important one. From energy density values of batteries (Table 1-1 & Fig. 1-3), [4] Li-ion battery and another type of lithium batteries show a good energy density value in all commercial power batteries and have large market share at the same time. With high energy density values, battery electric vehicles (BEVs) and plug-in hybrid electric vehicles (PHEVs) are already under use found in civil transportation. [5,6]

The materials used for cathode and anode material must show high practical specific density and high cell potential. Based on the above principles, typical secondary batteries have chosen Pd, Ni, and Li for anode metals or cathode metal materials. The cathode and anode material also limit the electrolytes materials which are combination of various liquid or solid.

Table 1.1. A comparison among the rechargeable battery systems

	Magnesium	Lead acid	Ni–Cd	Ni–MH	Li-ion I	Li-ion II	Li-ion III
Anode	Mg alloy	Pb	Cd	$MH(LaNi_5H_6)$	LiC_6	Sn–Co–C–Ti	LiC_6
Cathode	Mo_3S_4	PbO_2	NiOOH	NiOOH	$LiCoO_2$	$LiCoO_2$ + Li(Ni–Co–Mn)O_2	$LiFePO_4$
Electrolyte	$Mg(AlCl_2BuEt)$ in THF/TG	Aqueous H_2SO_4	Aqueous KOH	Aqueous KOH	$LiPF_6{}^a$	$LiPF_6{}^a$	$LiPF_6{}^a$
Specific energy density (theory) (W h kg^{-1})	135	170	220	220	410	226	560
Specific energy density (practical)(W h kg^{-1})	>60	30–40	40–60	75–100	120–150	158	95
Working voltage (V)	1.3–1.0	2.0–1.8	1.2–1.0	1.2–1.0	4.0–3.0	4.2–2.5	3.6–2.0
Working temperature (°C)	−20 to +80	−20 to +50	−40 to +45	−20 to +45	−30 to +80	−30 to +80	−30 to +80
Chemical overcharge protection	No	Yes	Yes	Yes	No^b	No^b	No^c
Chemical overdischarge protection	No	No	Yes	Yes	No^b	No^b	No^b
Cycle number, 100% DOD	>2000	>50	>1000	>1000	<1000	<1000	>3000
Relative toxicity	Low?	High	High	High	Medium	High	Low
Safety	High?	High	High	High	Medium	Medium	High
Estimated material costs	Low	Medium	Medium	Medium-high	High	Medium	Medium
Estimated manufacture cost	High	Low	Medium	Medium	High	High	High

^{a} Salt in aprotic organic solvents or polymers, DOD – depth of discharge. ^{b} Electronic control of the state of charge/discharge. ^{c} A123 uses redox shuttle mechanisms through additives, TG – tetraglyme.
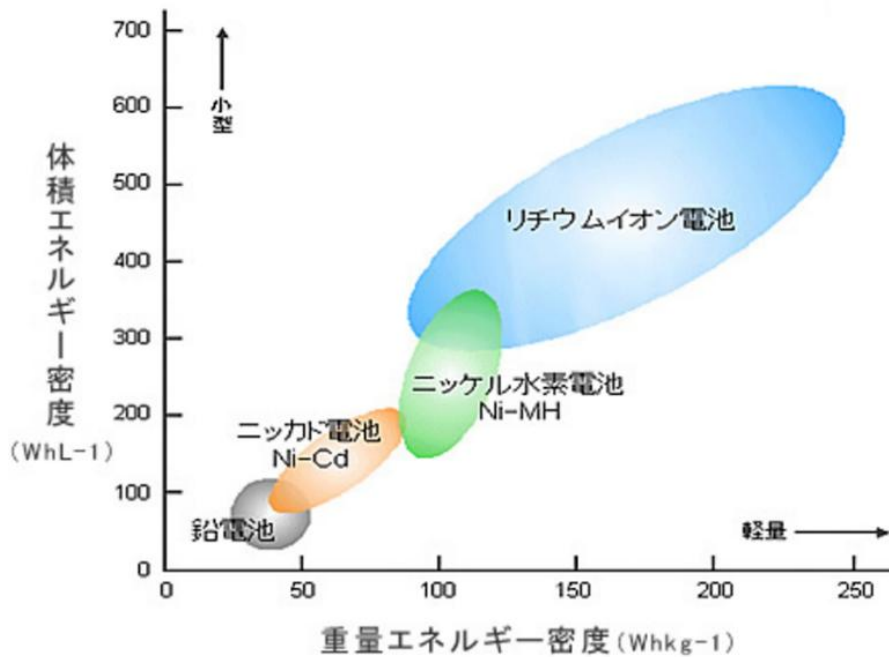
Fig. 1-3 Energy density values of secondary batteries

The lead–acid battery (Pb) is a type of rechargeable battery first invented in 1859 by French physicist Gaston Planté. It is the first type secondary battery ever created. The specific energy density of lead–acid battery is around 30-40Wh/Kg (Table 1.1). [7] Following is the total reaction.

$$2PbSO_4(s) + 2H_2O(l) \rightleftharpoons Pb(s) + PbO_2(s) + 2H_2SO_4(aq) \ (E^0_{cell}= 2.05V) \text{ equation 1}$$
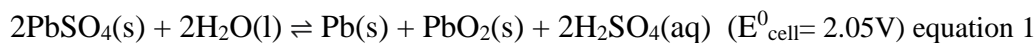
In 1980s, nickel-cadmium battery (Ni-Cd) and nickel metal hydride battery (Ni-MH) has become two widely used rechargeable batteries. The specific energy density of Ni-Cd and Ni-NH battery is around 40-60Wh/Kg (Ni-Cd) and 75-100Wh/Kg (Ni-Cd) (Table 1-1). The abbreviation of the Ni-Cd battery is derived from nickel (Ni) and cadmium (Cd). The chemical reaction at the positive electrode is similar in both of nickel-cadmium cell (Ni-Cd) and nickel metal hydride battery (Ni-MH). The differences between Ni-Cd and Ni-MH are choice of the anode materials. [8]
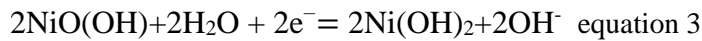
Ni-MH

$$H_2O + M + e^- = OH^- + MH \quad \text{equation 1}$$

Ni-Cd

$$Cd + 2OH^- = Cd(OH)_2 + 2e^- \quad \text{equation 2}$$

Oxide electrode

$$2NiO(OH) + 2H_2O + 2e^- = 2Ni(OH)_2 + 2OH^- \quad \text{equation 3}$$

After the Ni-Cd and Ni-MH batteries, a new type of battery that show a much higher gravimetric energy density is necessary. Li-ion battery demonstrated high specific energy density and low cost. As shown in Table 1-1 and Fig 1-3 lithium battery became the best choice for power battery pack.

In 1970s, M. Stanley Whittingham has discovered the intercalation electrodes based on a titanium disulfide cathode and a lithium-aluminium anode. John Goodenough invented lithium cobalt oxide as a cathode in 1980. In 1985, Li-ion battery's first commercial model was developed by Akira Yoshino, based on earlier research by John Goodenough utilizing graphite as anode.

Lithium-ion battery (Li-ion) is a rechargeable battery that mainly relies on the movement of lithium ions between the positive and negative electrodes. Lithium-ion batteries use an intercalated compound as electrode material. Anode material is typically graphite. Currently used cathode materials for lithium-ion batteries are lithium cobalt oxide ($LiCoO_2$), lithium manganate ($LiMn_2O_4$), lithium nickelate ($LiNiO_2$), and lithium iron phosphate ($LiFePO_4$), which are widely commercially used. The typical energy density of full packing commercial cell using various cathode materials is summarized in Table 1.2. [9-11]

Table 1.2. Energy density of Li-ion batteries anode material under full packing batteries.

Cathode materials	Nominal cell voltage	Energy density
$LiCoO_2$	3.7v	140 mAh/g
$LiMn_2O_4$	3.7v	100 mAh/g
$LiNiO_2$	3.3v	100 mAh/g
$LiFePO_4$	3.6v	115 mAh/g

With the advancement of material technology, the metal-air battery is becoming a new hot the secondary battery. The metal-battery was first discovered and researched in 1868 by Leclanche. There are various metal-air batteries such as zinc-air battery, aluminium-air battery. In 1932, zinc-air battery was designed and examined by Heise and Schumacher. Particularly Li-air batteries could exhibit very high energy density values of 11680 Wh/Kg, which are comparable to gasoline and ~10 times higher than that of Li-ion batteries (Fig. 1-4). [12]
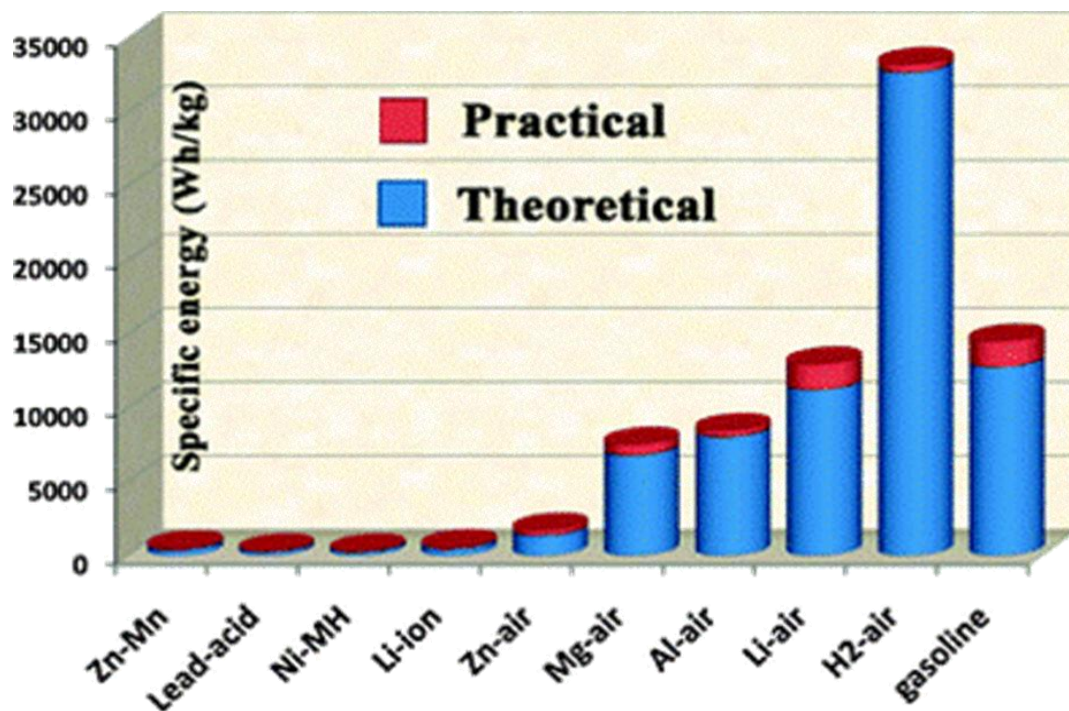

Fig. 1-4 Gravimetric energy density profile & Li-Air battery

This work deals with Li-air battery design and operation. Typically, lithium ions move across the electrolyte between the anode and cathode. During discharge, the electrons follow the external circuit to do electrical work, and the lithium ions migrate to the cathode. Both non-

aqueous (Li_2O_2 or LiO_2 as discharge product) and aqueous (LiOH as discharge product) Li-O_2 batteries were considered. Aqueous batteries require a protective layer on lithium for negative electrode from reacting with water. In Li-air battery oxidation of lithium at the anode and reduction of oxygen at the cathode cause current flow. One of the typical structures of the Li-air battery is shown in Figure 1-5. In detail, the electrolytes are different between four types of Li-air batteries, there are aprotic, aqueous, solid-state, and hybrid aqueous/ aprotic (Fig 1-6). [13,14]
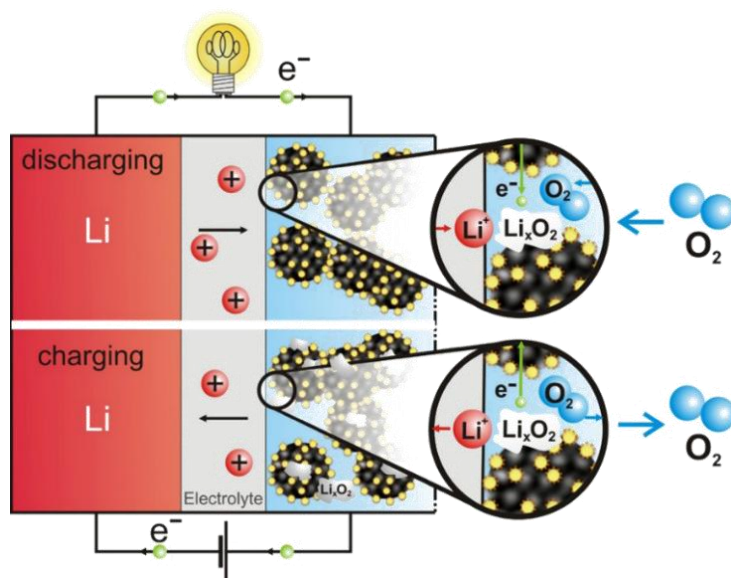

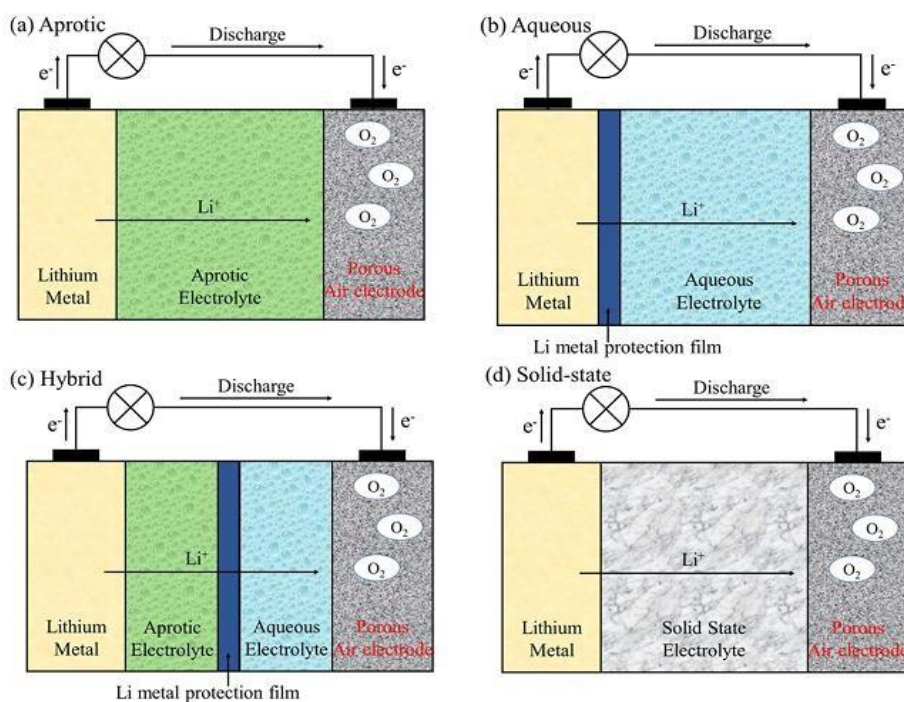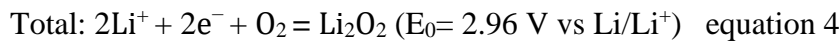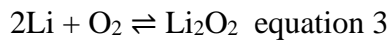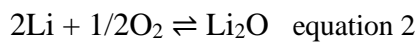Fig. 1-5 Schematic representation of typical Lithium Air (Li-air) battery

Fig. 1-6: Schematic representation of different types of Li-air batteries (Figure adopted from *Chem. Rev.*, **2014, 114, 5611–5640**)
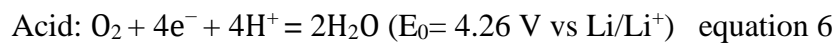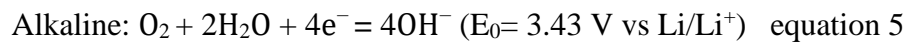
Lithium metal is the typical choice of anode. Lithium has a high specific capacity (3840 mAh/g) compared to other metal-air battery materials (820 mAh/g for zinc and 2965 mAh/g for aluminium). At the anode, lithium metal releases electrons via oxidation under electrochemical potential forces. [14,16] The half-reaction is:

$Li = Li^+ + e^-$ equation 1
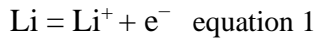
Li-air battery with high performance and energy density works under non-aqueous electrolyte. The reactions in Li-air battery are:

$2Li + 1/2O_2 \rightleftharpoons Li_2O$ equation 2

$2Li + O_2 \rightleftharpoons Li_2O_2$ equation 3

Total: $2Li^+ + 2e^- + O_2 = Li_2O_2$ ($E_0 = 2.96$ V vs Li/Li^+)   equation 4

Li-air battery with high performance and energy density works under aqueous electrolyte. The reactions in Li-air battery are:

Alkaline: $O_2 + 2H_2O + 4e^- = 4OH^-$ ($E_0 = 3.43$ V vs Li/Li^+)   equation 5

Acid: $O_2 + 4e^- + 4H^+ = 2H_2O$ ($E_0 = 4.26$ V vs Li/Li^+)   equation 6

Cathode is mixed with electrocatalyst. OER catalysts help in breaking of Li_xO_2. The half-reaction is:

$Li^+ + O_2 + e^- = Li_xO_2$ equation 7
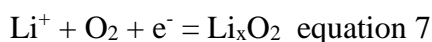
Li-air batteries do not have issues with fuel infrastructure. Then their specific energy density is much higher than the secondary batteries such as Ni-MH and Li-ion. The relationship between electrolyte and oxygen in cathode is shown in Figure 1-7. With equations 4-6, Li-air battery which operates under non-aqueous electrolyte could provide higher energy density than in aqueous electrolyte. Challenges to this battery systems are improvement in specific energy density and overall energy efficiency, charge-discharge cyclability, dendrite formation on all electrodes, instability of electrolytes and catalysts in the oxygen atmosphere, conductivity of electrolytes and electrodes, and so on. Charge-discharge current density of

typical Li-air batteries are 0.1−0.5 mA/cm^2. The major bottleneck of efficiency is oxygen reduction reaction and oxygen evolution reaction kinetics and uncontrollable side reactions of Li-O$_X$ systems.
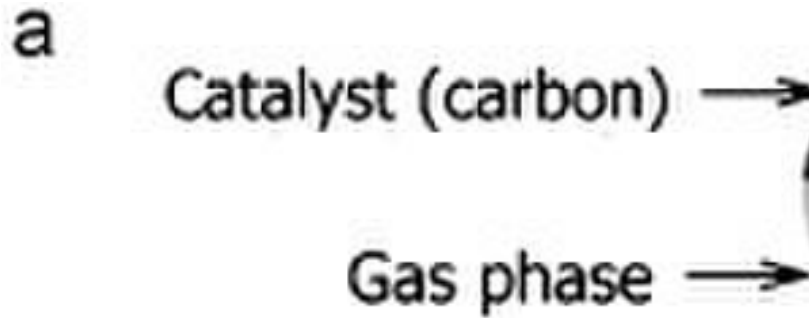
Fig. 1-7 Models of the reaction zones for catalytic reduction of oxygen: (a) a "three- phase reaction zone" for aqueous electrolyte metal/air battery and (b) a "two-phase reaction zone" for non-aqueous electrolyte Li–air battery (the original figure is insignificantly modified) [17]

In Li-air battery, cathode works on oxygen reduction reaction (ORR) and oxygen evolution reaction (OER). ORR and OER in nonaqueous systems follow the following mechanisms:

ORR:

$O_2 + 2e^- = O^{2-}$

$O_2^- + Li^+ \rightarrow LiO_2$

$2LiO_2 \rightarrow Li_2O_2 + O_2$

OER:

$Li_2O_2 = 2Li^+ + O_2 + 2e^-$
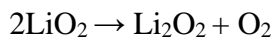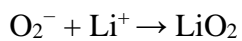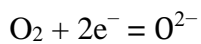
Under discharge, Li$^+$ containing non-aqueous electrolyte absorb the O$_2$ from air or oxygen gas and turns O$_2$ to O$_2^-$ and binds with Li$^+$ to form Li$_2$O (Fig.1-7 b), on the surface of the electrode. ORR and OER catalysts play an important role in determining efficiency and cyclability of Li-

air battery. [18,19]

The choice of electrolyte is important in nonaqueous electrolyte-based Li-air batteries. In such electrolytes superoxide radical (O^{2-}) formed by ORR shall be stable during discharge cycle. Some type of Li-ion batteries electrolytes could be used for Li-air batteries as well. But the Li-air batteries works in oxygen rich environments, and electrolytes shall be tested carefully. [20] Following are requirements for electrolytes in Li-air batteries

1. stability toward reaction with lithium metal

2. high boiling point and low volatility

3. high oxygen solubility and diffusivity

4. low viscosity to improve the rate performance

The lithium salts with $LiPF_6$, lithium bis[(trifluoromethyl)sulfonyl]imide (LiTFSI), $LiClO_4$, $LiCF_3SO_3$, $LiBF_4$, LiCl, and lithium bis(oxalato)borate (LiBOB) are supporting electrolyte usually. Specifically, for lithium air battery following are requirement for salts

1. Solubility is high enough in the solvent which could support smooth ion transport

2. Inert to the solvent and other cell components

3. Inert to the aggressive oxygen reduction species

Lithium bis[(trifluoromethyl) sulfonyl] imide (LiTFSI) is chosen for supporting electrolyte. LiI is employed as mediator.

1.3. Electrocatalyst for Cathode

It is important to have ORR and OER activities of electrocatalysts for the uses for Li-air battery. Carbon based materials can keep large specific surface area and conductivity, which makes it standard materials. The Oxygen Reduction Reaction (ORR) and the Oxygen Evolution Reaction (OER) are two type metal catalysed reaction. Under Li-air battery, ORR and OER activity is key for battery performance.

1.3.1. Oxygen Reduction Reaction (ORR)

1.3.1.1. Mechanism of ORR

The ORR is a complex process with diverse intermediates, the nature of which is influenced by the catalyst type and even by the reaction medium. Table 1.3 provides an overview about the ORR mechanism in various media, highlighting distinct intermediates and their associated thermodynamic potentials. This multifaceted understanding underscores the intricate dynamics of ORR, emphasizing the pivotal role of catalyst and environment in shaping the reaction pathway and thermodynamic considerations.

Table 1.3: Thermodynamic electrode potentials of electrochemical oxygen reduction reaction.

Electrolyte	ORR reactions	Thermodynamic electrode potential at standard conditions, V
Acidic aqueous solution	$O_2 + 4H^+ + 4e^- = H_2O$	1.229
	$O_2 + 2H^+ + 2e^- = H_2O_2$	0.70
	$H_2O_2 + 2H^+ + 2e^- = 2H_2O$	1.76
Alkaline aqueous solution	$O_2 + H_2O + 4e^- = 4OH^-$	0.401
	$O_2 + H_2O + 2e^- = HO_2^- + OH^-$	–0.065
	$HO_2^- + H_2O + 2e^- = 3OH^-$	0.867
Non-aqueous aprotic solvents	$O_2 + e^- = O_2^-$	a
	$O_2^- + e^- = O_2^{2-}$	b

Oxygen reduction reaction (ORR) could be classified as 4e⁻ process or 2e⁻ process. 4e⁻ process is key to produce water. Hydrogen peroxide is formed via in 2e⁻ process. In fuel cell, 4e⁻ pathway is preferred. In industrial H_2O_2 production, 2e⁻ reduction pathway is preferred. [21]

When the catalysts for Air-battery or fuel cell are designed larger electrochemical surface area has to be ensured. Usually, carbon-based supports are chosen.

1.3.1.2. Mechanism of ORR on Carbon Materials

ORR on graphite and glassy carbon: The following mechanism has been proposed for ORR catalysts. The following mechanism has been proposed.

$$O_2 \rightarrow O_{2(ads)} \qquad\qquad \text{equation 1}$$

$$O_2 + e- = [O_{2(ads)}]\text{-} \qquad\qquad \text{equation 2}$$

$$O_{2\,(ads)} \rightarrow O_{2\,[ads]}\text{ -} \qquad\qquad \text{equation 3}$$

$$O_2^-{}_{(ads)} + H_2O \rightarrow HO_2 + OH^- \qquad \text{equation 4}$$

$$HO_2 + e^- = HO_2^-{}_{(ads)} \qquad\qquad \text{equation 5}$$

$$HO_2^-{}_{(ads)} \rightarrow HO_2^- \qquad\qquad \text{equation 6}$$
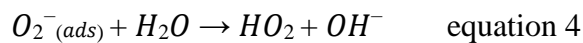
Corresponded species adsorbed on the electrode surface are marked as subscript *ads*. The reactants and products in Reaction 3 are two different forms of superoxide ions. [22]

1.3.1.3. ORR on Carbon Nanotubes

Carbon nanotubes (CNTs) have attracted significant interest due to their unique electronic, mechanical, and thermal properties. These properties make CNTs promising materials for various applications, such as energy storage, biosensors, and catalysis. In particular, the catalytic properties of CNTs have been extensively investigated, and they have been found to be effective in catalyzing many chemical reactions, including the oxygen reduction reaction (ORR). [23]

The activity of CNTs in ORR is strongly influenced by their preparation method. In the dihexyl hydrogen phosphate synthesis method, the CNTs showed a catalytic activity for ORR through a two-electron process. This method involved the formation of a thin film of the dihexyl hydrogen phosphate on a glassy carbon electrode, followed by the deposition of CNTs. The CNTs showed a high electrocatalytic activity for ORR due to the presence of nitrogen-containing functional groups on their surface.

On the other hand, when poly-diallyl dimethylammonium chloride was used to synthesize multi-walled carbon nanotubes, the electron transfer number was found to be between 3 and 3.5. The higher electron transfer number suggests that the CNTs prepared by this method had a higher number of active sites for ORR. The high activity of CNTs in ORR makes them potential candidates for use in fuel cells and other electrochemical devices.

To further enhance the performance of CNT-based catalysts for ORR, efforts are being made to modify the surface of the CNTs to increase their hydrophilicity, promote gas scavenging, and improve their durability. These modifications include doping the CNTs with heteroatoms, such as nitrogen or boron, and introducing defects in the CNT structure. Overall, the unique properties and versatile applications of CNTs make them an exciting area of research for the development of new and improved electrocatalytic materials.

1.3.1.4. ORR on Heteroatom Doped Carbon Atoms

Doping carbon with heteroatoms has been shown to be an effective way of enhancing ORR activity. Nitrogen has been the most commonly used dopant. In fact, doping carbon fibres with nitrogen has been shown to shift the ORR potential by nearly 70 mV, and the number of electron transfers was close to 4. Other heteroatoms such as boron, sulfur, fluorine, and phosphorus can also be used to dope carbon and enhance ORR activity, although the exact mechanism behind this is not yet fully understood. It is believed that the introduction of heteroatoms into the carbon structure creates active sites near the heteroatom and facilitates the breaking of the O=O bond in O_2, leading to enhanced ORR activity. [24]

1.3.1.5. ORR on Pretreated Carbon Surface

Electrode surface pretreatment has been found to be an effective way to improve ORR performance. Various methods such as vacuum heat treatment, electrode polishing, radio frequency plasma treatment, in-situ laser treatment, low-pressure heating, and electrochemical oxidation have been used to pretreat the electrodes. These methods have been found to increase the surface area of the electrodes to generate more functional groups and defects and expose new edges. This leads to more active sites on the electrode surface, which can enhance the ORR performance. However, the optimal pretreatment method may vary depending on the specific type of electrode material and the intended application. [25]

1.3.1.6. ORR Activity on Precious Metals

Platinum (Pt) is considered to be the most efficient catalyst for ORR. Despite efforts to find a single metal with similar activity, none have been found to match platinum. While the exact mechanism by which platinum catalyses ORR is not yet fully understood, research has suggested a possible pathway involving multiple intermediates as illustrated in Figure 1.8. According to this pathway, oxygen is fully reduced to water by losing 4 electrons without any intermediate states being formed during the process. [26]
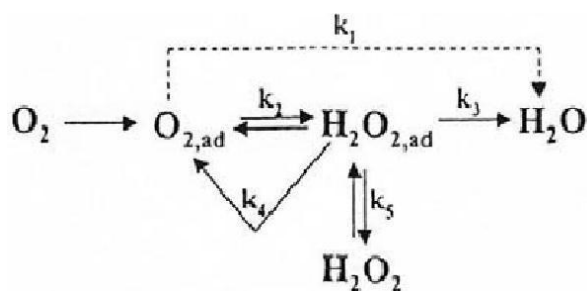
Fig 1.8: Mechanism of ORR on Pt

As we can see in Figure 1.6, O_2 can be reduced directly to H_2O with a rate constant of K_1, or it can be reduced to H_2O_2 via an intermediate formation with a rate constant of K_2. In addition, this intermediate can be reduced to HO^- with a rate constant K_3 or can be desorbed in the electrolyte with a rate constant K_5 or can be decomposed at the electrolyte surface with a rate constant K_4. It is widely accepted, however, that the most favourable route is to form water directly with the electron number of 4 transfer.

Two mechanisms were proposed based on DFT calculations. They are the association mechanism and the dissociation mechanism. The association mechanism is suitable for regions of high current density.

The dissociation mechanism is suitable under low current density regions where the O=O bond in O_2 splits and atomic O forms OH^- and H_2O. Other metals (such as Au, Cu, Pd, Ir, and Rh) can also exhibit ORR activities, but no other metal can maintain or exceed the catalytic activity of Pt.

1.3.1.7. Fuel-cell and Li-air Battery

ORR is well demonstrated and highly efficient in nature. The specific capacity (mass energy density) with Lithium is 3840 mAh/g or 43MJ/kg and the specific energy of hydrogen is 141.6 MJ/kg. As a comparison, gasoline is 46.4 MJ/kg, diesel is 44.8 MJ/kg and Li-ion battery is 0.46-0.73MJ/kg. The metals for ORR activity are shown in Figure 1-9 (volcano plot of ORR catalyst).

Regarding ORR activity, Pt is top of all materials, also the ORR catalyst is mainly used for fuel cell system.
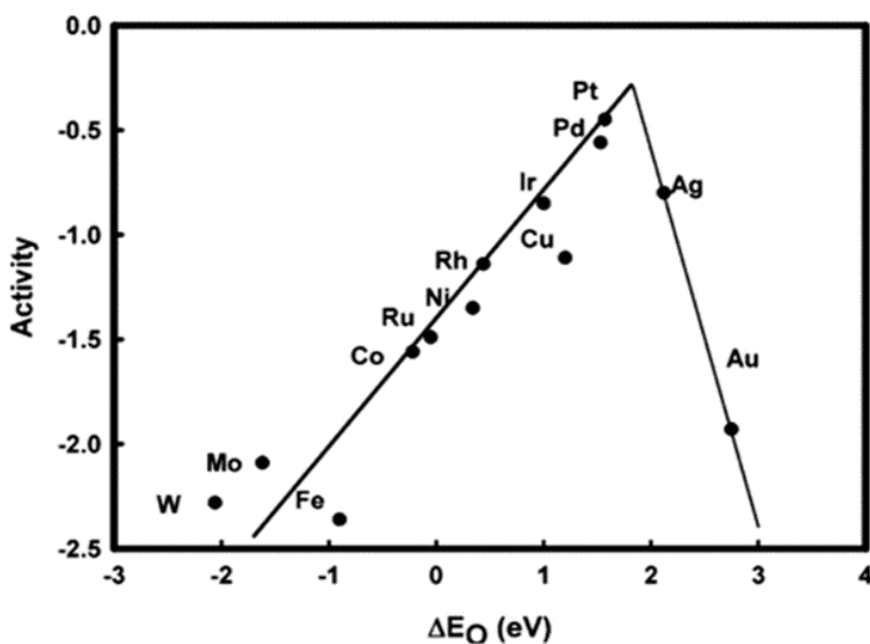
volcano plot of ORR catalyst

Fig. 1-9 Trends in oxygen reduction activity plotted as a function of the oxygen binding energy[26]

Fuel cells have many advantages over traditional power generation methods, such as internal combustion engines, because they can operate at higher efficiency, lower noise levels, and produce fewer emissions. They are also scalable, which means they can be used as power for anything from small portable devices to large industrial applications. Fuel cells are particularly attractive for transportation applications because they have the potential to provide a zero-emission source of power, which is critical for reducing greenhouse gas emissions and combating climate change. [27]

There are several types of fuel cells, each with different operating characteristics and materials. For example, proton exchange membrane (PEM) fuel cells are widely used in transportation applications because they can operate at low temperatures and have a high power density. Solid oxide fuel cells (SOFCs) operate at high temperatures and are typically used in large stationary power generation applications.

Despite their many advantages, fuel cells still face several challenges that limit their widespread adoption. One major challenge is the cost of materials and manufacturing, which is still relatively high compared to other power generation methods. Another challenge is the limited availability of hydrogen fuelling infrastructure, which is necessary for hydrogen fuel cells to be used in transportation applications. Researchers and engineers are working to address these challenges and improve the efficiency and cost-effectiveness of fuel cells, in order to make them more accessible and practical for a wide range of applications.

Typical Proton Exchange Membrane Fuel Cell (PEMFC) design is shown below in Figure 1-10. The reaction of fuel cell is:

$$H_2 = 2H^+ + 2e^- \qquad E^0 = 0 \; V \; vs \; SHE$$

$$\frac{1}{2}O_2 + 2H^+ + 2e^- = H_2O \qquad E^0 = 1.23 \; V \; vs \; SHE$$
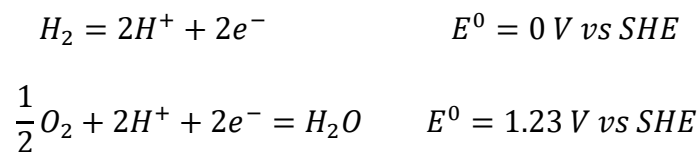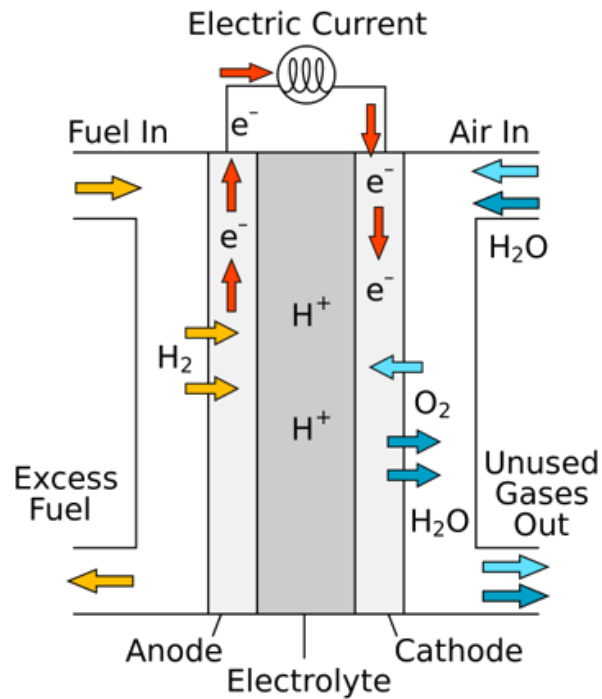
Fig 1-10. Schematic Representation of Proton Exchange Membrane Fuel Cell (PEMFC)

When the PEMFC works, the ORR happens in cathode where the catalyst layer is loaded. The electrochemical performance of fuel cell is decided on the surface which is marked under red line in Figure 1-11. [28]
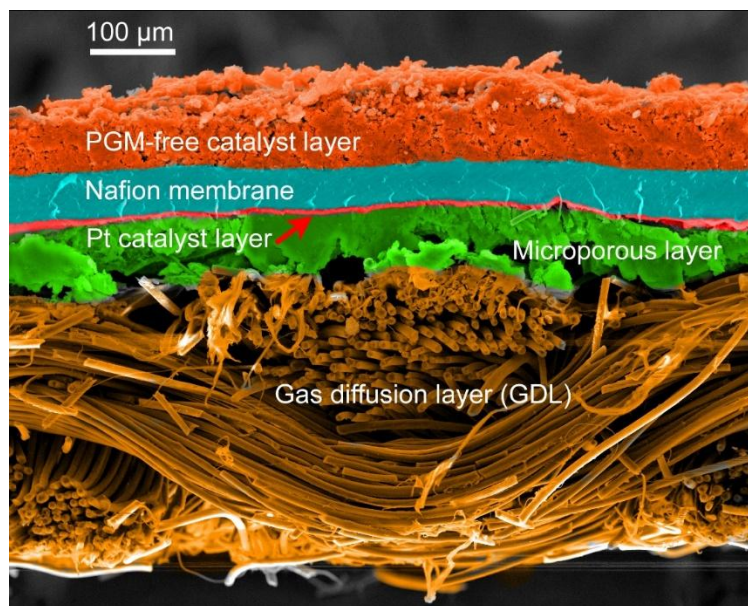

Fig 1-11. Oxygen Reduction Reaction (ORR) & Proton Exchange Membrane Fuel Cell (PEMFC)

1.3.2. Oxygen Evolution Reaction (OER)

1.3.2.1. Mechanism of OER

The Oxygen Evolution Reaction (OER) is also called Water oxidation reaction, which is one of the half reactions of water splitting. Basic reaction is

$2H_2O = O_2 + 4H^+ + 4e^-$ Oxidation (generation of dioxygen) (a)

$4H^+ + 4e^- = 2H_2$ Reduction (generation of dihydrogen) (b)

$2H_2O = 2H_2 + O_2$ Total Reaction (c)

Equation (b) (HER) and Equation (c) (OER) are two concurrent catalytic half-cell reactions. Though oxygen evolution is a 4-electron process, it is more complicated than evolution of hydrogen, as several surface-adsorbed intermediates are involved. The electrocatalysis process of water in each process must be discussed with respect to voltage and efficiency losses. The HER using selected noble metals setting exhibits very high exchange current density j_0, which is a measure of the internal turnover frequency of an electrochemical half-cell process (Figure 1-12). [29,30]

In electrocatalysis, overpotential is a fundamental concept of characterizing catalytic processes on surfaces, which is important in OER and ORR activity. The overpotential is generally considered to be a dynamical phenomenon, which can be divided into various factors such as ohmic overpotential or transport overpotential in the process of charge flow.
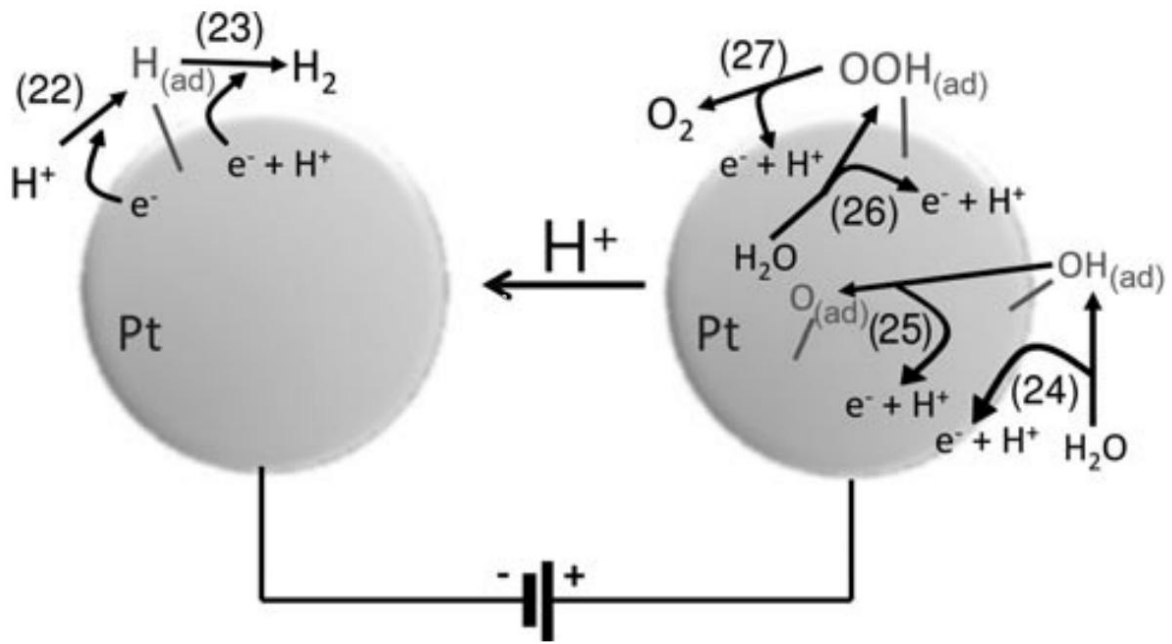
Figure 1-12. **Catalytic reactions associated with electrochemical water electrolysis.** An external voltage, symbolized by the battery symbol, drives the evolution of hydrogen at the cathode (HER) and the evolution of oxygen at the anode (OER). Protons are migrating from anode to cathode. Both mechanisms are depicted assuming a sequence of proton-coupled single-electron redox reactions. While HER shows one adsorbed intermediate, OER has three. The spheres symbolize a metal electrode, for example, Pt, covered with an oxide layer. The numbers in parentheses refer to chemical equations given in the text. [31]

1.3.2.2. Mechanism of OER on Carbon Materials

Carbon materials are widely used in electrocatalysis. From the discussion in 1.3.2.1, OER happened on the surface of the noble metals. How to keep the large area is a challenge with catalyst. In general, as results of OER and HER bubbles could be found on the surface of the electrode surface, so the speed of gas scavenging could limit the activity.

Improved hydrophilicity, keeping a large surface may resolve the limited gas diffusion on the catalyst surface. [31]

1.3.2.3. OER Activity on Metals

Metal selection for OER can be based on the volcano plot of ORR catalyst, as shown in Figure 1-13. Among the metals studied for ORR, Ru exhibits the best performance, followed closely by Pt. However, when discussing OER activity, it is important to consider heterogeneous OER, which is highly dependent on the surface where the reaction occurs and is influenced by the pH of the solution. In fuel cells and Li-air batteries, the pH during operation is usually below 7. According to Figure 1-14, even under ideal conditions, OER activity with Ru and Pt catalysts operating at 6 mV/s and 1600 rpm in 0.1 M $HClO_4$ at room temperature only reaches 30% of the theoretical values. [32]
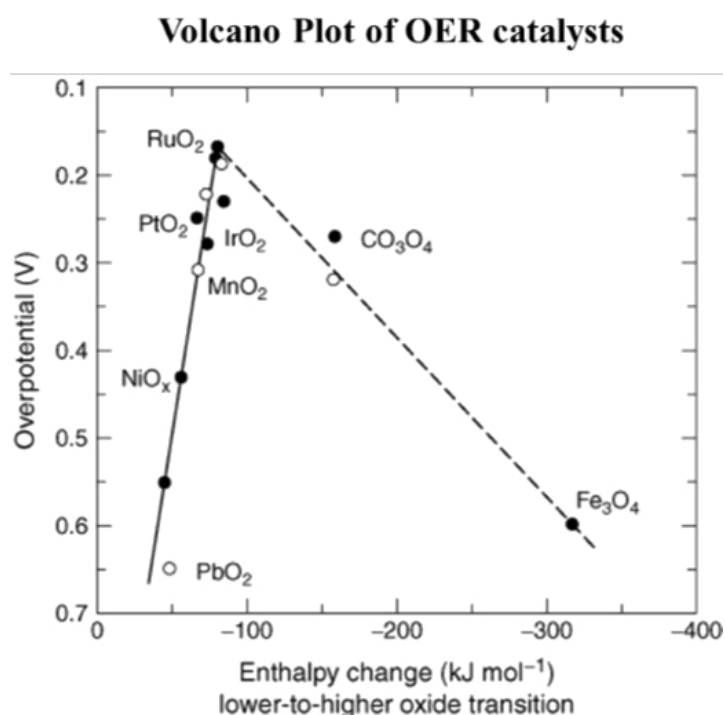

Fig. 1-13 Trends in oxygen evolution activity plotted as a function of the oxygen dis-binding energy
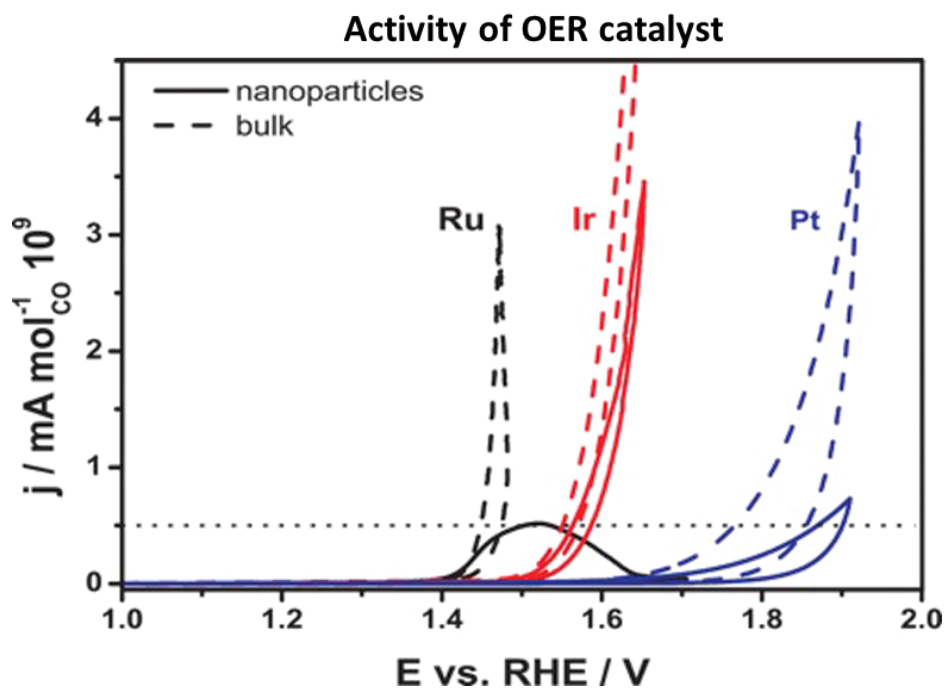
21

Activity of OER catalyst

Fig 1-14. First quasi stationary OER scan for bulk and nanoparticle catalysts of Ru, Ir, and Pt recorded with 6 mV/s and 1600 rotations per minute (rpm) in deaerated 0.1 M HClO$_4$ at RT. The current is normalized to the number of surface sites determined from CO stripping experiments.

[33]

1.3.2.4. Li-Air Battery Using Metals

In Li-air batteries, the metal catalysts used for OER are crucial for the battery's performance. The most commonly used metals are noble metals, such as platinum (Pt), ruthenium (Ru), and iridium (Ir), due to their high catalytic activity for OER. However, their scarcity and high cost limit their practical application. Therefore, researchers have been investigating alternative metal catalysts that are more abundant and cost-effective, such as transition metals and their oxides, including cobalt (Co), manganese (Mn), nickel (Ni), iron (Fe). These metals and their oxides have shown promising OER activity, but their catalytic activity is generally lower than that of noble metals. Therefore, improving the catalytic activity of these metals and their oxides is a key research area for developing more efficient and cost-effective Li-air batteries.

Catalyst design aims to achieve high performance at a lower cost, and for this reason, Ir is often the best choice, even though it may lose some activity under acidic conditions during OER activity. Both fuel cells and Li-air batteries use the same site for ORR and OER reactions. However, when ORR catalysts are used under OER conditions, their performance is significantly reduced, and they may even become damaged. This is because, under acidic conditions, water binds to the catalyst surface and irreversibly removes one electron and one proton, forming metal hydroxide. In alkaline solutions, typically, an oxide surface is presumed to form prior to oxygen evolution during OER.

1.3.3. Application of Bi-functional Catalyst and Li-Air Battery Design

Developing improved catalysts for ORR and OER is the key to the advancement of in metal-air batteries.

In this work, a catalyst needs to be designed for the Li-air battery in which new catalyst would work for ORR and OER. That means this catalyst must deal with two key problems at same time.

In this study, a catalyst is needed to be designed for Li-air batteries that can operate efficiently under both ORR and OER conditions. This means that the catalyst must address two critical challenges: firstly, it must maintain high ORR and OER activity, and secondly, it should exhibit stable performance under both ORR and OER conditions. It is the catalyst with Pt which works for ORR activity and Ir for OER activity. In section 1.2 the Li-air battery has been discussed; the catalyst is loaded on carbon-coated Ni mesh. The battery structure is shown in Figure 1-15.
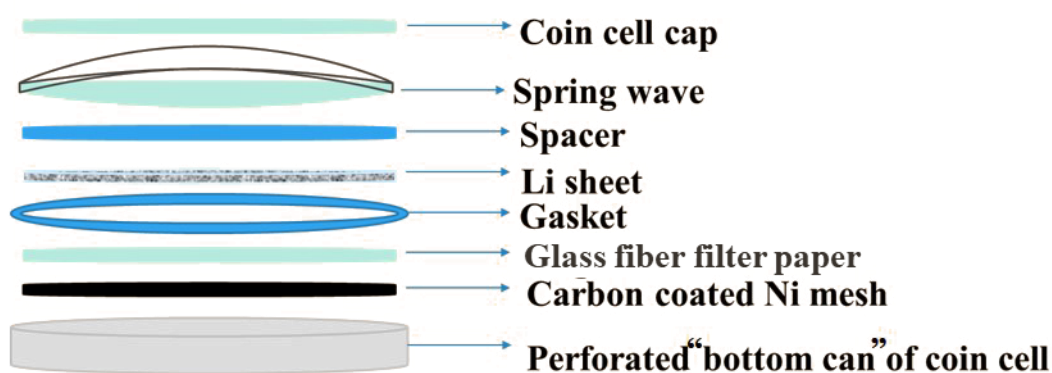
Coin cell configuration showing various components and the inset shows the perforated bottom can of the coin cell

Fig 1-15. Structure of Li-air battery

1.4. Introduction on Carbon-metal Based ORR and OER Catalyst

Carbon materials loaded with nanomaterials have been used in heterogeneous catalysis. These kinds of carbon-based materials have been used in catalysis as catalysts or even as supports of catalysts. Advantages are i) high chemical stability, ii) high thermal stability, iii) less corrosion capability, iv) easy recovery after reaction or synthesis and v) easy modification by chemical or physical method. However, over the surface of the carbon, their acid–base character and redox properties could be controlled by concentration and nature of the organic functional groups that are bearing different heteroatoms such as O, N, H, Cl, S, etc. (Fig 1-16). These affect morphological properties of carbon and show crucial role in catalytic behaviour. [34]
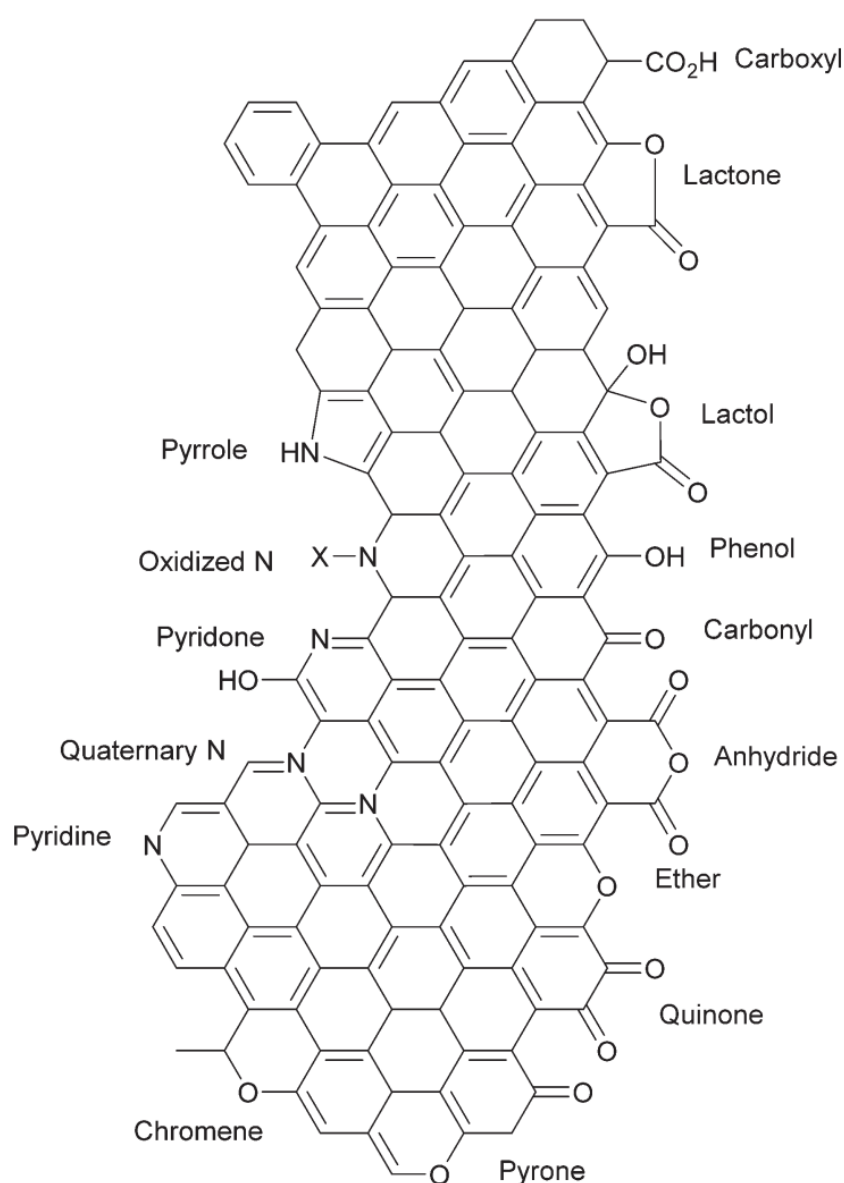

Fig 1-16. Organic functional groups on carbon materials

1.5. Facet Controlled Catalysis

The facet-controlled ORR has gained significant global research attention for achieving high performance. Low-index Pt nano-surfaces have been extensively studied in perchloric acid. In perchloric acid, Pt (100) << Pt (111)~Pt (110) in terms of activity has been reported. However, when operating within an acidic aqueous electrolyte system, Pt (100) is more reactive than Pt (111) due to the surface coverage of Pt (111) by bisulfate ions. It was further established that the arrangement of surface atoms, i.e., the morphological features, affects the catalytic performance. Shape-controlled synthetic strategies for transferring active catalytic surfaces from single crystals to practical nanophases show enhancement of the ORR activity of platinum. El-Sayed et al. successfully synthesized different facets of Pt, including nano-tetrahedra with (111) and nano-cubic composition of (100) as well as "approximately spherical" nanocrystals containing a mixture of {111} and {100} surfaces. [35]

Sun et al. conducted research on the synthesis of one-sided Pt nano-cubes (100) using a high-temperature method and found that the resulting catalyst exhibited a 2-fold higher ORR (oxygen reduction reaction) activity compared to commercially available Pt catalysts. The group also demonstrated that 7 nm (100) Pt nano-cubes showed better activity than other morphological forms of nanoparticles, highlighting the importance of facets as well as the shape dependence of nano-catalysts.

Another research group led by Xia et al. reported the synthesis of Pt concave nano-cubes with high-refractive-index faces such as {510}, {720}, and {830}. These catalysts exhibited higher electrocatalytic activity per unit surface area compared to catalysts with low-index planes, such as {100} and {111}. Despite the observed higher activity of these higher-index facets, the underlying mechanism remains unclear. Additionally, these highly faceted nanocrystals exhibited lower mass activity compared to other highly active ORR catalysts.

In summary, facet-controlled synthesis of Pt nano-catalysts has been shown to be a promising strategy for enhancing ORR activity. The surface morphology and atomic arrangement of Pt nanocrystals play critical roles in determining their electrocatalytic performance. High-index facets have been shown to exhibit higher activity, although the mechanism behind this is not yet fully understood. Further research is needed to optimize nano-catalyst synthesis and design, with a particular focus on balancing activity and stability for practical fuel cell applications.

1.6. Enhancement of Catalytic Activity of These Alloys

Bimetallic core-shell nanoparticles have been shown to exhibit improved activity and stability compared to their bulk counterparts, due to the unique synergistic effects between the two different metals. The core-shell structure consists of a metallic core surrounded by a shell layer of another metal. The metal shell can act as a protective barrier against dissolution, preventing the leaching of non-Pt metals, while the metal core maintains the activity of the catalyst.

Furthermore, the properties of the core-shell structure can be further tuned by controlling the size, composition, and morphology of the particles. For example, by varying the thickness of the shell layer, the activity and selectivity of the catalyst can be adjusted. In addition, the use of highly dispersed alloy nanoparticles can also improve the performance of the catalyst, as the high surface area to provide more active sites for the reaction.

In recent years, various methods have been developed for the synthesis of core-shell nanoparticles, including chemical reduction, solvothermal synthesis, and galvanic replacement. These methods allow precise control over the size, composition, and morphology of the particles, enabling the development of highly efficient and stable electrocatalysts for ORR applications.

Overall, the use of bimetallic core-shell nanoparticles offers a promising approach for overcoming the limitations of traditional alloy catalysts and provides a path for the design and development of highly efficient and stable ORR catalysts. [36]

1.7. Synthesis of Core Shell Nanoparticles:

There are various strategies for the synthesis of core-shell nanoparticles.

A core metal is selected and a shell was deposited on this already formed core.

Removal of unwanted constituents from alloys also can be carried out.

The alloy is treated in such a way that one of the alloy constituents' segregates to the surface to form a shell.

Figure 1.17 schematically illustrates the diverse methodologies employed in the development of core-shell nanoparticles. Researchers are benefited from the versatility in synthesis methods, allowing them to tailor nanoparticles to specific requirements.
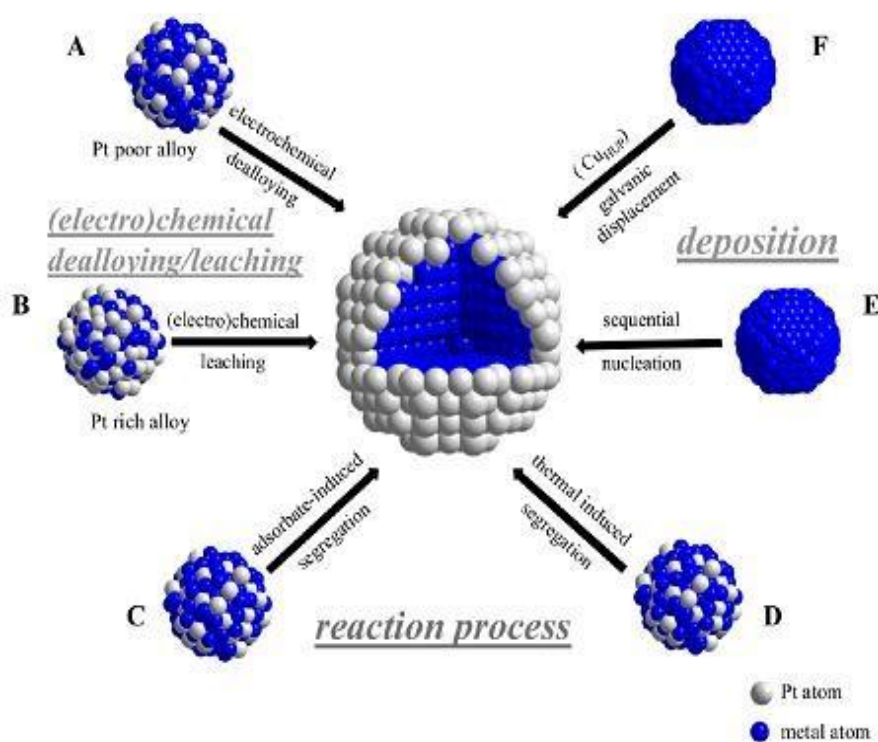

Fig 1.17: Various synthetic methods for core shell nanoparticles

(Figure adapted from *J. Phys. Chem. Lett., 2013, 4, 3273–3291*)

In this work, a carbon-supported Pt/Ir alloy nano-particles was synthesized and examined for Li-air battery.

1.8.   Design and Utilization of FAB Based Catalyst

Carbon has been used as the support for metal loading for many years in industrial catalyst. In electrocatalyst filed, oil-furnace blacks and acetylene blacks are two main types of carbon black being used as supports for Pt/C catalyst. In some research, carbon can affect the dispersion of the Pt particles. Usually, acetylene blacks typically have surface areas below 100 m^2g^{-1}, and furnace blacks show surface areas ranging from 20 to 1500 m^2g^{-1}, which were summarized in Table 1.4.

Table 1.4 Carbon blacks that have been used as support for Pt catalysts in PEMFCs

| Carbon	Supplier	Type of carbon	BET surface area $(m^2 \, g^{-1})$[a]	DBP adsorption (units)[b]
Vulcan XC72	Cabot Corp.	Furnace black	250	190
Black Pearls 2000	Cabot Corp.	Furnace black	1500	330
Ketjen EC300J	Ketjen Black International	Furnace black	800	360
Ketjen EC600JD	Ketjen Black International	Furnace black	1270	495
Shawinigan	Chevron	Acetylene black	80	-
Denka black	Denka	Acetylene black	65	165

a BET: Brunauer–Emmett–Teller method.

b DBP: dibutyl phthalate number (measure of carbon void volume).

Acetylene black (AB) (Fig 1-18) is one of carbon black, which has lower polycyclic aromatic hydrocarbon (PAH) content, and function group is less than 1%. When carbon support shows better affinity to metal nanoparticle, such affinity is key to control the nanoparticles size to enable larger surface area. When appropriate functional groups are present on the surface of AB particles, an increase in their surface area is observed.

Pt/Ir alloy nanoparticles and FAB as carbon support, was combined to form a new class of electrocatalyst, which is Bifunctional Pt/Ir Nano-particles Decorated Functionalized Acetylene Black. These systems are expected to exhibit higher performance in ORR and OER at same time along with long life.
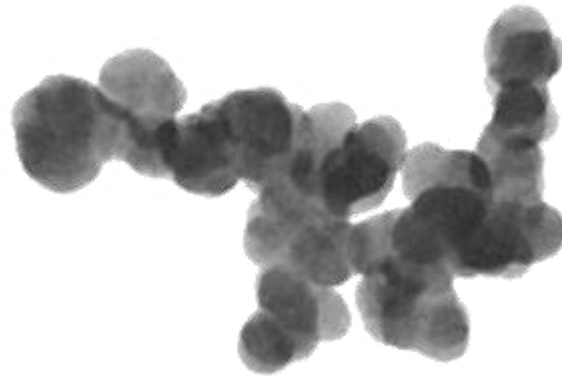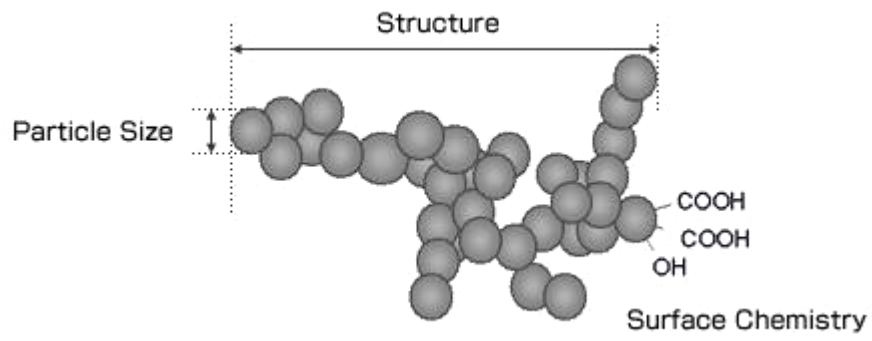
Fig 1-18. Structure (a) and TEM (b) of Acetylene black

1.9. Important Evaluation Methods and Basic Principles

Electrochemical Measurements

Three-electrodes set up was used for cyclic voltammetry. Typical three-electrodes set up is represented in Figure 1-23. Under three-electrodes system, current flows between the working electrode and the counter electrode was measured. Electric potential on working electrode has been controlled by an independent reference electrode, that means the electric potential on working electrode could be kept and monitored steadily.
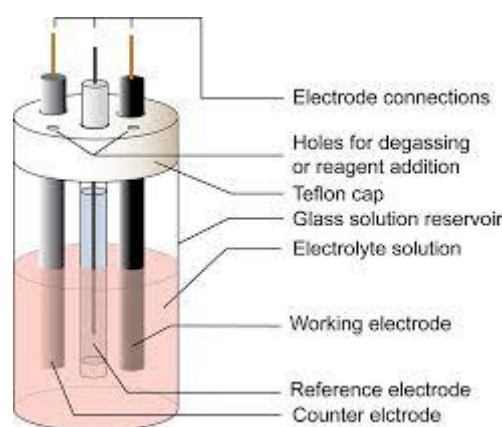

Fig. 1-23 three-electrodes assay

In this study, aqueous and organic electrolytes were chosen for ORR performance determination. Cyclic voltammetry (CV) and linear sweep voltammetry (LSV) were carried out under aqueous electrolytes. Cyclic voltammetry (CV) was measured under organic electrolytes as well.

Cyclic voltammetry (CV) is an electrochemical technique that is supported by the Nernst equation. The potential of the working electrode undergoes a smooth change that is measured against reference electrode, as shown in Figure 1-24. The Figure 1-24 is forward scan, which starts from a greater potential (a) and ends at a lower potential (d). The potential maximum (d) are called as the switching potential, where the voltage is sufficient enough to complete an oxidation or reduction. From (d) to (g) is positive scans, which turns to the reverse scan thereafter. The scans speed is the slope between (a) to (d). Figure 1-24 shows a cyclic voltammetry image resulting from an reduction and oxidation, which demonstrate reversible reaction. The reduction occurs during (a) and (d).

Linear sweep voltammetry (LSV) is another voltametric method. Under sweeping the potential between the working electrode and a reference electrode linearly by time, voltammogram is
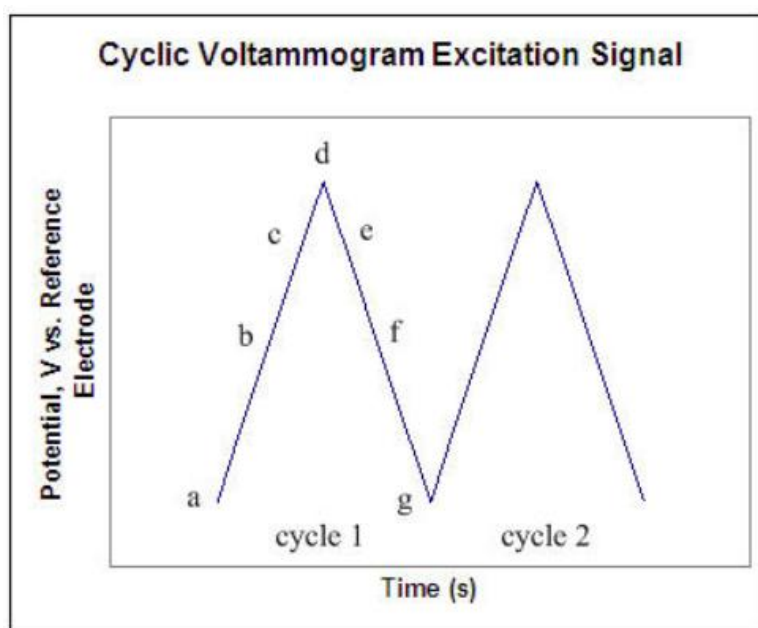
obtained as shown in Figure 1-25.
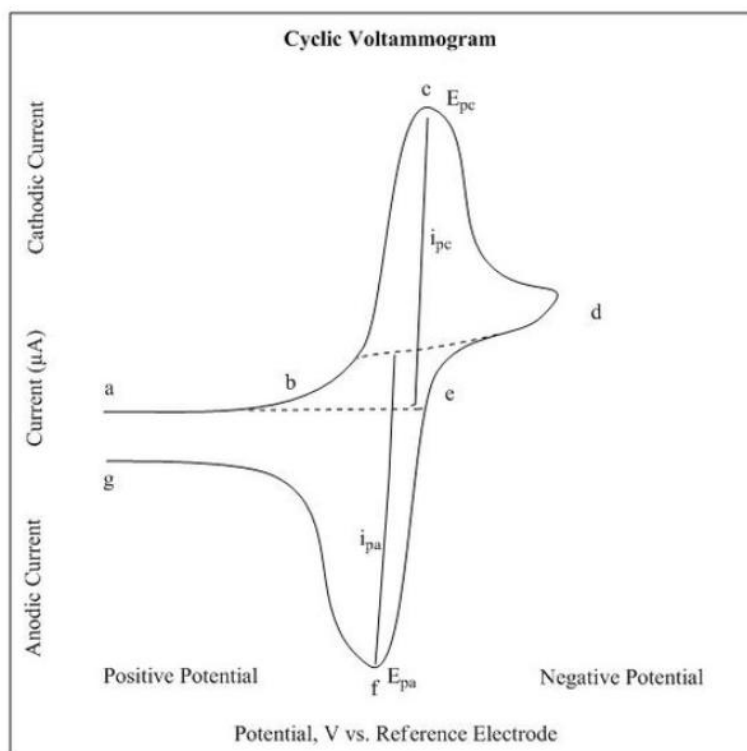

Fig. 1-24 CV Excitation Signal

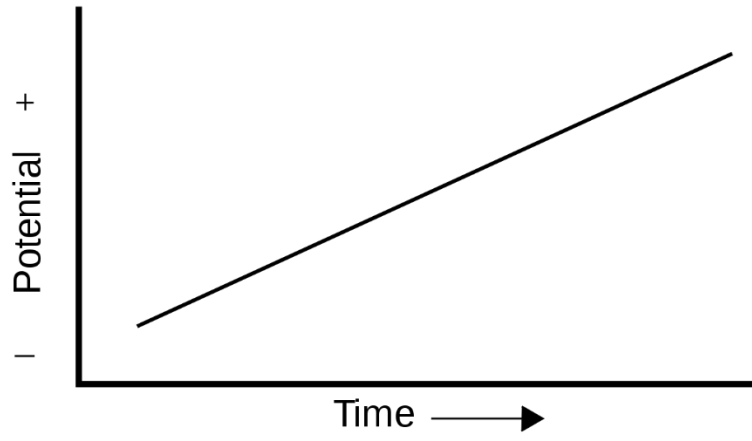Fig. 1-25 Voltammogram of a Single electron oxidation-reduction

Fig. 1-26 Linear potential sweep

1.10. Conclusion and Outlook about This Research

Li-air battery system is one of metal batteries; this type of battery could keep very high energy density, however, the limited of electrocatalyst is bottleneck of this technology. Bifunctional Pt/Ir Nano-particles Decorated Functionalized Acetylene Black as new type of catalyst, which has dual catalytic activity both for ORR and OER at once, will demonstrate advantage of this electrocatalyst design.

References

[1] Our World in Data. Retrieved, < https://ourworldindata.org>, (2019).

[2] NASA GISS Surface Temperature Analysis (v4), <https://data.giss.nasa.gov/gistemp/graphs_v4/>, (2019).

[3] Reddy, Thomas B. "David Linden Editor." (2002).

[4] Aravindan, V., Gnanaraj, J., Lee, Y. S., & Madhavi, S. (2013). LiMnPO 4–A next generation cathode material for lithium-ion batteries. Journal of Materials Chemistry A, 1(11), 3518-3539.

[5] 独立行政法人 新エネルギー・産業技術総合開発機構(NEDO), 「ＮＥＤＯ二次電池技術開発ロードマップ (Battery RM2010)」 (2010).

[6] 独立行政法人 新エネルギー・産業技術総合開発機構(NEDO), 「NEDO 二次電池技術開発ロードマップ 2013 （Battery RM2013）」 (2013).

[7] May, G. J., Davidson, A., & Monahov, B. (2018). Lead batteries for utility energy storage: A review. Journal of energy storage, 15, 145-157.

[8] Putois, F. (1995). Market for nickel-cadmium batteries. *Journal of Power Sources*, *57*(1-2), 67-70

[9] Kwon, S. J., Lee, S. E., Lim, J. H., Choi, J., & Kim, J. (2018). Performance and life degradation characteristics analysis of NCM LIB for BESS. *Electronics*, *7*(12), 406.

[10] Vicente, J. R., Kordesch, M. E., & Chen, J. (2021). Stabilization of mixed-halide lead perovskites under light by photothermal effects. *Journal of Energy Chemistry*, *63*, 8-11

[11] "The Nobel Prize in Chemistry 2019". *Nobel Prize*. Nobel Foundation. 2019. Retrieved 1 January 2020

[12] 国立研究開発法人 物質・材料研究機構(NIMS), 「リチウム空気電池について」, (2018).

[13] Girishkumar, G., McCloskey, B., Luntz, A. C., Swanson, S., & Wilcke, W. (2010). Lithium− air battery: promise and challenges. *The Journal of Physical Chemistry Letters*, *1*(14), 2193-2203.

[14] Abraham, K. M., & Jiang, Z. (1996). A polymer electrolyte-based rechargeable lithium/oxygen battery. *Journal of the Electrochemical Society*, *143*(1), 1.

[15] Girishkumar, G., McCloskey, B., Luntz, A. C., Swanson, S., & Wilcke, W. (2010). Lithium− air battery: promise and challenges. *The Journal of Physical Chemistry Letters*, *1*(14), 2193-2203.

[16] Ogasawara, T., Débart, A., Holzapfel, M., Novák, P., & Bruce, P. G. (2006). Rechargeable Li_2O_2 electrode for lithium batteries. *Journal of the American Chemical Society*, *128*(4), 1390-1393.

[17] Kraytsberg, A., & Ein-Eli, Y. (2011). Review on Li–air batteries—Opportunities, limitations and perspective. *Journal of Power sources*, *196*(3), 886-893.

[18] Peng, Z., Freunberger, S. A., Hardwick, L. J., Chen, Y., Giordani, V., Bardé, F., ... & Bruce, P. G. (2011). Oxygen reactions in a non-aqueous Li^+ electrolyte. *Angewandte Chemie International Edition*, *50*(28), 6351-6355

[19] Geng, D., Ding, N., Hor, T. A., Chien, S. W., Liu, Z., Wuu, D., ... & Zong, Y. (2016). From lithium‐oxygen to lithium‐air batteries: challenges and opportunities. Advanced Energy Materials, 6(9), 1502164.

[20] Di Censo, D., Exnar, I., & Graetzel, M. (2005). Non-corrosive electrolyte compositions containing perfluoroalkylsulfonyl imides for high power Li-ion batteries. *Electrochemistry communications*, *7*(10), 1000-1006.

[21] Taylor, R. J., & Humffray, A. A. (1975). Electrochemical studies on glassy carbon electrodes: II. Oxygen reduction in solutions of high pH (pH> 10). *Journal of Electroanalytical Chemistry and Interfacial Electrochemistry*, *64*(1), 63-84.

[22] Singh, S. K., Takeyasu, K., & Nakamura, J. (2019). Active sites and mechanism of oxygen reduction reaction electrocatalysis on nitrogen-doped carbon materials. Advanced Materials, 31(13), 1804297.

[23] Tang, H., Chen, J. H., Huang, Z. P., Wang, D. Z., Ren, Z. F., Nie, L. H., ... & Yao, S. Z. (2004). High dispersion and electrocatalytic properties of platinum on well-aligned carbon nanotube arrays. *Carbon*, *42*(1), 191-197.

[24] Maldonado, S., & Stevenson, K. J. (2005). Influence of nitrogen doping on oxygen reduction electrocatalysis at carbon nanofiber electrodes. *The Journal of Physical Chemistry B*, *109*(10), 4707-4716.

[25] Šljukić, B., Banks, C. E., & Compton, R. G. (2005). An overview of the electrochemical reduction of oxygen at carbon-based modified electrodes. *Journal of the Iranian Chemical Society*, *2*, 1-25.

[26] Zhang, S., Yuan, X. Z., Hin, J. N. C., Wang, H., Friedrich, K. A., & Schulze, M. (2009). A review of platinum-based catalyst layer degradation in proton exchange membrane fuel cells. *Journal of Power Sources*, *194*(2), 588-600.

[27] Tiwari, J. N., Lee, W. G., Sultan, S., Yousuf, M., Harzandi, A. M., Vij, V., & Kim, K. S. (2017). High-affinity-assisted nanoscale alloys as remarkable bifunctional catalyst for alcohol oxidation and oxygen reduction reactions. *ACS nano*, *11*(8), 7729-7735.

[28] Yin, X., Lin, L., Chung, H. T., Babu, S. K., Martinez, U., Purdy, G. M., & Zelenay, P. (2017). Effects of MEA fabrication and ionomer composition on fuel cell performance of PGM-free ORR catalyst. *ECS Transactions*, *77*(11), 1273.

[29] Ghosh, S. K., & Rahaman, H. (2019). Noble metal–manganese oxide hybrid nanocatalysts. In *Noble Metal-Metal Oxide Hybrid Nanoparticles* (pp. 313-340). Woodhead Publishing.

[30] Dotan, H., Landman, A., Sheehan, S. W., Malviya, K. D., Shter, G. E., Grave, D. A., ... & Grader, G. S. (2019). Decoupled hydrogen and oxygen evolution by a two-step electrochemical–chemical cycle for efficient overall water splitting. *Nature Energy*, *4*(9), 786-795.

[31] Ghosh, S. K., & Rahaman, H. (2019). Noble metal–manganese oxide hybrid nanocatalysts. In *Noble Metal-Metal Oxide Hybrid Nanoparticles* (pp. 313-340). Woodhead Publishing.

[32] Nørskov, J. K., Rossmeisl, J., Logadottir, A., Lindqvist, L. R. K. J., Kitchin, J. R., Bligaard, T., & Jonsson, H. (2004). Origin of the overpotential for oxygen reduction at a fuel-cell cathode. *The Journal of Physical Chemistry B*, *108*(46), 17886-17892.

[33] Tahir, M., Pan, L., Idrees, F., Zhang, X., Wang, L., Zou, J. J., & Wang, Z. L. (2017). Electrocatalytic oxygen evolution reaction for energy conversion and storage: a comprehensive review. *Nano Energy*, *37*, 136-157.

[34] Kasprzak, A., Zuchowska, A., & Poplawska, M. (2018). Functionalization of graphene: does the organic chemistry matter. Beilstein journal of organic chemistry, 14(1). 2018-2026.

[35] Wang, Y., Nie, Y., Ding, W., Chen, S. G., Xiong, K., Qi, X. Q., ... & Wei, Z. D. (2015). Unification of catalytic oxygen reduction and hydrogen evolution reactions: highly dispersive Co nanoparticles encapsulated inside Co and nitrogen co-doped carbon. *Chemical communications*, *51*(43), 8942-8945.

[36] Hong, J. W., Kang, S. W., Choi, B. S., Kim, D., Lee, S. B., & Han, S. W. (2012). Controlled synthesis of Pd–Pt alloy hollow nanostructures with enhanced catalytic activities for oxygen reduction. ACS nano, 6(3), 2410-2419.

2. Chapter 2

Material Preparing Discussion.

2.1. Abstract

In this work, we report a high feasibility catalyst design on Acetylene Black (AB) based nanoparticles loading materials. The AB needs to be pre-processed before loading with metal nanoparticles. Pt alloy nanoparticles have been chosen to enhance the activity of the AB, with respect to oxygen reduction reaction (ORR) and oxygen evolution reaction (OER). The successful formation of bifunctional Pt/Ir nanoparticles decorated functionalized Acetylene Black, such as FAB180-Pt and FAB(x)-Pt/Ir catalyst, has been demonstrated. Materials characterization was carried out by impedance analysis, scanning electron microscopy-energy-dispersive X-ray spectroscopy (SEM-EDS), transmission electron microscopy (TEM), thermogravimetric analysis (TGA), and X-ray photoelectron spectroscopy (XPS).

2.2. Introduction

The challenge of controlling and reducing global warming is a worldwide concern, and finding alternative energy sources is crucial to addressing this issue. [1] Use for renewable energy is one of the best solutions, and wind and solar power are becoming more prevalent methods of generating electricity. The development of batteries that can efficiently store and discharge electricity will further enhance the viability of renewable energy sources. The use of clean energy systems is becoming increasingly desirable, not only to reduce greenhouse gas emissions but also to reduce reliance on fossil fuels, which are finite resources. The adoption of renewable energy and the implementation of clean energy systems are essential steps in achieving sustainable development and combating climate change. It is crucial that individuals, businesses, and governments work together to invest in and promote the use of renewable energy sources and clean energy systems.

According to Figure 2-1, metal-air batteries have highest energy densities compared to other types of batteries. This is because they use anodes made from pure metal and an external cathode of ambient air. Due to the small amount of actual mass in the battery, the calculated energy density is high.[2] Aluminium, which has 3 valence electrons compared to lithium's 1 valence electron, also contributes to the high energy density. The Ragone plot shown in Figure 2-1 confirms that metal-air batteries have good energy density. Chemical energy storage is becoming increasingly important as a way to store electricity, and metal-air batteries are a promising technology in this regard. By further developing and optimizing these batteries, we can potentially overcome some of the limitations of other battery types and achieve more efficient and sustainable energy storage.
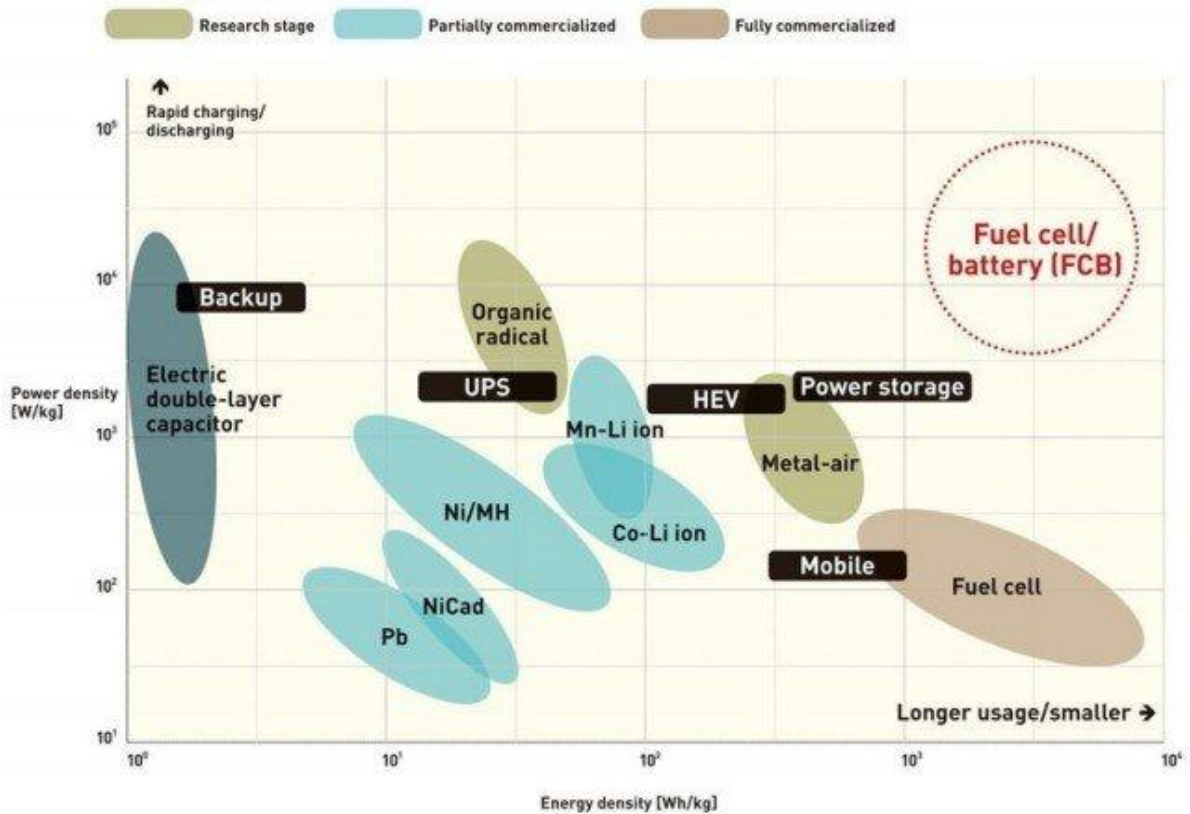
Fig 2-1 energy density for various types of batteries. [3]

The research presented in this thesis aims to design and test a new type of electrocatalyst for use in Li-air batteries.[4] Li-air batteries are a promising energy storage technology with a high theoretical energy density, making them ideal for use in electric vehicles and other applications. The designed material must exhibit both ORR (oxygen reduction reaction) and OER (oxygen evolution reaction) activities simultaneously. ORR is the process in which oxygen receives electrons to form water or Li_xO_y,[5] while OER is the opposite process in which water or Li_xO_y is split into oxygen and electrons. Both of these reactions are crucial for the proper functioning of a Li-air battery. In the case of Li-air batteries, an efficient catalyst is crucial for achieving high energy density and long cycle life. Therefore, the research presented in this thesis focuses on designing that exhibits high ORR and OER activity at the same time, with the goal of enhancing the performance of Li-air batteries. This research has important implications for the development of more efficient and sustainable energy storage technologies.

2.3. Materials Synthesis

The materials chosen for electrocatalyst synthesis in this thesis to enhance the performance of Li-air batteries are based on carbon and precious metals. Acetylene Black was selected for its excellent electrical conductivity, high surface area and high density of functional groups when oxidated. While Pt and Ir were chosen for their high catalytic activity towards the ORR and OER, respectively. The combination of these materials is expected to result in a electrocatalyst that exhibits both ORR and OER activities simultaneously, which is crucial for the proper functioning of a Li-air battery. This research has important implications for the development of more efficient and sustainable energy storage technologies.

Table 2-1 Reagent

Perchloric acid	60 %	Kanto Chemical Co.
LiTFSI (Lithium bis[trifluoro methanesulfonyl]imide)	>98.0 %	Kanto Chemical Co.
TEGDME (Tetraethyleneglycol dimethyl ether)	≥99 %	Sigma-Aldrich
Methanol	99.8 %	Kanto Chemical Co.
Acetone	99.0 %	Kanto Chemical Co.
Hexane	96.0 %	FUJIFILM Wako Pure Chemical Co.
2-propanol	98.0 %	FUJIFILM Wako Pure Chemical Co.
5% Nafion Dispersion^{TM}	DE521 CS タイプ	FUJIFILM Wako Pure Chemical Co.
Acetylene black	2.2 g/cm^3 (20 °C)	MERCK
Chloroplatinic acid	97.0+ %	FUJIFILM Wako Pure Chemical Co.
Chloroiridic acid	97.0+ %	Sigma-Aldrich
Sulfuric acid	95 %	FUJIFILM Wako Pure Chemical Co.
Nitric acid	60 %	FUJIFILM Wako Pure Chemical Co.
LiI(Lithium iodide)	97.0+ %	FUJIFILM Wako Pure Chemical Co.
LiTFSI (Lithium bis [trifluoro methanesulfonyl] imide)	>98.0 %	Kanto Chemical Co.
TEGDME (Tetraethyleneglycol dimethyl ether)	≥99 %	Sigma-Aldrich

Table 2-2 Instrumentation

Ultrasonic cleaning machine	UT-106	SHARP Co.
Electrochemical analyser station	VSP Potentiostat	Bio-logic Science Instruments
Rotating ring disk electrode device	RRDE-3A	BAS
Magnetic stirrer	CT-1AN	AS ONE
Vacuum glove box	UN-650F	UNICO

2.3.1. AB Carbon

Acetylene Black, a widely used was type of carbon black in various industrial processes, serves as an essential basic material in battery systems as conductive additive. The generic structure of Acetylene Black is shown in Figure 2-2. Additionally, it contains oxygen-containing hydrophilic functional groups, due to structural defects based on sp^3 carbon.

The research presented in this thesis focuses on designing a material that exhibits high ORR and OER activity, with the goal of enhancing the performance of Li-air batteries.
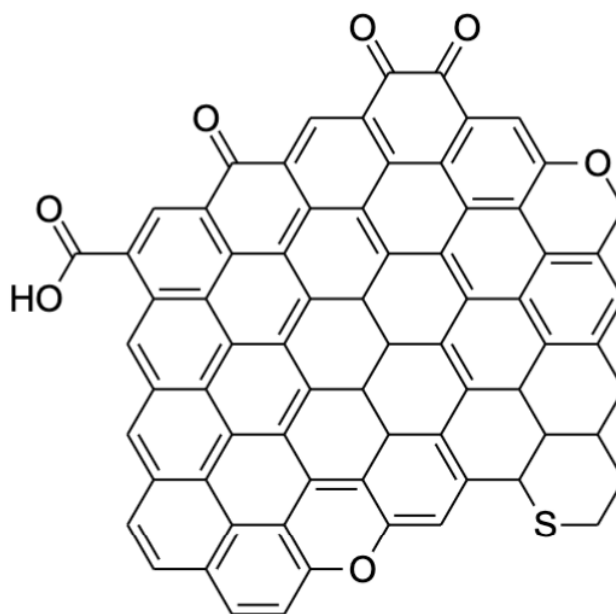
Fig 2-2 The generic structure of carbon black.

2.3.2. FAB carbon and preparation

For this study, Functional Acetylene Black (FAB) was selected as the carbon support material. However, before it could be used, Acetylene Black (AB) needed to be modified to introduce functional groups into the system.

Functional Acetylene Black (FAB) is a derivative of AB that is produced through a process known as acid corrosion. This process introduces functional groups such as -OH and -COOH onto the surface of the AB particles, which can improve their compatibility with other materials and enhance their performance in certain applications.

One key difference between AB and FAB is their diffusivity in water. AB has a relatively high diffusivity due to its highly porous structure, which allows water to penetrate and move through the material easily but it all most cannot disperse in water. In contrast, FAB has a higher diffusivity in water due to the presence of functional groups on its surface, which can interact with water molecules.

The synthesis of Functional Acetylene Black (FAB) involved several steps. Firstly, a mixed acid was prepared by combining H_2SO_4 and HNO_3 with water. Then, 1000 mg of Acetylene Black (AB) was mixed with the mixed acid and subjected to ultrasonic irradiation for varying lengths of time (60, or 180 minutes). During this process, the AB particles were dispersed and reacted with the mixed acid to introduce -COOH functional groups onto the surface of the resulting FAB.

The amount of -COOH functional groups in the FAB could be controlled by adjusting the reaction time. Specifically, samples synthesized under 60, and 180 minutes of reaction time were produced with varying amounts of -COOH functional groups. The resulting FAB samples were then thoroughly washed with deionized water and vacuum-dried at room temperature for over 12 hours. Table 2-3 displays the FAB samples that were synthesized for this study, along with the specific reaction time used to produce each sample.

Table 2-3 FAB carbon

Sample name	Reaction time
FAB-60	60min
FAB-180	180min

The synthesized FAB samples were intended for use as a substrate for metals deposition. The introduction of -COOH functional groups onto the surface of FAB is expected to enhance its compatibility with metal ions and improve the efficiency of metals deposition.

2.3.3. Pt Carbon

Pt/C catalyst is widely used in electrochemical applications, particularly in fuel cell technologies. Some examples of fuel cell vehicles that use Pt/C catalyst include the Toyota Mirai and Honda Clarity. These vehicles rely on fuel cell technology to generate electricity, and the Pt/C catalyst plays a critical role in facilitating the electrochemical reactions that produce this electricity.

In this study, Pt/C played a key role in comparing the performance of different types of Pt including catalysts in an air battery system. Specifically, the study aimed to assess the performance of catalysts with single metal or composite metals. The objective was to identify alternative catalyst materials that could potentially offer comparable or improved performance for use in electrochemical applications, particularly in air battery systems. By using Pt/C as a benchmark catalyst, the study sought to evaluate the performance of novel Pt including composite metal-based catalyst materials.

The synthesis of Pt metal catalyst (FAB180-Pt 10%) was carried out as follows: to perform metal deposition onto the FAB-180 carbon support, a 300 ml two-necked flask was chosen as the reaction container. A solution was prepared by mixing 100 mg of FAB and 100 ml of ethylene glycol, which was subjected to ultrasonic irradiation for 1 hour. A 100 ml dropping funnel was connected to the side neck of the flask, and a condenser was attached to the main neck. Next, a metal salt solution containing 6.9 ml 0.01 M $H_2PtCl_6 \cdot xH_2O$ mixed with 40 ml of ethylene glycol was added to the dropping funnel. The flask was then immersed in an oil bath, and the temperature was maintained at 150°C for 12 hours. During the heating process, the switch of the constant pressure funnel was opened, and the metal salt solution was added dropwise into the flask. After heating, the solid part was thoroughly washed with deionized water and then vacuum-dried at 80°C for 12 hours. Tiled of FAB180-Pt 10% was 109 mg.

Table 2-4 FAB180-Pt10% catalyst

	Carbon Standers	Pt &Weight Percent	Designed Metal Weight Percent	Amount
FAB180-Pt 10%	FAB-180 @100mg	6.9 ml@12.5 mg 10%wt	10% wt	109 mg

2.3.4. Pt/Ir Carbon

The Pt/Ir catalyst is a type of composite metal-based electrochemical catalyst. The fundamental idea behind using composite metal cores is to retain two or more physical and chemical properties simultaneously. In the case of the Pt/Ir catalyst, the combination of platinum and iridium allows the catalyst to exhibit both ORR and OER catalytic activity.

This type of composite metal-based catalyst is particularly useful in electrochemical reactions, where the presence of both metals enhances the performance of the catalyst. For this reason, the Pt/Ir catalyst is designed to hold both ORR and OER activity simultaneously. Therefore, a Pt and Ir alloy has been proposed and systematically tested as a composite metal electrochemical catalyst.

The synthesis of FAB60-Pt/Ir 1:1 was carried out as follows: to perform metal deposition onto the FAB-60 carbon support, a 300 ml two-necked flask was chosen as the reaction container. A solution was prepared by mixing 100 mg of FAB-60 and 100 ml of ethylene glycol, which was subjected to ultrasonic irradiation for 1 hour. A 100 ml dropping funnel was connected to the side neck of the flask, and a condenser was attached to the main neck. Next, a metal salt solution containing 6.9ml 0.01 M $H_2PtCl_6 \cdot xH_2O$ and 6.9 ml $H_2IrCl_6 \cdot xH_2O$ mixed with 40 ml of ethylene glycol was added to the dropping funnel. The flask was then immersed in an oil bath, and the temperature was maintained at 150°C for 12 hours. During the heating process, the switch of the constant pressure funnel was opened, and the metal salt solution was added dropwise into the flask. After heating, the solid part was thoroughly washed with deionized water and then vacuum-dried at 80°C for 12 hours. Tiled of was 121 mg.

The synthesis of FAB60-Pt/Ir 2:1 was carried out as follows: to perform metal deposition onto the FAB-60 carbon support, a 300 ml two-necked flask was chosen as the reaction container. A solution was prepared by mixing 100 mg of FAB-60 and 100 ml of ethylene glycol, which was subjected to ultrasonic irradiation for 1 hour. A 100 ml dropping funnel was connected to the side neck of the flask, and a condenser was attached to the main neck. Next, a metal salt solution containing 9.2 ml 0.01 M $H_2PtCl_6 \cdot xH_2O$ and 4.6 ml $H_2IrCl_6 \cdot xH_2O$ mixed with 40 ml of ethylene glycol was added to the dropping funnel. The flask was then immersed in an oil bath, and the temperature was maintained at 150°C for 12 hours. During the heating process, the switch of the constant pressure funnel was opened, and the metal salt solution was added dropwise into the flask. After heating, the solid part was thoroughly washed with deionized water and then vacuum-dried at 80°C for 12 hours. Tiled of was 117 mg.

The synthesis of FAB180-Pt/Ir 1:1 was carried out as follows: to perform metal deposition onto the FAB-180 carbon support, a 300 ml two-necked flask was chosen as the reaction container. A solution was prepared by mixing 100 mg of FAB-180 and 100 ml of ethylene glycol, which was subjected to ultrasonic irradiation for 1 hour. A 100 ml dropping funnel was connected to the side neck of the flask, and a condenser was attached to the main neck. Next, a metal salt solution containing 6.9ml 0.01 M $H_2PtCl_6 \cdot xH_2O$ and 6.9 ml $H_2IrCl_6 \cdot xH_2O$ mixed with 40 ml of ethylene glycol was added to the dropping funnel. The flask was then immersed in an oil bath, and the temperature was maintained at 150°C for 12 hours. During the heating process, the switch of the constant pressure funnel was opened, and the metal salt solution was added dropwise into the flask. After heating, the solid part was thoroughly washed with deionized water and then vacuum-dried at 80°C for 12 hours. Tiled of 119 mg.

The synthesis of FAB180-Pt/Ir 2:1 was carried out as follows: to perform metal deposition onto the FAB-180 carbon support, a 300 ml two-necked flask was chosen as the reaction container. A solution was prepared by mixing 100 mg of FAB-180 and 100 ml of ethylene glycol, which was subjected to ultrasonic irradiation for 1 hour. A 100 ml dropping funnel was connected to the side neck of the flask, and a condenser was attached to the main neck. Next, a metal salt solution containing 9.2 ml 0.01 M $H_2PtCl_6 \cdot xH_2O$ and 4.6 ml $H_2IrCl_6 \cdot xH_2O$ mixed with 40 ml of ethylene glycol was added to the dropping funnel. The flask was then immersed in an oil bath, and the temperature was maintained at 150°C for 12 hours. During the heating process, the switch of the constant pressure funnel was opened, and the metal salt solution was added dropwise into the flask. After heating, the solid part was thoroughly washed with deionized water and then vacuum-dried at 80°C for 12 hours. Tiled of was 119 mg.

Table 2-5 FAB(x)-Pt/Ir catalysts

	Carbon Standers	Pt & Weight Percent	Ir & Weight Percent	Designed Metal Weight Percent	Yield
FAB60-Pt/Ir 1:1	FAB-60 @ 100 mg	6.9 ml @ 12.5 mg 10%wt	6.9 ml @ 12.5 mg 10%wt	20%wt	121 mg
FAB60-Pt/Ir 2:1	FAB-60 @ 100 mg	9.2 ml @ 16.7 mg 10%wt	4.6 ml @ 8.3 mg 10%wt	20%wt	117 mg
FAB180-Pt/Ir 1:1	FBA-180 @ 100 mg	6.9 ml @ 12.5 mg 10%wt	6.9 ml @ 12.5 mg 10%wt	20%wt	119 mg
FAB180-Pt/Ir 2:1	FAB-180 @ 100 mg	9.2 ml @ 16.7 mg 10%wt	4.6 ml @ 8.3 mg 10%wt	20%wt	119 mg

2.4. Analysis and Discussion

This section focuses on the use of TGM, SEM-EDS, TEM, and XPS to analyse the structures of the AB carbon material and the FAB(x)-Pt/Ir catalysts. The aim is to identify and discuss the structural aspects of materials.

2.4.1. SEM-SED

SEM-EDS (Scanning Electron Microscopy-Energy Dispersive X-ray Spectroscopy) is a powerful technique used to identify and quantify the elemental composition of materials. By analyzing the characteristic X-rays emitted from the sample, the technique can provide valuable information about the spatial distribution and concentration of various elements. In this study, SEM-EDS was employed to investigate the elemental composition of obtained carbon materials.

SEM-EDS was utilized to conduct elemental analysis on AB, FAB, FAB-Pt, and FAB-Pt/Ir materials. Table 2-6 presents the weight percentage of C, O, Pt, and Ir for each material.

Table 2-6 The weight percentage of rations elements in catalysts by SEM-EDS

Sample	Element Weight (percent)				
	C	O	Pt	Ir	Metal Total (%)
AB	96.29	3.71	-	-	
FAB-60	93.47	6.53	-	-	
FAB-180	88.95	11.05	-	-	
FAB180-Pt10%	84.62	6.65	8.73	-	8.73
FAB60-Pt/Ir 1:1	75.77	4.43	8.61	11.63	20.24
FAB60-Pt/Ir 2:1	76.13	7.25	11.59	5.03	16.62
FAB180-Pt/Ir 1:1	78.07	3.96	9.04	8.92	17.96
FAB180-Pt/Ir 2:1	77.01	5.09	12.91	4.99	17.90

As for AB carbon, the percentage of oxygen increased from 3.71% to 6.53% in FAB-60 and to 11.05% in FAB-180 after reaction. This increase in oxygen percentage suggests that functional groups were introduced into the carbon material, altering its surface structure. The results

demonstrate that the AB carbon underwent significant changes in surface after reaction, which could have important implications for its electrochemical performance.

In the case of FAB180-Pt10%, the presence of 8.73% Pt in the catalyst led to a decrease in oxygen content to 6.65%. This reduction in oxygen content indicates disapperance of some C-O bonds.

The FAB(x)-Pt/Ir catalysts are the main focus of present study. The elemental analysis of metal composites of FAB-60 and FAB-180 carbons revealed that the oxygen percentage in FAB-60-Pt/Ir was higher than in FAB-180-Pt/Ir, regardless of the metal percentage, which can explain the difference in functional group percentage between the two carbons. The study then focused on the metal component of the catalysts, where the weight ratio of Pt/Ir was either 2:1 or 1:1. It was found that the oxygen weight percent was higher when the Pt/Ir weight ratio was 2:1, compared to 1:1. This observation can be further investigated with TEM and XPS data, which provide information about the morphology, size distribution, and chemical state of the catalyst particles.

Understanding how metal percentage and weight load affect the oxygen percentage and functional group distribution in carbon can lead to the development of more efficient catalyst materials. In this work, the oxygen percentage and functional group distribution in FAB carbon were modified, leading to changes in the structure and surface of Pt and Ir. This was confirmed through clear data obtained from TEM and XPS analyses.

Map Sum Spectrum				FAB-60
Element	Line Type	Weight %	Weight % Sigma	Atomic %
C	K series	93.47	0.20	95.02
O	K series	6.53	0.20	4.98
Total		100.00		100.00

Map Sum Spectrum				FAB-180
Element	Line Type	Weight %	Weight % Sigma	Atomic %
C	K series	88.95	0.25	91.47
O	K series	11.05	0.25	8.53
Total		100.00		100.00
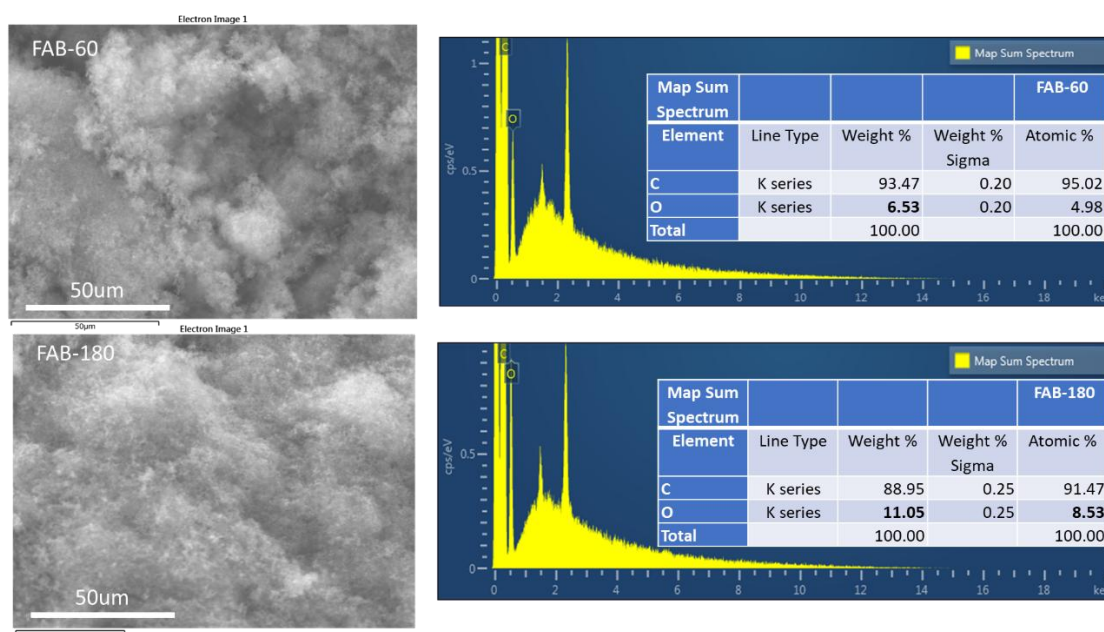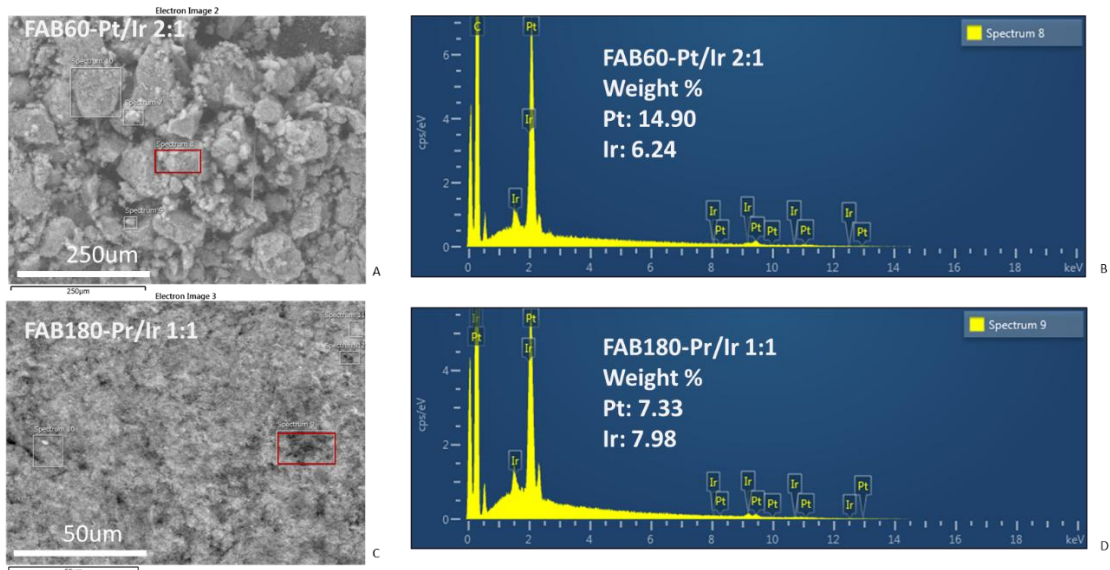
Fig. 2.4 SEM images of FAB-60 and FAB-180
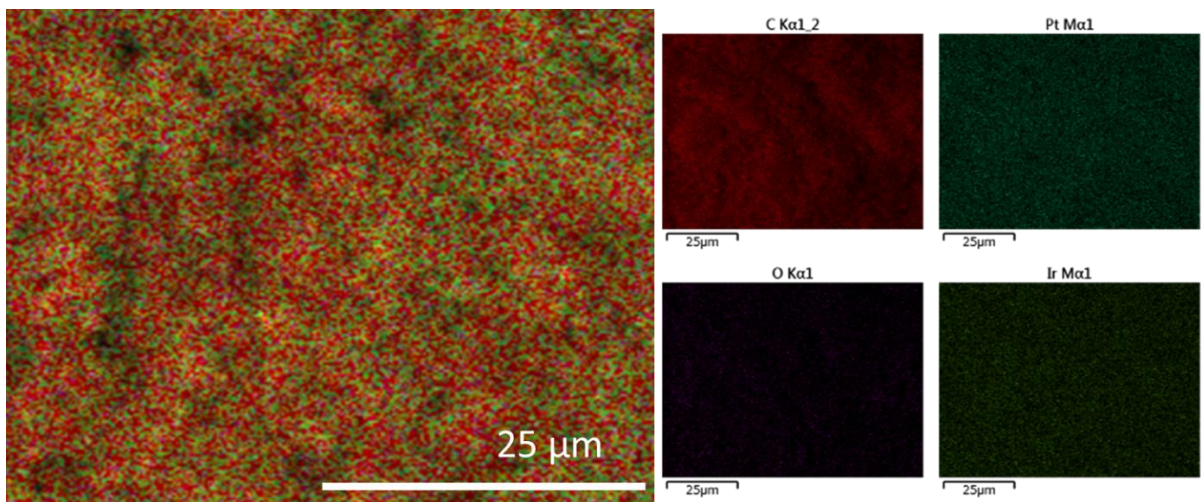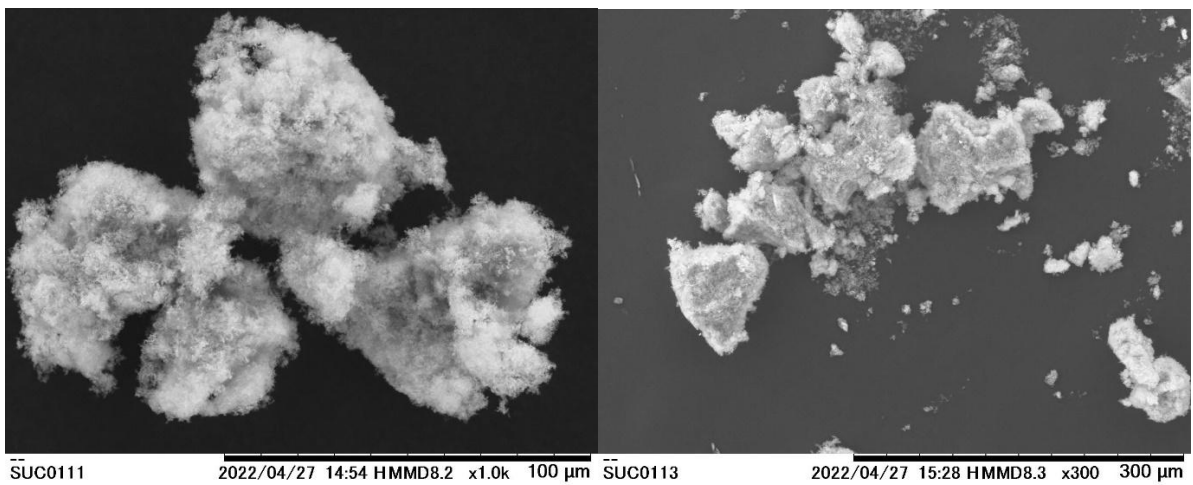
Fig. 3-5 SEM images of FAB- FAB(x)-Pt/Ir

2.4.2. TGA

Thermogravimetric analysis (TGA) is a technique used in materials science and chemistry to analyze the thermal stability and composition of a sample by measuring its weight changes as a function of temperature or time.

TGA is being used to calibrate the weight with metal in the FAB180-Pt/Ir 2:1 catalyst. The weight percent of Pt and Ir alloy in the catalyst is then compared with the data obtained from scanning electron microscopy with energy-dispersive X-ray spectroscopy (SEM-EDS), as shown in part 2.4.2.

The data in Figure 2-4 indicates that the weight percent of Pt and Ir alloy in the FAB180-Pt/Ir 2:1 catalyst is 18.95%, which is consistent with the results obtained from SEM-EDS.

Overall, TGA is a valuable tool for analyzing the thermal properties and composition of materials and can provide important insights into their characteristics and performance.
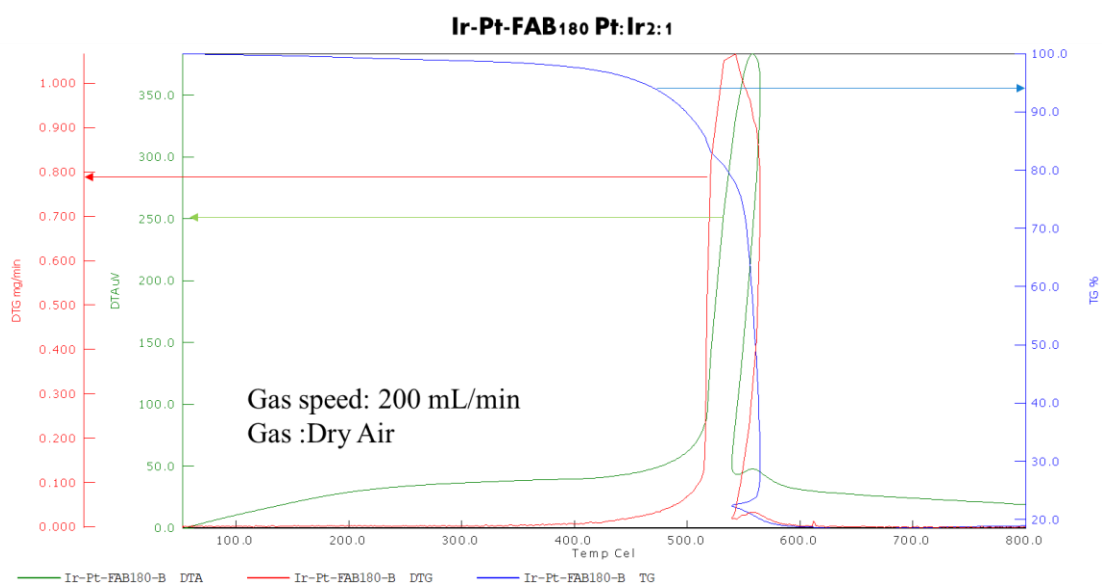
Fig 2-6 TGM for FAB180- Pt/Ir 2:1

2.4.3. TEM
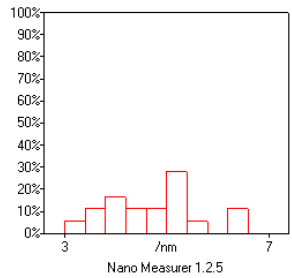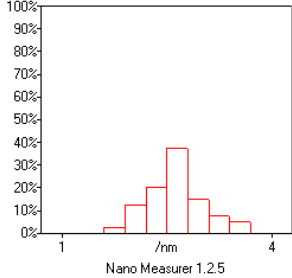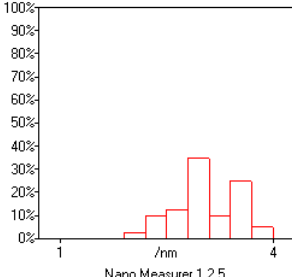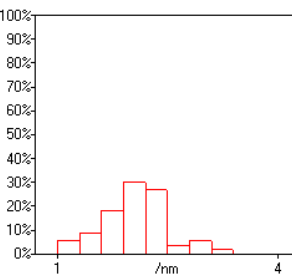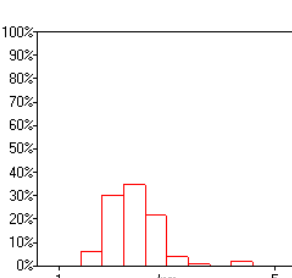
After SEM-EDS, TEM was measured to check nano-particles sizes and structure. TEM image is shown in Figure 2-7.

In addition to the nano-particle size, the distribution of nanoparticles within the carbon material also plays a crucial role in the oxygen content of the catalyst. It was found that in FAB-180-based catalysts with a large number of functional groups, the metal nanoparticles could be distributed more uniformly within the carbon material. This is due to the fact that the functional groups provide more surface area and sites for the metal particles to attach to, leading to a more even distribution.

The catalysts were analyzed through selected area electron diffraction (SAED) pattern analysis, revealing that the metal nanoparticles containing Pt and Ir were oriented with Pt(111) and Ir(111), respectively. This was further confirmed through high-resolution transmission electron microscopy (HRTEM) images, which showed distinct variations between the various catalysts. In comparison to FAB-60-based catalysts, the FAB-180-based catalysts exhibited a complete lattice structure, while it was challenging to obtain reliable crystal phase information for the FAB-60-based catalysts. Finally, the HAADF image of FAB180-Pt/Ir 1:1 was obtained, displaying the corresponding component mapping of Pt and Ir elements. As per the HAADF image, it was observed that Pt and Ir remained alloyed in the catalyst.

TEM images showed desired materials with uniform loading of metal nanoparticle on FAB was successfully prepared. Further, alloyed bimetallic structure and orientation of Pt/Ir was also clarified.

Table 2-7 Nano metal particles size in catalysts.

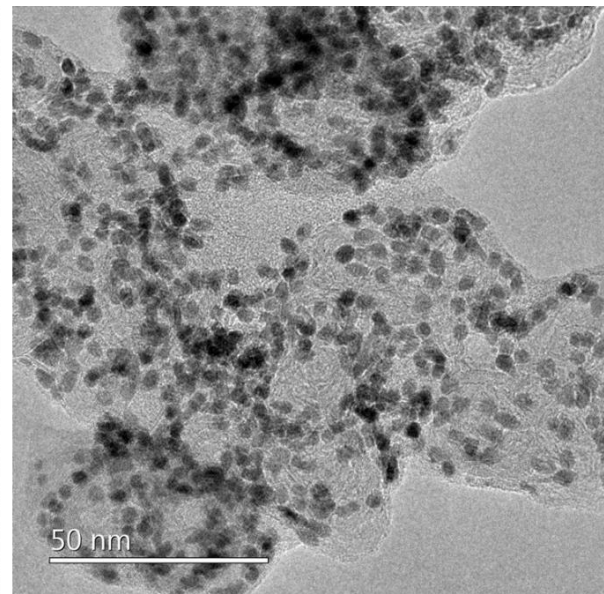| Sample	Mean/nm	Distr./nm	Freq.	Fig
FAB180-Pt10%	4.75	5-5.4	27.78%	
FAB60-Pt/Ir 1:1	2.61	2.5-2.8	37.50%	
FAB60-Pt/Ir 2:1	3.07	2.8-3.1	35.00%	
FAB180-Pt/Ir 1:1	2.06	1.9-2.2	30.36%	
FAB180-Pt/Ir 2:1	2.39	2.2-2.6	35.00%	
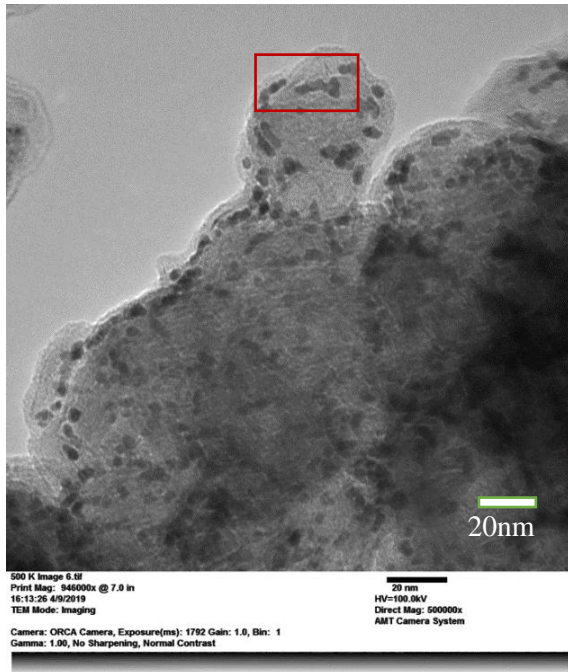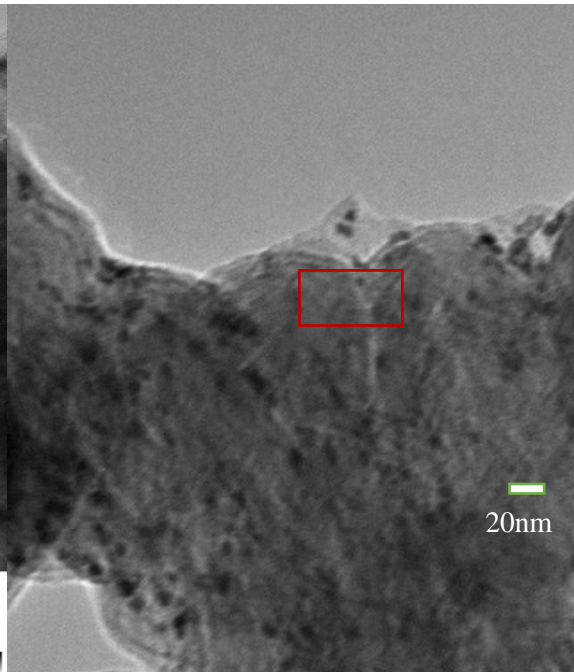
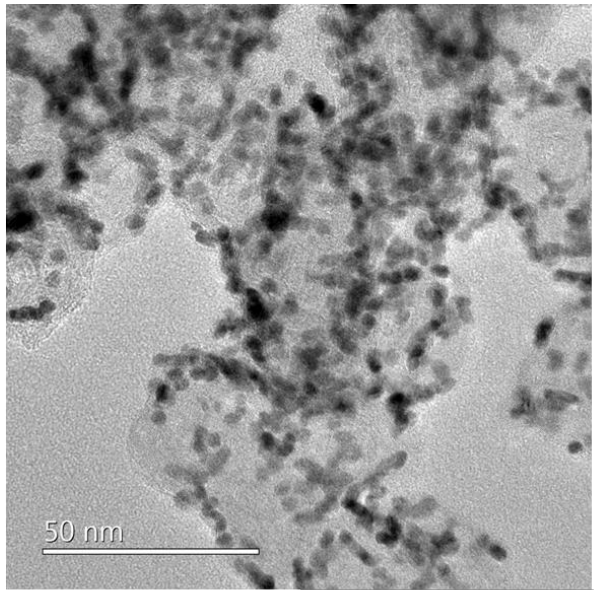FAB60-Pt/Ir 2:1   FAB180-Pt/Ir 1:1
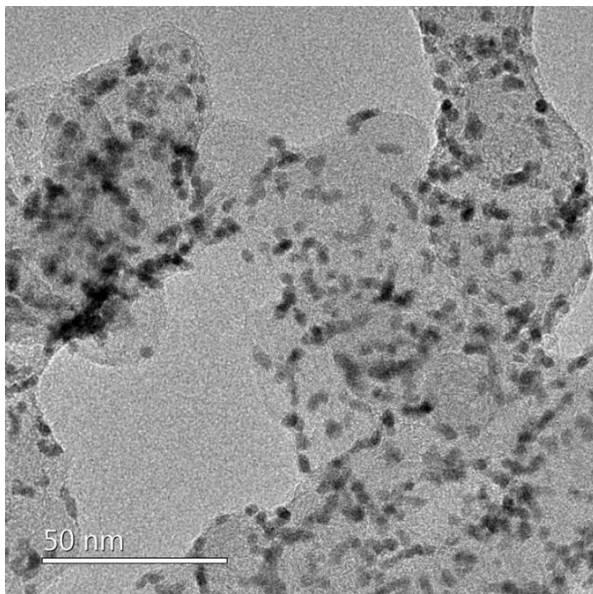
FAB-180 Pt:Ir 1:1   FAB-180 Pt:Ir 2:1

FAB-60 Pt:Ir 1:1

FAB-60 Pt:Ir 2:1
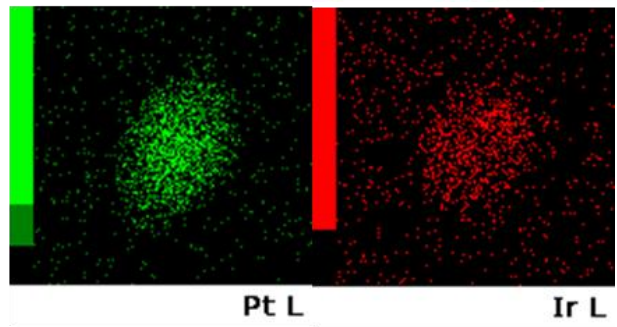
50 nm

5 nm

10 1/nm
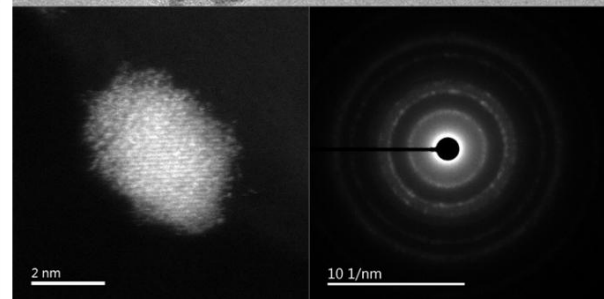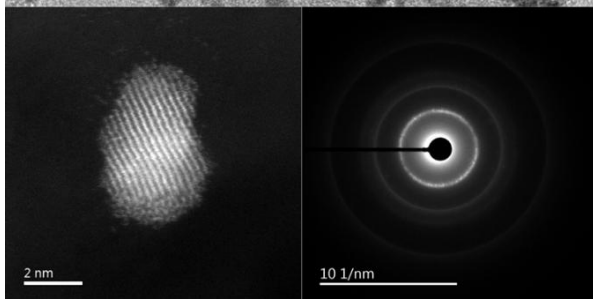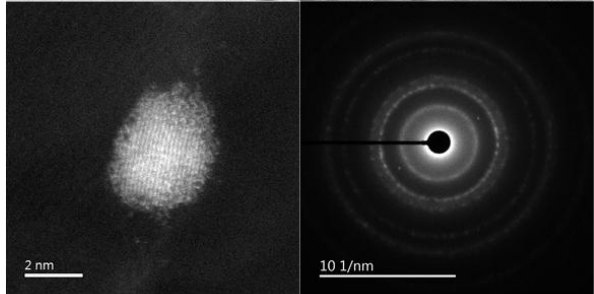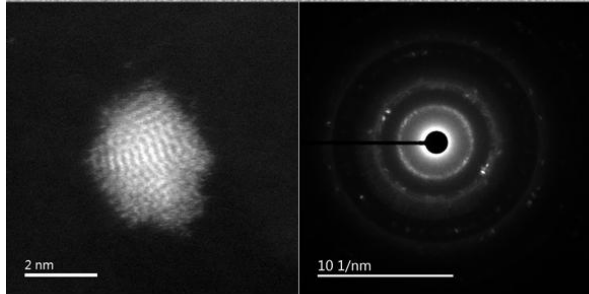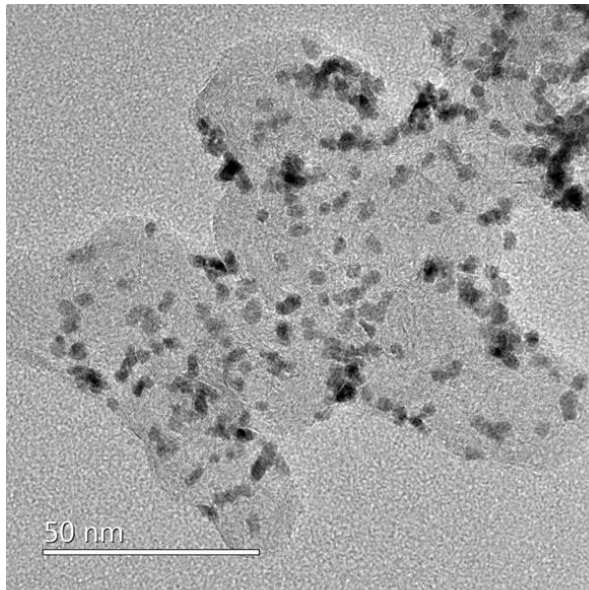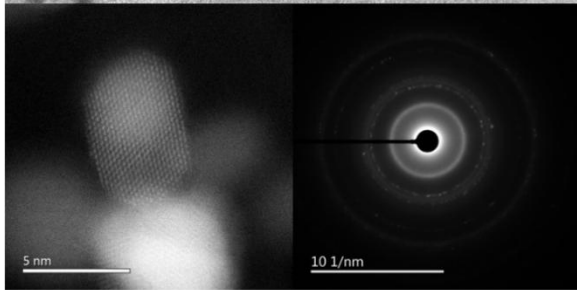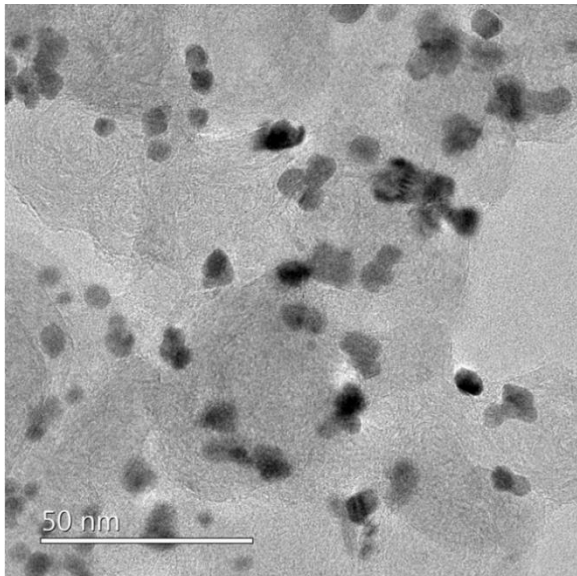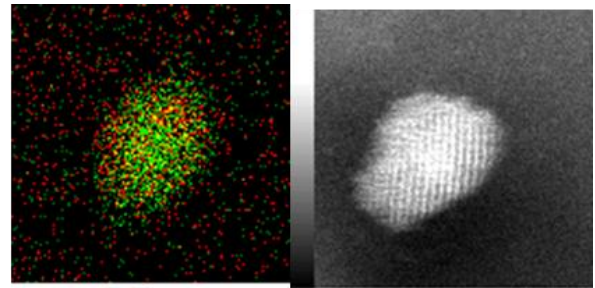
FAB180-Pt10%

2.5 nm

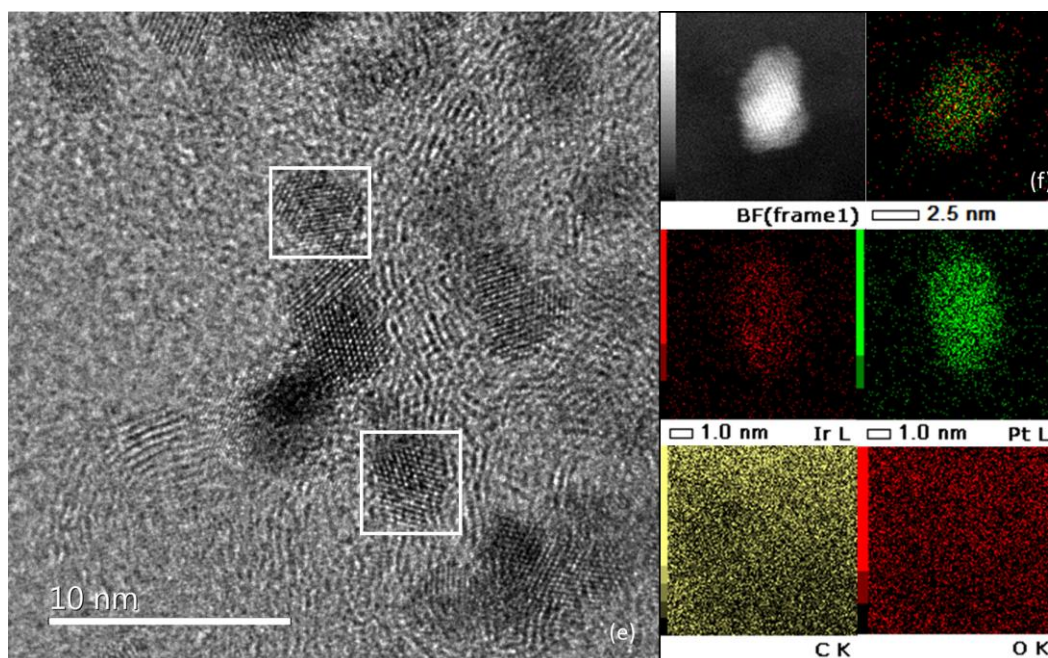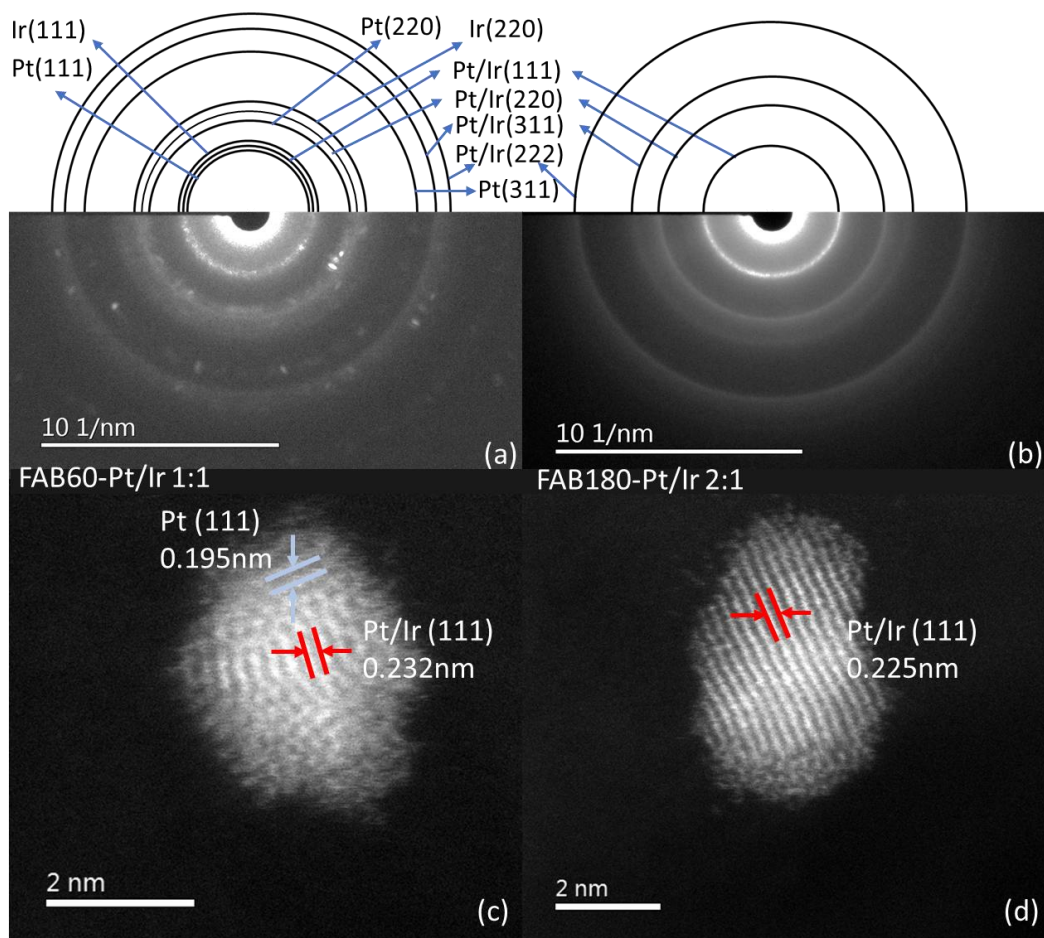BF

Pt L

Ir L

FAB180-Pt/Ir 1:1

Fig 2-7 TEM image with catalyst: SAED patterns, (a) FAB60-Pt/Ir 1:1, (b) FAB180-Pt/Ir 1:1; HAADF-STEM image, (c) FAB60-Pt/Ir 1:1, (d) FAB180-Pt/Ir 1:1; HR-TEM image (e) FAB180-Pt/Ir 1:1 and EDS elemental mapping images (f) FAB180-Pt/Ir 1:1.

2.4.4. XPS

The analysis of X-ray photoelectron spectroscopy (XPS) data revealed notable differences between the AB carbon before and after the oxidation. Initially, the main O 1s peak was observed at 533 eV with a weak peak at 528.7 eV. However, after 60 minutes of reaction, the main peak shifted to 533.3 eV and the weak peak shifted to 531.7 eV with the same peak area. After 180 minutes of oxidation, further peak shift did not occur, but the peak area of C=O was doubled compared to that of C-O. The C-C peak in C 1s spectrum of in AB carbon was initially observed at 284.5 eV. However, after the oxidation, the peak area shifted slightly to lower energy region, FAB-60 at 284.2 eV, FAB-180 at 284.0 eV. Similarly, in the spectral O 1s spectrum, the C=O peak shifted to lower energy region and was observed at 288.5 eV in FAB-180 compared to 289.0 eV in FAB-60. The peak area also changed, and the C-O and C=O peaks became larger in FABs than in AB. These changes suggest that more functional groups were added in the carbon structure after the oxidation.
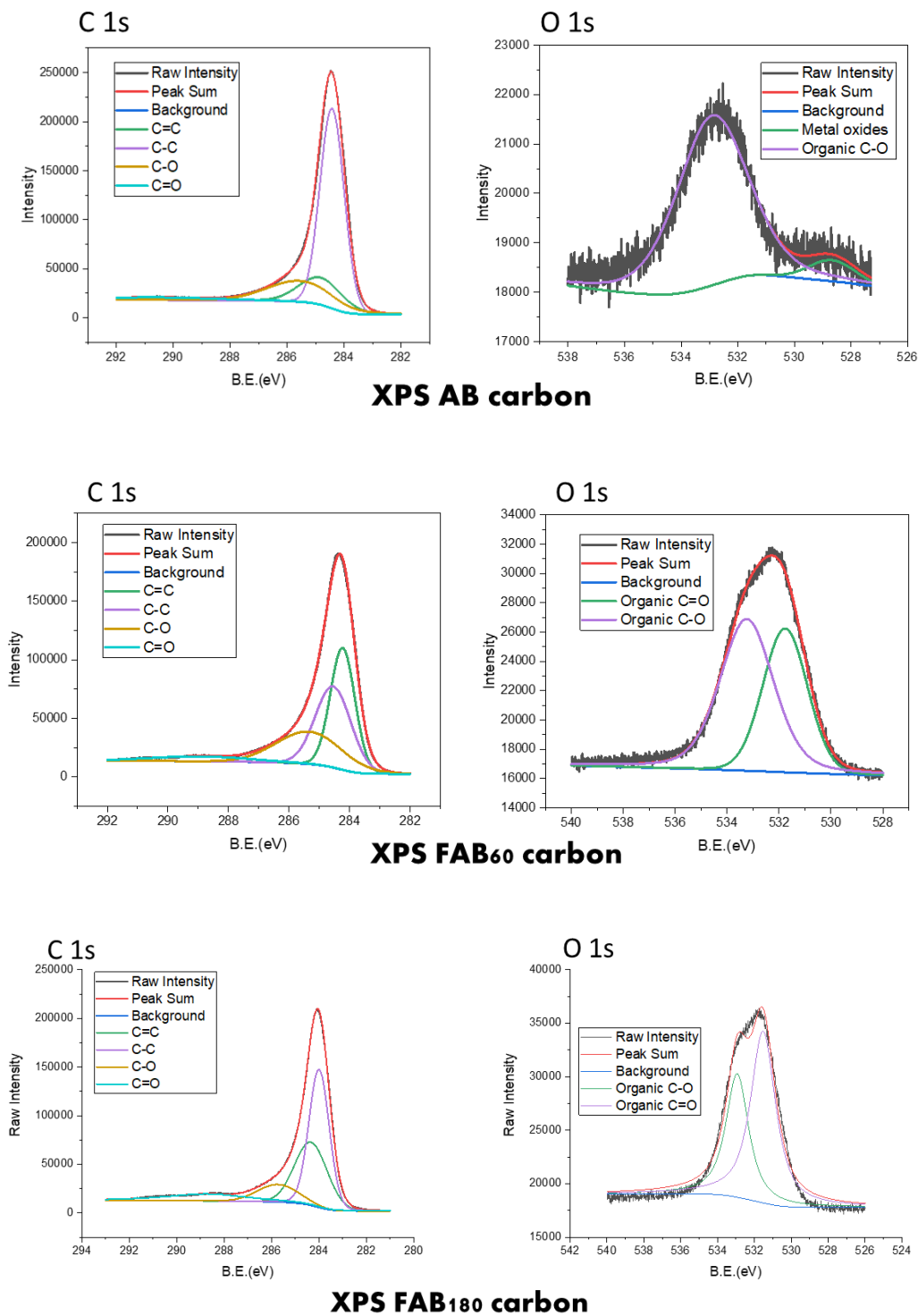
Fig 2-8 XPS with carbon standers

When analyzing the C 1s spectrum of the catalysts, it was observed that the C=O peak disappeared after introducing the metal. The O 1s peak showed a shift to the left, with raw intensities of 531.9 eV and 532.1 eV for the FAB-60 and FAB-180 based catalysts, respectively.

Interestingly, both of these carbon-based catalysts showed the same peak shift as the metal weight changed. The only exception was the Pt/Ir 2:1 catalyst, which had a very weak signal.

Further analysis revealed that the Pt-O/Organic C-O peak in the FAB60-Pt/Ir 1:1 and FAB180-Pt/Ir 1:1 catalysts were located at 531.0 eV, while in the FAB60-Pt/Ir 2:1 and FAB180-Pt/Ir 2:1 catalysts, they were located at 531.5 eV. These results suggest that the presence of Pt and Ir in the catalysts plays a crucial role in the changes observed in the C and O spectra. It is clear that the type and weight of the metals used in the catalysts affect the chemical environment of the carbon structure, which may have implications for the catalytic activity and selectivity of these materials in electrocatalysis.
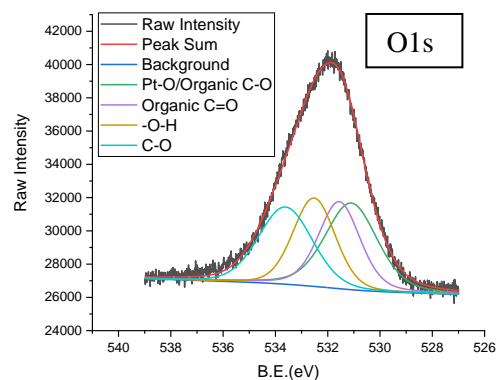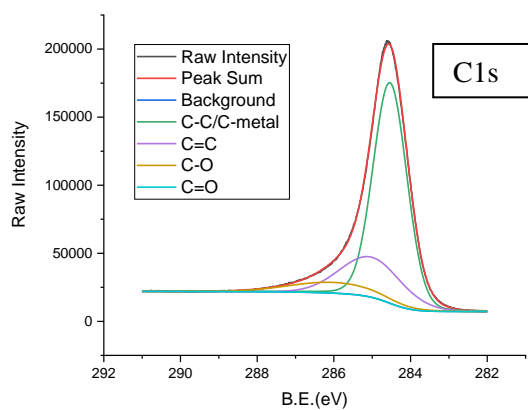
FAB-60 Pt:Ir 1:1
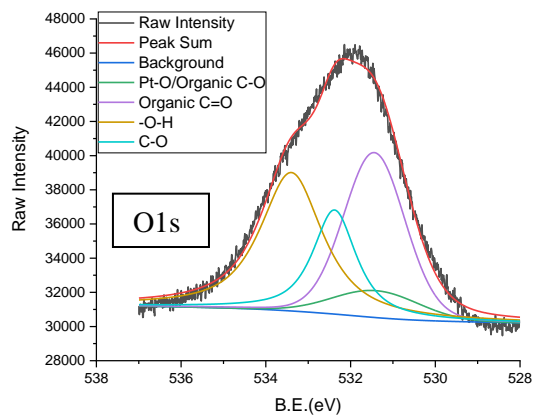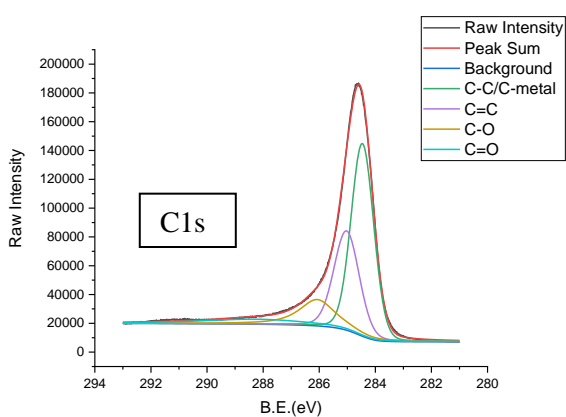
FAB-60 Pt:Ir 2:1
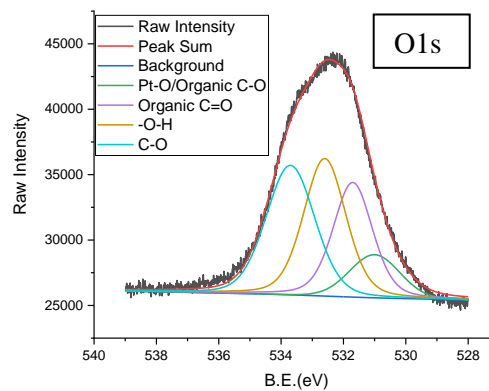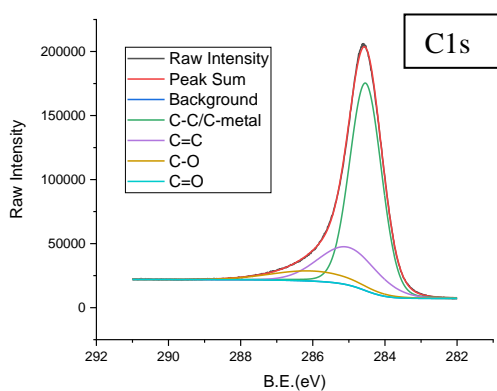
FAB-180 Pt:Ir 1:1

FAB-180 Pt:Ir 2:1

Fig 2-9 XPS with catalyst on C1s and O1s

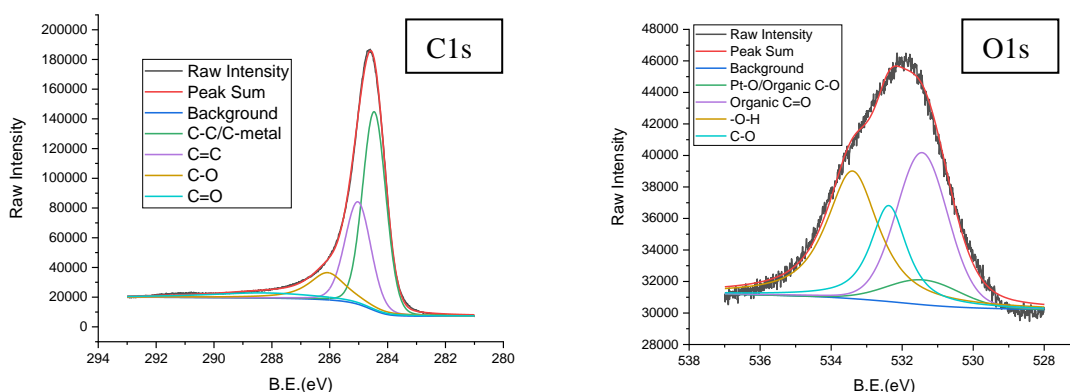Further analysis of the data revealed some interesting trends. The Pt peaks of Pt 7/2 in the FAB60-Pt/Ir 1:1 and FAB60-Pt/Ir 2:1 catalysts were located at 71.20 eV and 71.19 eV, respectively, while in the FAB180-Pt/Ir 1:1 and FAB180-Pt/Ir 2:1 catalysts, they were located at 71.13 eV and 71.03 eV. Similarly, the Pt 2+ peaks in the FAB60-Pt/Ir 1:1 and FAB60-Pt/Ir 2:1 catalysts were located at 72.35 eV and 72.34 eV, respectively, while in the FAB180-Pt/Ir 1:1 and FAB180-Pt/Ir 2:1 catalysts, they were located at 72.28 eV and 72.18 eV. It was observed that all Pt peaks in the FAB-60 based catalysts shifted to higher binding energy region when compared to those in the FAB-180 based catalysts.

Further analysis also revealed that the Ir peaks of Ir 7/2 in the FAB180-Pt/Ir 1:1 and FAB60-Pt/Ir 1:1 catalysts were located at 60.41 eV and 60.60 eV, respectively, while in the FAB180-Pt/Ir 2:1 and FAB60-Pt/Ir 2:1 catalysts, they were located at 60.65 eV and 60.63 eV. The peaks of Ir 4+ in the FAB180-Pt/Ir 1:1 and FAB60-Pt/Ir 1:1 catalysts were located at 61.51 eV and 61.70 eV, respectively, while in the FAB180-Pt/Ir 2:1 and FAB60-Pt/Ir 1:1 catalysts, they were located at 61.75 eV and 58.73 eV. It was observed that the Ir peaks in the FAB-180 based catalysts shifted to lower banding energy region compared to those in the FAB-60 based catalysts under Pt:Ir ratio of 1:1 loading. However, when the Pt:Ir loading was changed to 2:1, the data was almost the same.

The peak area between Ir 7/2 and Ir 4+ (7/2) revealed that when Pt:Ir was loaded in a 1:1 ratio, the FAB60-Pt/Ir 1:1 catalyst had 40.9% of Ir 7/2 and 7.3% of Ir 4+, while FAB180-Pt/Ir 1:1 had 16.5% of Ir 7/2 and 37.3% of Ir 4+. This suggests that in FAB180-Pt/Ir 1:1, the Ir was

predominantly loaded as IrO_2, while in FAB60-Pt/Ir 1:1, the Ir was predominantly loaded as Ir metal.

Fig 2-10 Peaks of Pt 4f for FAB60 Pt:Ir 1:1

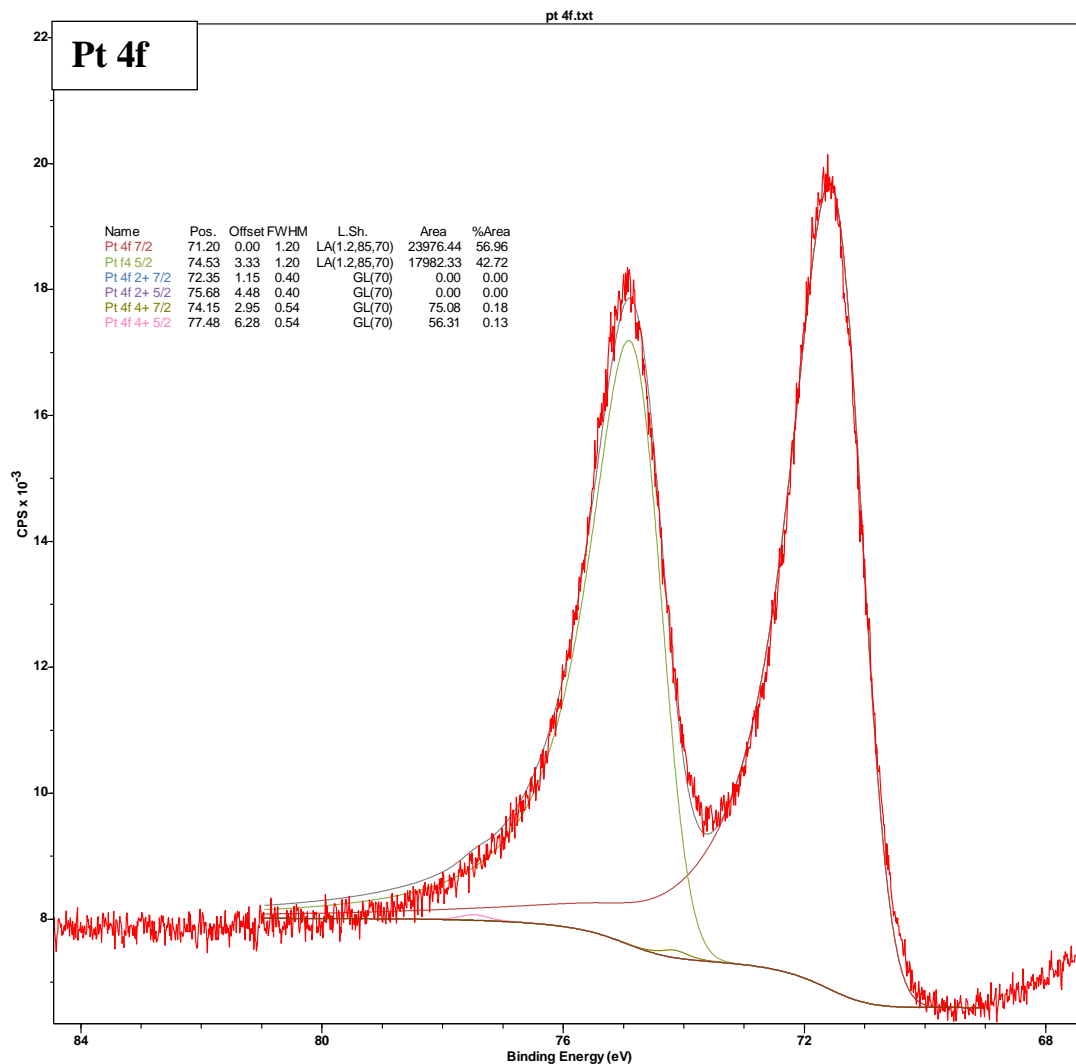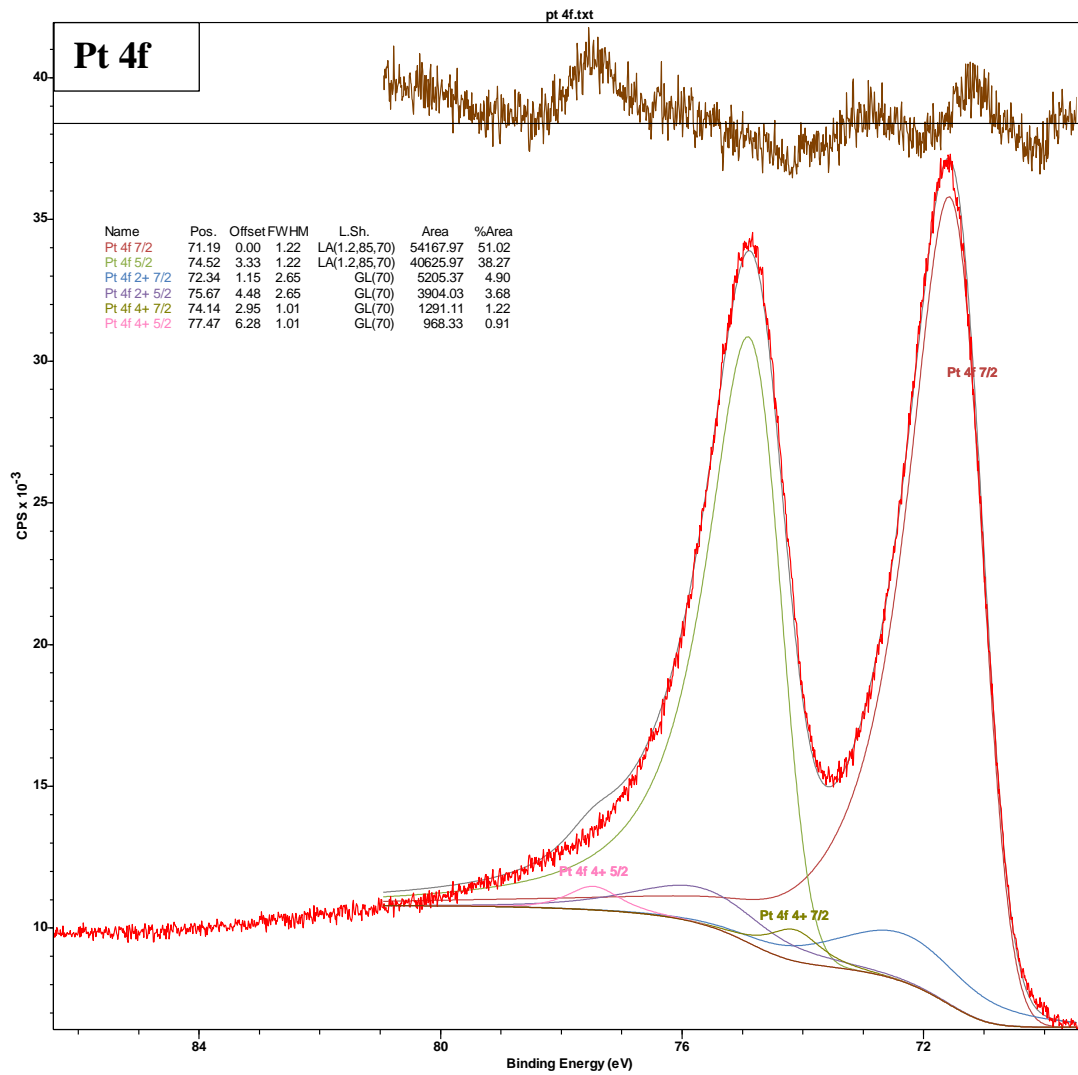| Name	Pos.	Offset	FWHM	L.Sh.	Area	%Area
Pt 4f 7/2	71.19	0.00	1.22	LA(1.2,85,70)	54167.97	51.02
Pt 4f 5/2	74.52	3.33	1.22	LA(1.2,85,70)	40625.97	38.27
Pt 4f 2+ 7/2	72.34	1.15	2.65	GL(70)	5205.37	4.90
Pt 4f 2+ 5/2	75.67	4.48	2.65	GL(70)	3904.03	3.68
Pt 4f 4+ 7/2	74.14	2.95	1.01	GL(70)	1291.11	1.22
Pt 4f 4+ 5/2	77.47	6.28	1.01	GL(70)	968.33	0.91

Fig 2-11 Peaks of Pt 4f for FAB60 Pt:Ir 2:1

66

Fig 2-12 Peaks of Pt 4f for FAB180 Pt:Ir 1:1

Pt 4f

Name	Pos.	Offset	FWHM	L.Sh.	Area	%Area
Pt 4f 7/2	71.03	0.00	1.23	LA(1.2,85,70)	39902.78	55.89
Pt f4 5/2	74.36	3.33	1.23	LA(1.2,85,70)	29927.08	41.92
Pt 4f 2+ 7/2	72.18	1.15	9.27	GL(70)	0.00	0.00
Pt 4f 2+ 5/2	75.51	4.48	9.27	GL(70)	0.00	0.00
Pt 4f 4+ 7/2	73.98	2.95	1.79	GL(70)	894.91	1.25
Pt 4f 4+ 5/2	77.31	6.28	1.79	GL(70)	671.18	0.94

pt 4f.txt

68
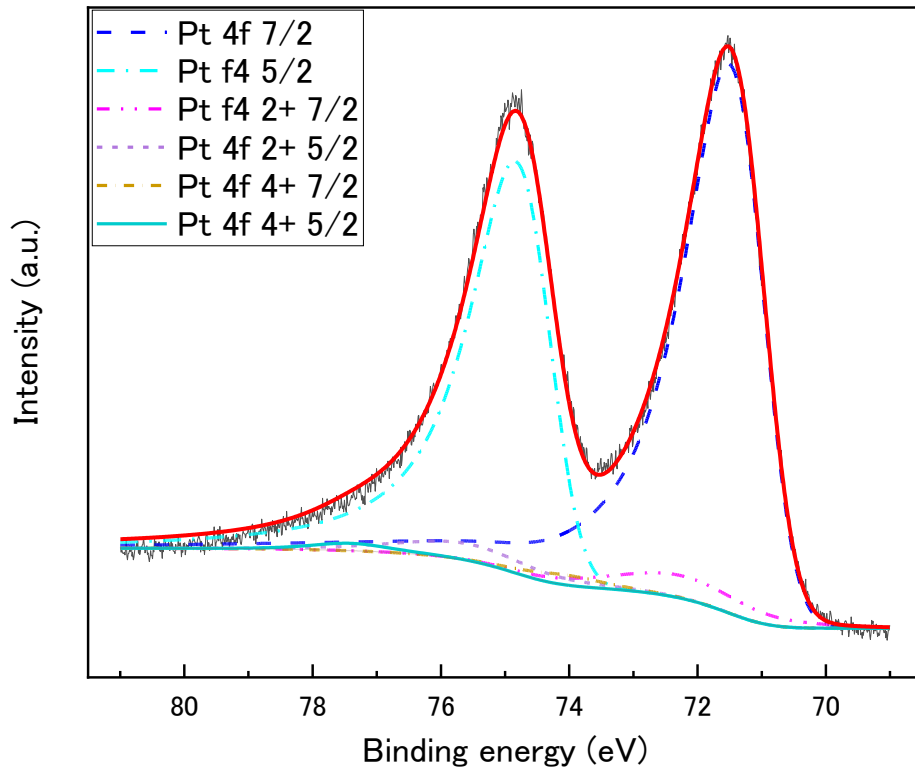
Fig 2-13 Peaks of Pt 4f for FAB180 Pt:Ir 1:1
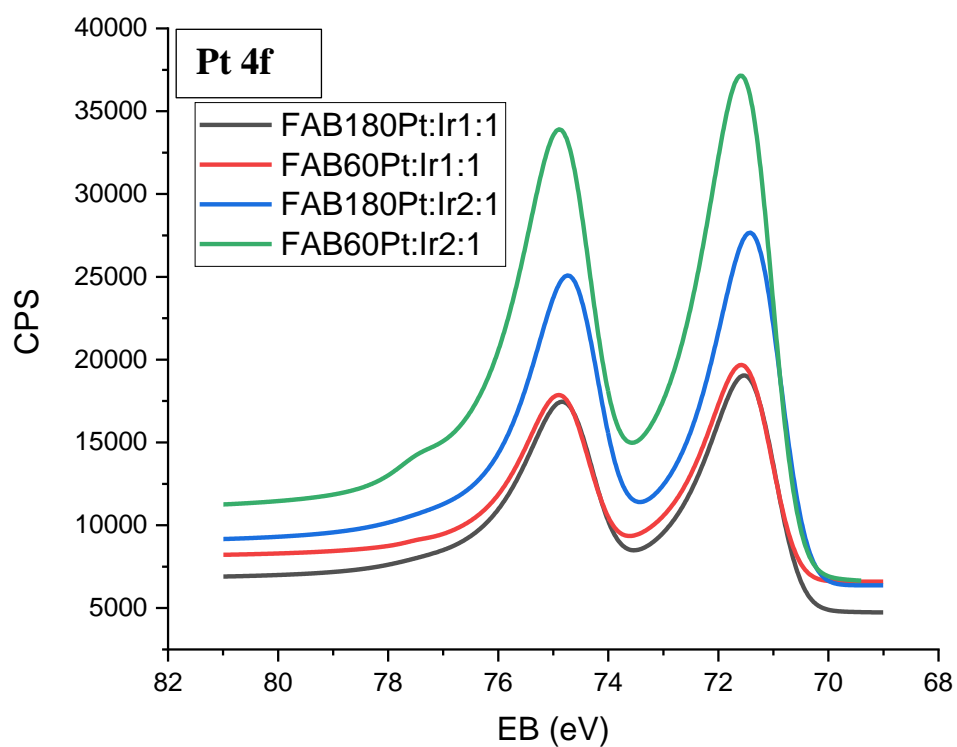
Fig 2-14 XPS with catalyst on Pt 4f

Table 2-8 Pt 4f peaks shifts (eV)

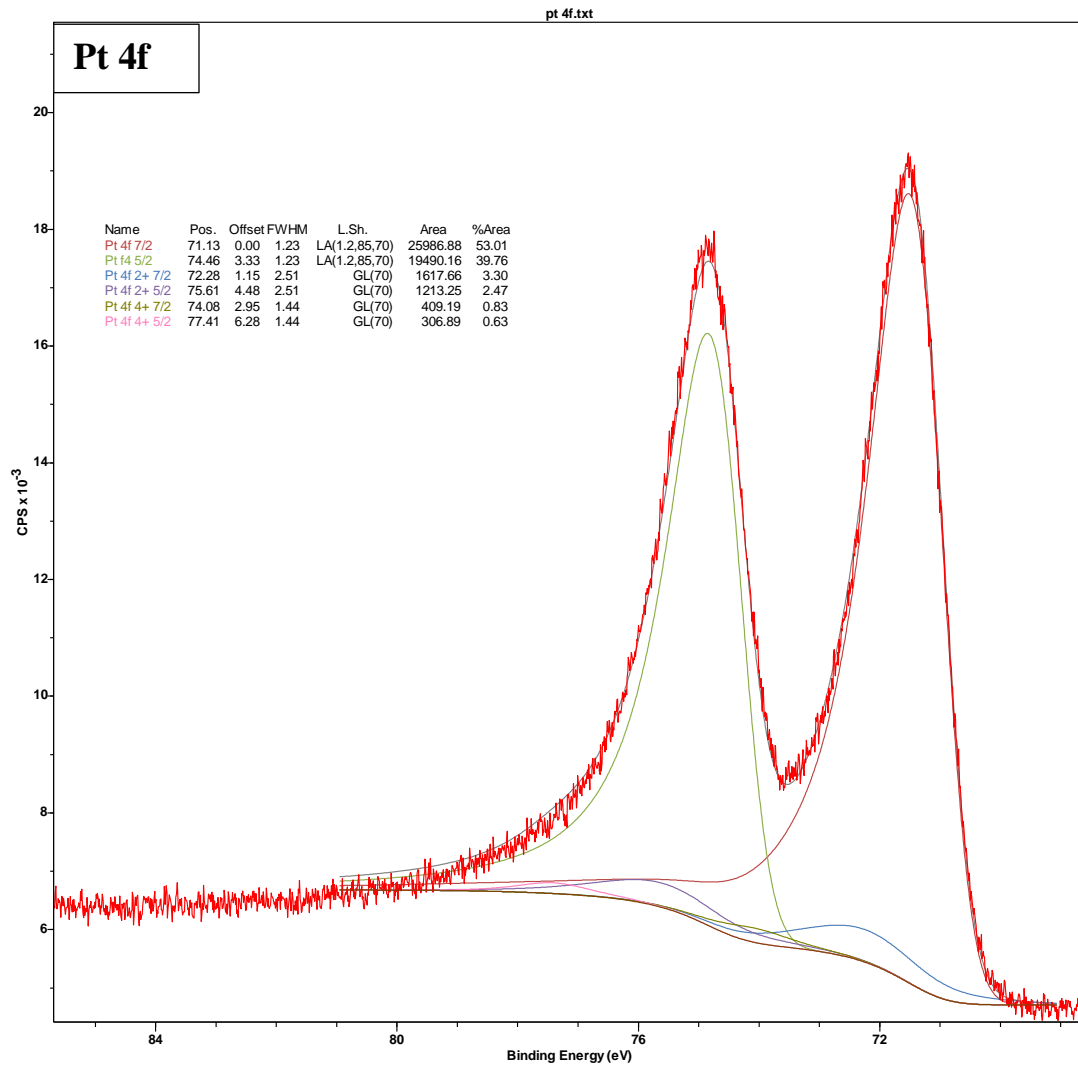|	FAB180 Pt:Ir 1:1	FAB60 Pt:Ir 1:1	FAB180 Pt:Ir 2:1	FAB60 Pt:Ir 2:1
Pt 7/2	71.13	71.20	71.03	71.19
Pt 2+	72.28	72.35	72.18	72.34
Pt 4+	74.08	74.15	73.98	74.14
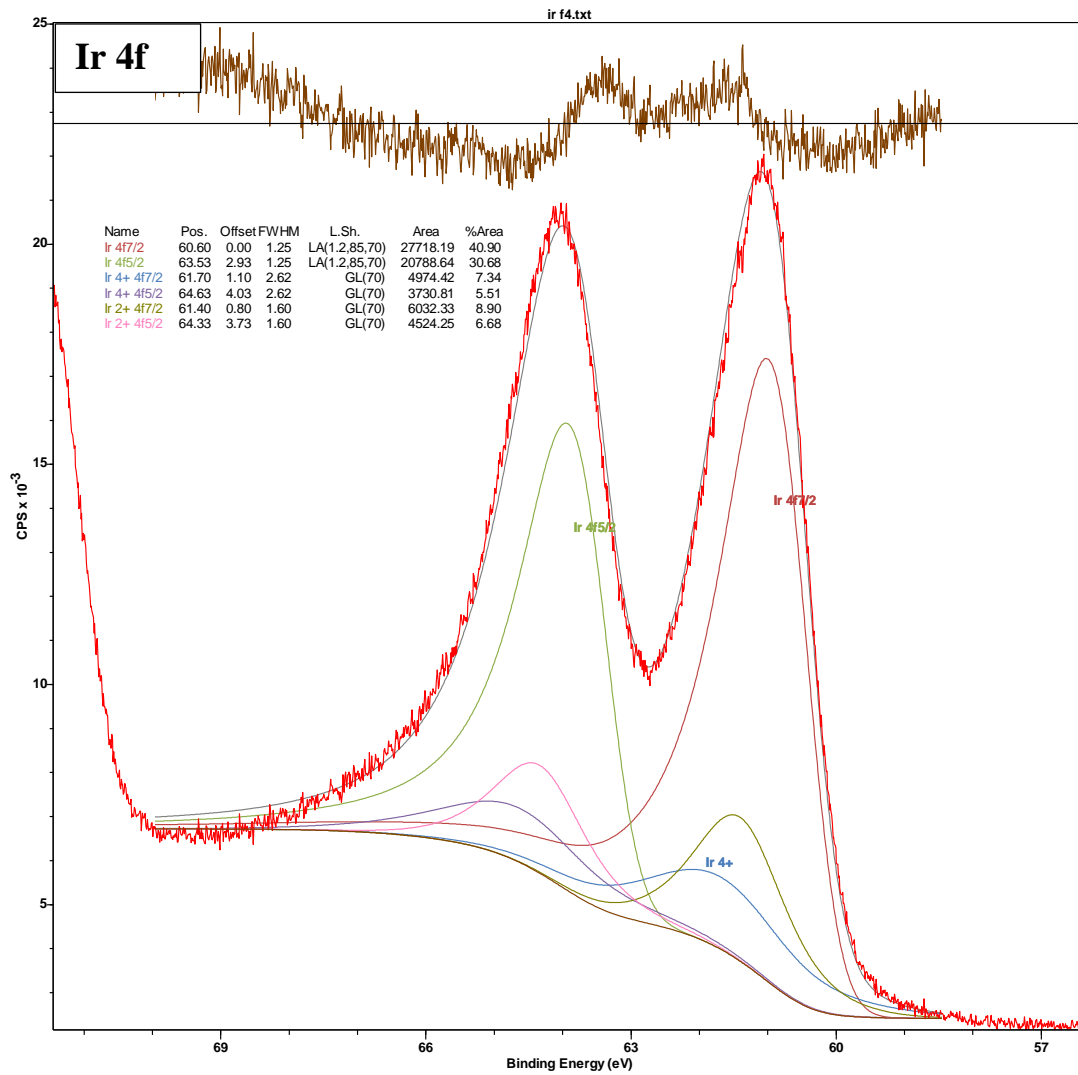
Fig 2-15 Peaks of Ir 4f for FAB60 Pt:Ir 1:1
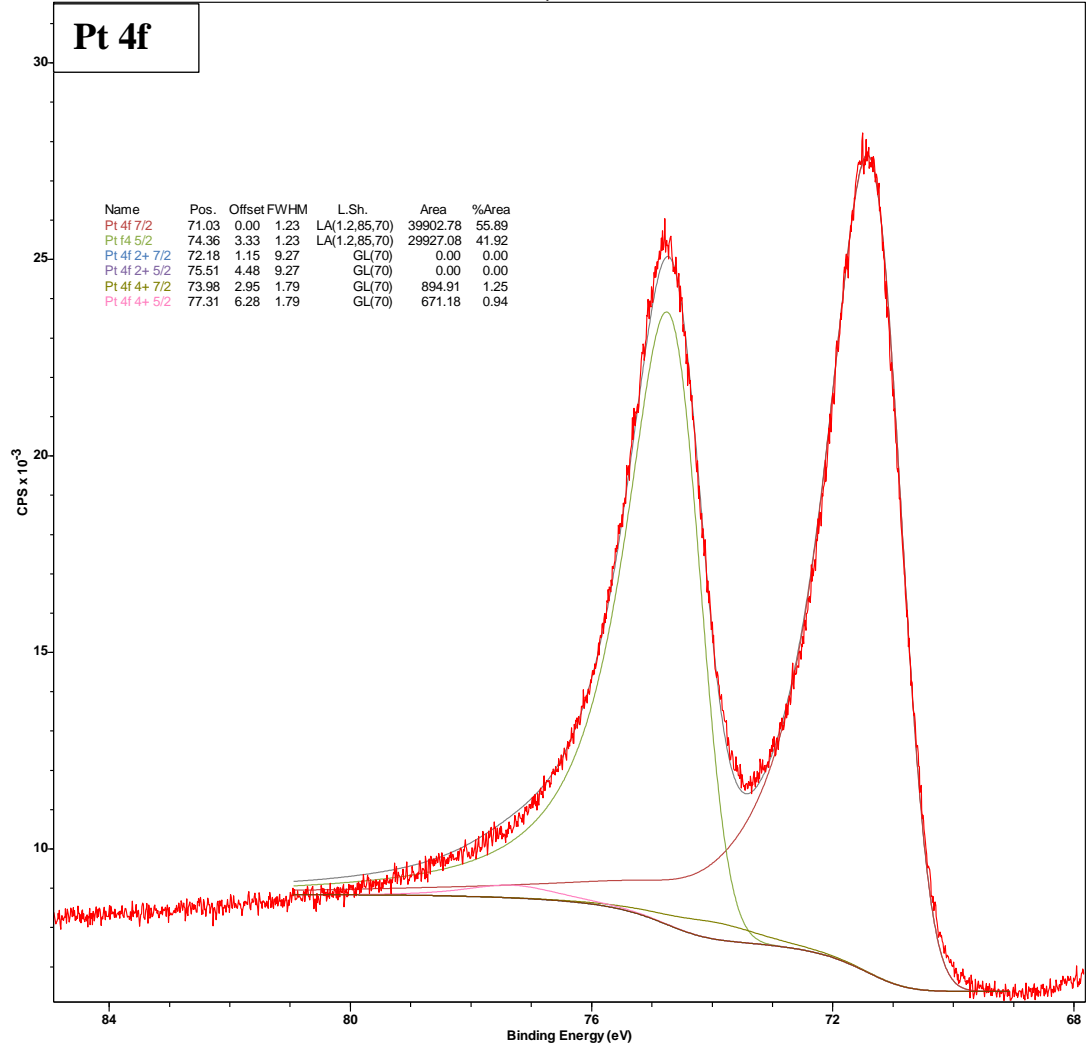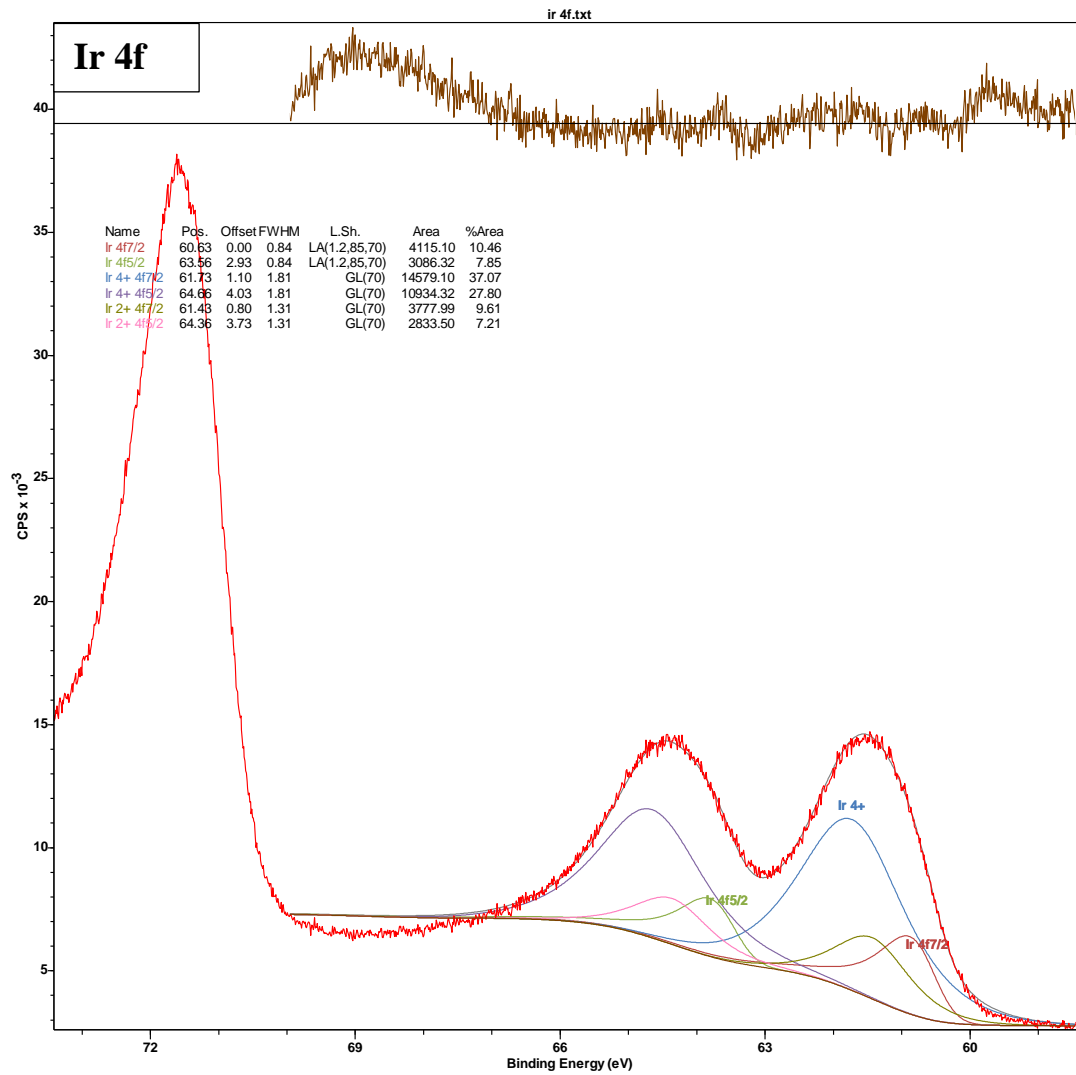
Fig 2-16 Peaks of Ir 4f for FAB60 Pt:Ir 2:1

Ir 4f

Name	Pos.	Offset	FWHM	L.Sh.	Area	%Area
Ir 4f7/2	60.41	0.00	0.89	LA(1.2,85,70)	5387.56	16.49
Ir 4f5/2	63.34	2.93	0.89	LA(1.2,85,70)	4040.67	12.37
Ir 4+ 4f7/2	61.51	1.10	1.89	GL(70)	12174.44	37.27
Ir 4+ 4f5/2	64.44	4.03	1.89	GL(70)	9130.83	27.95
Ir 2+ 4f7/2	61.21	0.80	0.77	GL(70)	1102.47	3.38
Ir 2+ 4f5/2	64.14	3.73	0.77	GL(70)	826.85	2.53
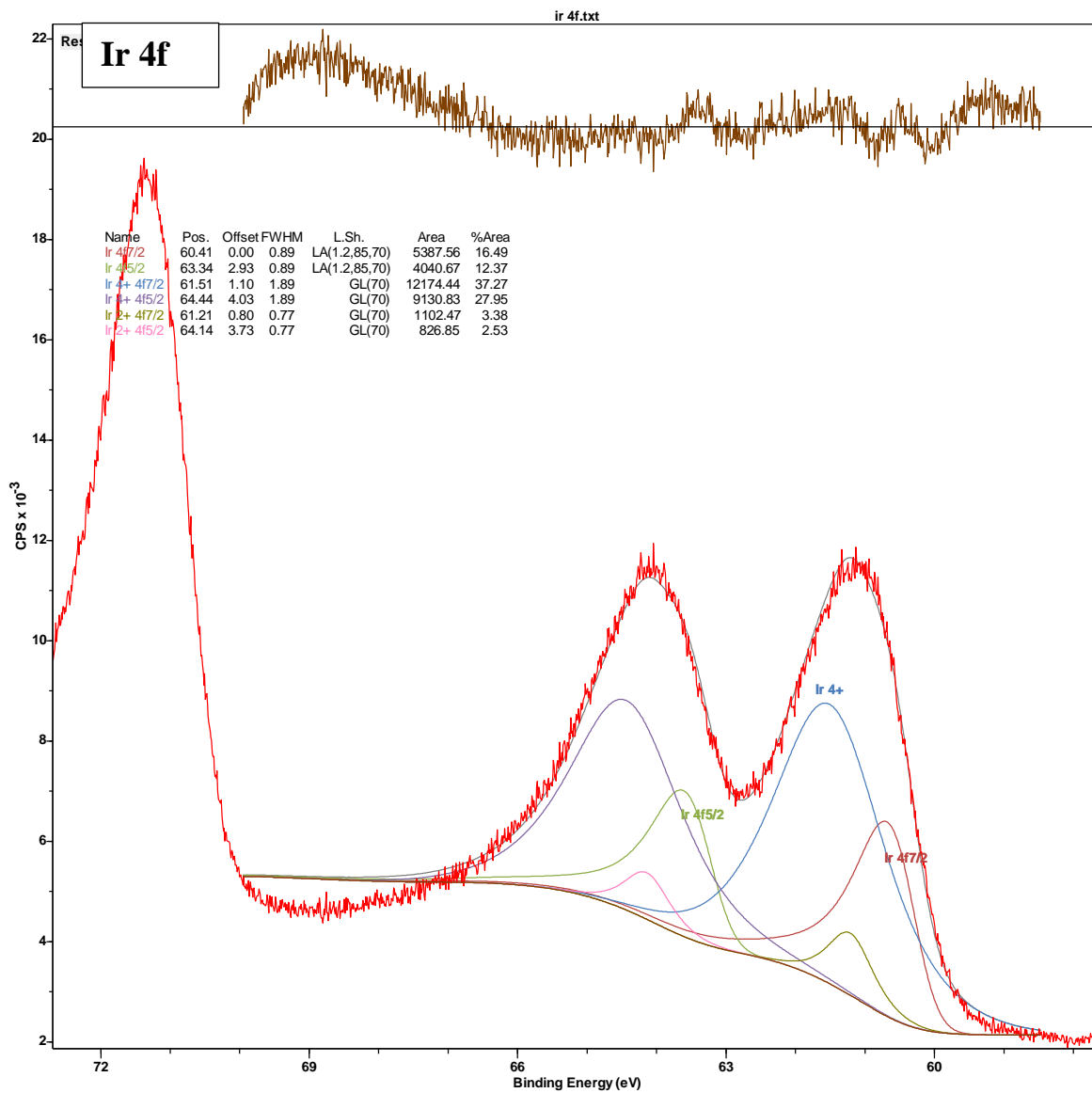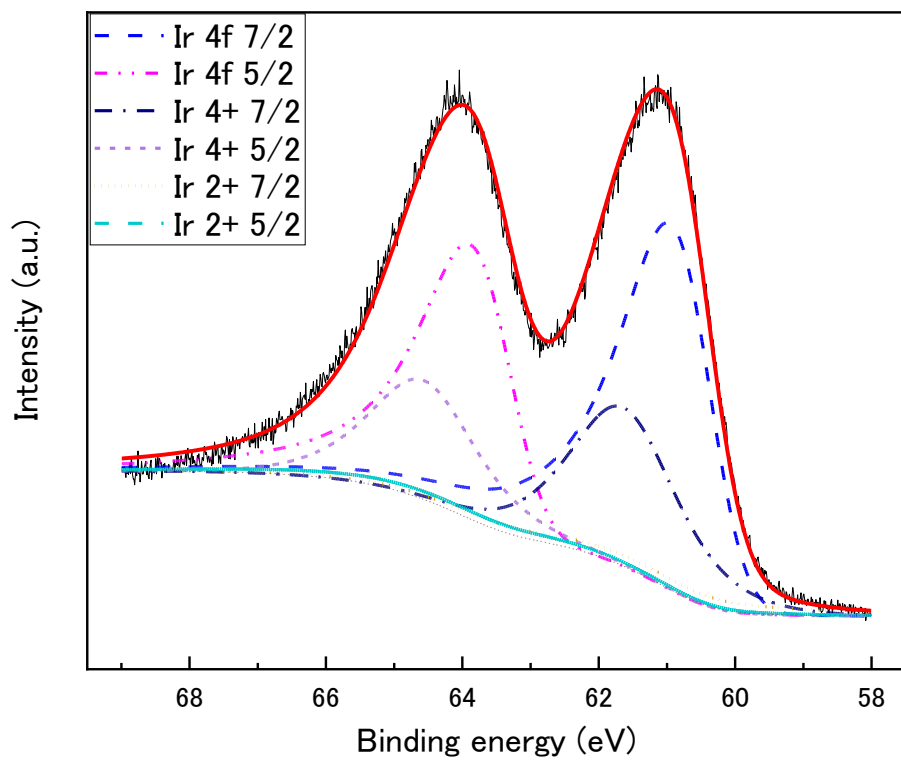
Fig 2-17 Peaks of Ir 4f for FAB180 Pt:Ir 1:1

Name	Pos.	Offset	FWHM	L.Sh.	Area	%Area
Ir 4f7/2	60.65	0.00	1.05	LA(1.2,85,70)	11063.25	21.82
Ir 4f5/2	63.58	2.93	1.05	LA(1.2,85,70)	8297.44	16.36
Ir 4+ 4f7/2	61.75	1.10	1.97	GL(70)	13790.38	27.20
Ir 4+ 4f5/2	64.68	4.03	1.97	GL(70)	10342.78	20.40
Ir 2+ 4f7/2	61.45	0.80	1.16	GL(70)	4121.02	8.13
Ir 2+ 4f5/2	64.38	3.73	1.16	GL(70)	3090.76	6.10
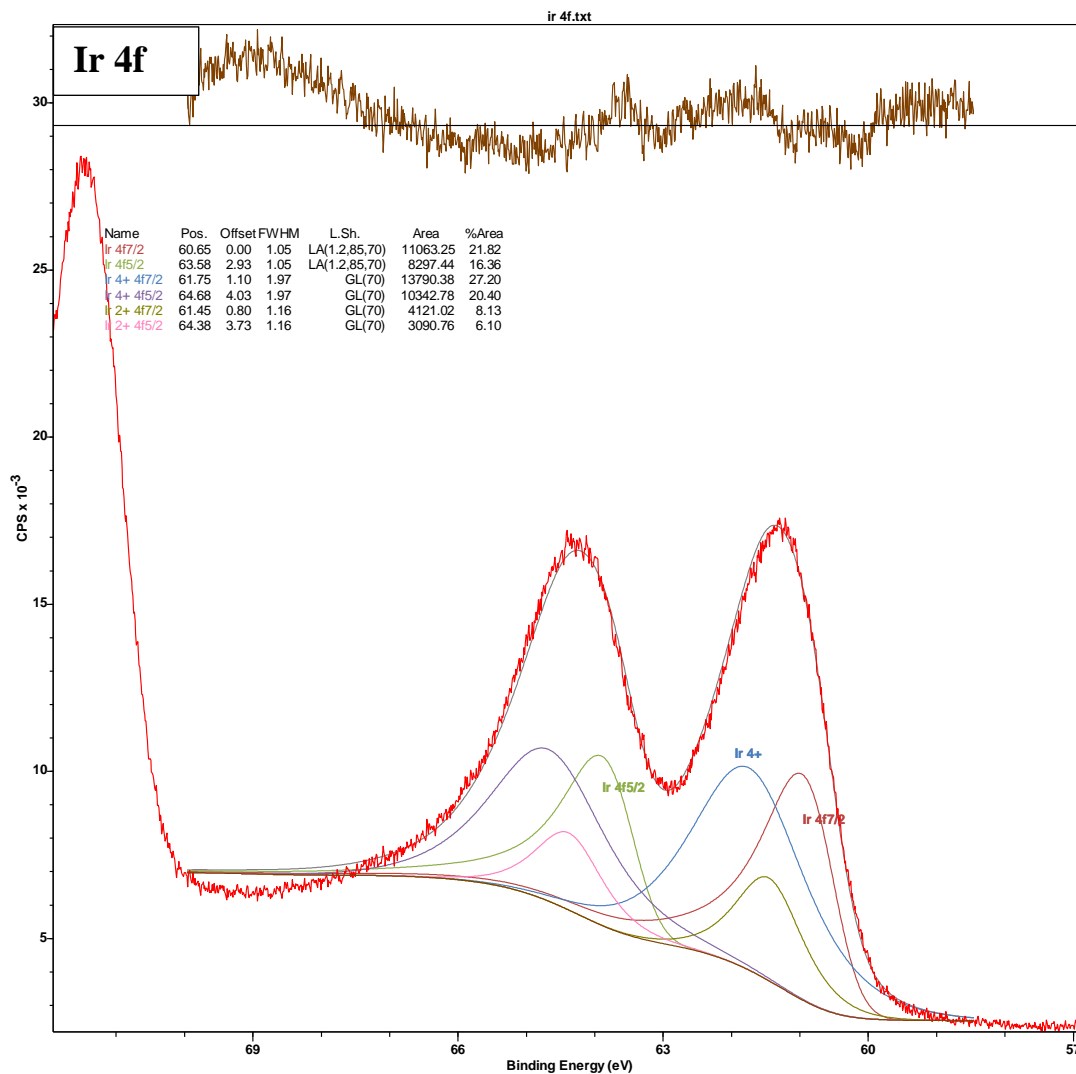
Fig 2-18 Peaks of Ir 4f for FAB180 Pt:Ir 2:1

Table 2-9 Ir 4f peaks shifts (eV)

	FAB180 Pt:Ir 1:1	FAB60 Pt:Ir 1:1	FAB180 Pt:Ir 2:1	FAB60 Pt:Ir 2:1
Ir 7/2	60.41	60.60	60.65	60.63
Ir 4+	61.51	61.70	61.75	61.73
Ir 2+	61.21	61.40	61.45	61.48

2.5. Conclusion

In this study, two carbon based materials for bi-functionalized catalysts were obtained by varying the reaction time for oxidation of AB carbon: FAB-60 and FAB-180, which have different oxygen contents and physical and chemical properties were prepared. Four types of electrochemical catalysts were designed, synthesized, and tested by controlling the weight percent of the metals loaded on carbon materials. The microstructure of the FAB(x)-Pt/Ir family catalysts was found to be influenced by the functional groups present in the carbon and the weight percent of the metal. If the carbon has sufficient functional groups for metal bonding, the size of the nanoparticles can be controlled to be uniform and in the nanoscale range.

References

[1] Aravindan, V., Gnanaraj, J., Lee, Y. S., & Madhavi, S. (2013). *Journal of Materials Chemistry A*, *1*(11), 3518-3539.

[2] NASA GISS Surface Temperature Analysis (v4), <https://data.giss.nasa.gov/gistemp/graphs_v4/>, (2019).

[3] Christensen, L., Fischer, N., Kroffke, S., Lemburg, J., & Ahlers, R. (2011). Cost-effective autonomous robots for ballast water tank inspection. Journal of ship production and design, 27(3), 127.

[4] Kraytsberg, A., & Ein-Eli, Y. (2011). Review on Li–air batteries—Opportunities, limitations and perspective. *Journal of Power sources*, *196*(3), 886-893.

[5] Peng, Z., Freunberger, S. A., Hardwick, L. J., Chen, Y., Giordani, V., Bardé, F., ... & Bruce, P. G. (2011). Oxygen reactions in a non-aqueous Li+ electrolyte. *Angewandte Chemie International Edition*, *50*(28), 6351-6355

3. Chapter 3

A series of FAB(x)-Pt/Ir catalysts for Li-air battery

3.1. Abstract

Despite extensive research on secondary batteries for improving electrochemical performance, the key factor in metal-air batteries is the control of oxygen reduction reaction (ORR) and oxygen evolution reaction (OER) activity during charge and discharge cycles. The challenge is to develop batteries with long lifespan and minimal attenuation. In this study, the FAB(x)-Pt/Ir catalyst family will be tested using linear sweep voltammetry (LSV) and cyclic voltammetry (CV) before full charge-discharge cycles are performed in a Li-air battery, in order to evaluate the ORR and OER performance.

3.2. Introduction

Based on Figure 3-1, it can be observed that different materials have different energy densities. Hydrogen and natural gas are capable of storing high energy per unit mass, while metals are capable of storing high energy per unit volume. It is worth noting that the energy density of a material is an important factor in determining its suitability for use in energy storage applications. For instance, Li-ion batteries have a lower energy density compared to Li-air batteries, which makes Li-air batteries more attractive for high-energy applications. [1] Similarly, the high energy density of metals makes them promising candidates for use in metal-air batteries. Advances in material technology have made it possible to explore the potential of metal-air batteries as a viable option for high-energy density applications. [2]

The development of new materials has made metal-air batteries an exciting area of research in the field of secondary batteries. These cutting-edge energy devices, such as Li-air batteries, offer remarkably high energy density values that are comparable to gasoline and about ten times higher than those of Li-ion batteries. This means that metal-air batteries have the potential to revolutionize energy storage, especially in applications where weight and space are at a premium, such as in electric vehicles and portable electronics. While there are still some challenges to overcome, such as improving the durability and stability of these batteries, the progress that has been made so far is promising. As materials science continues to advance, it is likely that metal-air batteries will become increasingly efficient, reliable, and cost-effective, making them a key technology for the future of energy storage. [3]
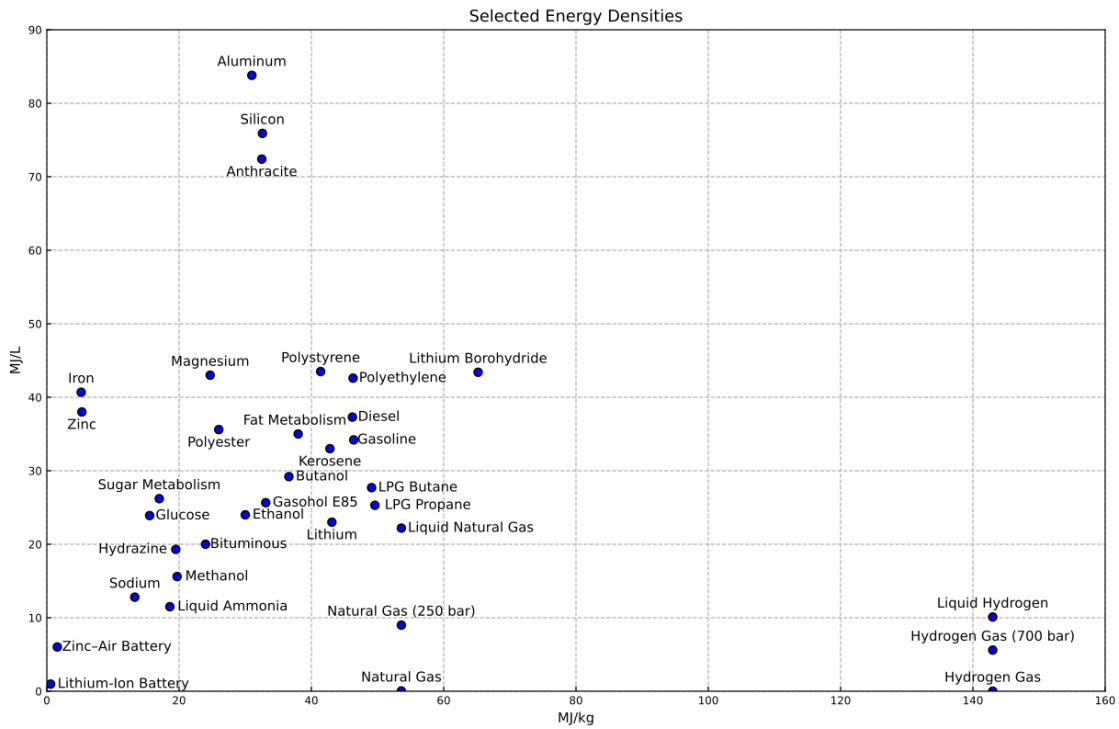
Fig 3-1 Energy densities plot

The metal-air battery typically consists of three parts: the anode (1), cathode (2), and electrolyte (3). The anode is typically a pure metal. With widely used metals include aluminum (4300 Wh/kg), sodium (1677 Wh/kg), magnesium (2789 Wh/kg), and lithium (5210 Wh/kg). Electrolytes are available in states: liquid solvent, a mixture of polymer and liquid solvent, and polymer-based solid etc. [4]

Similar to a fuel cell, the cathode in a metal-air battery is where the key reaction takes place. In a metal-air battery, the cathode needs to maintain activity for OER and ORR for charge-discharge. For this reason, catalyst design needs to follow three main criteria: (1) high ORR and OER activity at the same time, (2) low overpotential during charge-discharge, and (3) a large surface area.

Li-air batteries have been considered as one of the most promising next-generation energy storage systems due to their high energy density. However, the development of Li-air batteries has been limited by several challenges, particularly at the cathode. The cathode is responsible for the oxygen reduction reaction (ORR) during discharge and the oxygen evolution reaction (OER) during charging, which are essential for the battery's performance. [5]

80

In this context, the FAB(x)-Pt/Ir catalysts has shown potential for enhancing the performance of Li-air batteries. FAB(x)-Pt/Ir catalysts exhibit excellent activity for both the ORR and OER, which are advantageous for efficient Li-air battery operation. Further analysis has also revealed that the oxygen percentage and functional group distribution in the carbon can significantly affect the performance of the catalyst. By understanding the effects of metal percentage and metal loading factors, we can develop more efficient and effective catalyst materials for Li-air batteries.

3.3. Materials and Experimental

3.3.1. Catalyst

In this chapter, the focus is on the electrochemical evaluation and charge-discharge performance of the FAB(x)-Pt/Ir catalyst based cells in LAB. The selection of the catalyst is crucial as it must exhibit high activity for both the oxygen reduction reaction (ORR) and oxygen evolution reaction (OER) to enable efficient battery operation. The discussion will provide insights into the performance of the FAB(x)-Pt/Ir catalysts based cells in LAB.

Table 3-1 FAB(x)-Pt/Ir catalysts

Sample	Element Weight percent (Follow By SEM-EDS)					Design Metal Weight Percent	Deviation With Design
	C	O	Pt	Ir	Metal Total		
FAB60-Pt/Ir 1:1	75.77	4.43	8.61	11.63	20.24	20%wt	+1.2%
FAB60-Pt/Ir 2:1	76.13	7.25	11.59	5.03	16.62	20%wt	-16.9%
FAB180-Pt/Ir 1:1	78.07	3.96	9.04	8.92	17.96	20%wt	-10.2%
FAB180-Pt/Ir 2:1	77.01	5.09	12.91	4.99	17.90	20%wt	-10.5%

3.3.2. Electrochemical Detection

Electrochemical measurements are essential in determining the activity of cathode materials for Li-air batteries. In this chapter, the performance of bifunctional Pt/Ir nanoparticles-based electrodes was evaluated through electrochemical analysis to determine their ORR and OER activity. The results provide important insights into the efficiency of the FAB(x)-Pt/Ir catalyst family and their potential use in Li-air batteries. The electrochemical methods impedance involved cyclic voltammetry (CV), linear sweep voltammetry (LSV), and charge-discharge, which enabled the determination of various electrochemical parameters such as over potential, internal resistance, capacity, CE, and charge-discharge stability.

3.3.3. Air-Battery

The positive electrode for the Li-air battery was prepared by coating a Pt-Ir-FAB ink onto a coated carbon cloth. The ink was made by mixing the FAB-based catalyst with a polyvinylidene fluoride (PVDF) binder in a 9:1 ratio in N-methyl pyrrolidone (NMP) via ultrasonication. The cathode was produced using a brush coating technique, and the coated electrode was then dried in a vacuum oven at 80°C for 2 hours. Subsequently, the electrode was hot-pressed at 80°C for 12 hours to obtain a uniform coating. Lastly, 15 mm diameter discs were punched out to use as the cathode.

The fabrication of the Li-air battery involved the use of the cathode prepared in section 3.3.1, as shown in Figure 3-2. The Li-air battery was based on a 2025-coin cell, with a bottom cap that had a 1cm hole for oxygen exchange. All coin cell components were kept under an 80°C vacuum oven for 5 hours after washing with acetone. Glass fiber paper was used as a separator, which was cut into disks of 18mm diameter, and a 15 mm diameter lithium disk was cut from lithium foil. The cell was fabricated in an argon Ar gas glove box.

The electrolyte was prepared with 0.1M LiI (Lithium iodide) and 0.1M LiTFSI (Lithium bis[trifluoro methanesulfonyl] imide) in TEGDME (Tetraethyleneglycol dimethyl ether). The electrolytes were sufficiently dehydrated via vacuum drying.
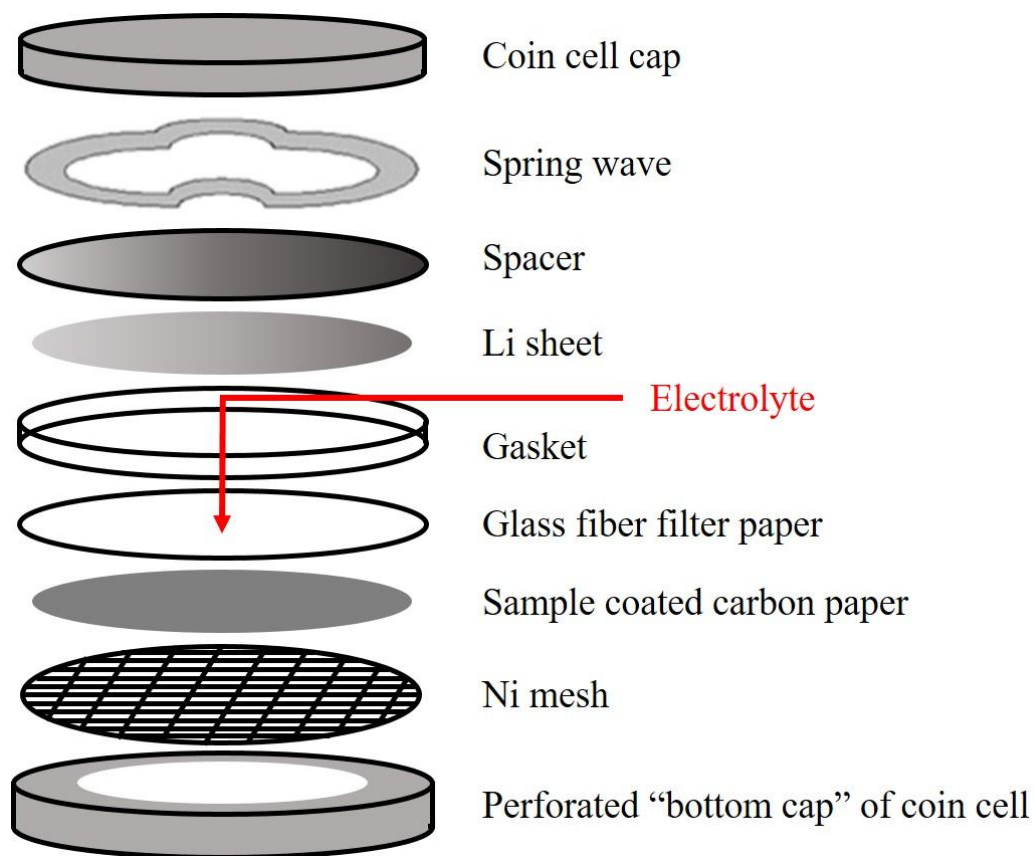
Fig. 3-2 Construction of Li-air battery

Li-air battery charge- discharge testing was carried under test chamber as shown in Figure 3-3.
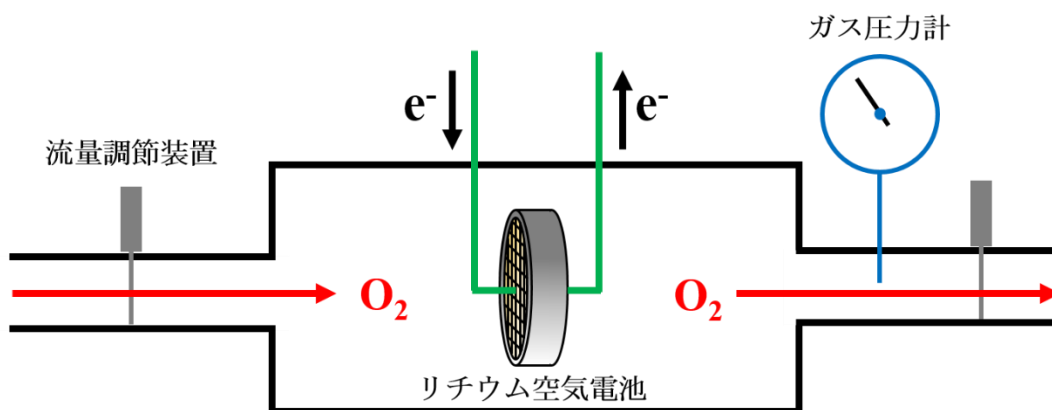

Fig. 3-3 schematic diagram of Li-air battery test chamber

Before conducting the Li-air battery charge-discharge tests, the test chamber was purged with oxygen gas to eliminate any moisture or other gas contamination. During the tests, the chamber

atmosphere was maintained at 99.9% oxygen, and the pressure was controlled to achieve the desired level within the chamber. The pressure was monitored every 12 hours to ensure it remained within the target range which is keep in to 0.1 MPa.

3.4. Analysis and Discussion

This section of the thesis discusses the application of three electrochemical techniques, impedance, linear sweep voltammetry (LSV), cyclic voltammetry (CV), and charge-discharge, to investigate the performance of the FAB(x)-Pt/Ir catalysis. The objective is to analyse their activity and behaviour among the catalyst materials. Through these analyses, the differences between the catalysts will be identified and further discussed.

3.4.1. LSV

The LSV analysis was carried out for a comparison of the ORR and OER activities of the FAB(x)-Pt/Ir catalysts, which is important to estimate their potential utility in Li-air batteries.

LSV measurements were carried out under 0.1M $HClO_4$ aq. (perchloric acid). The results of measurements are shown in Figure 3-4.
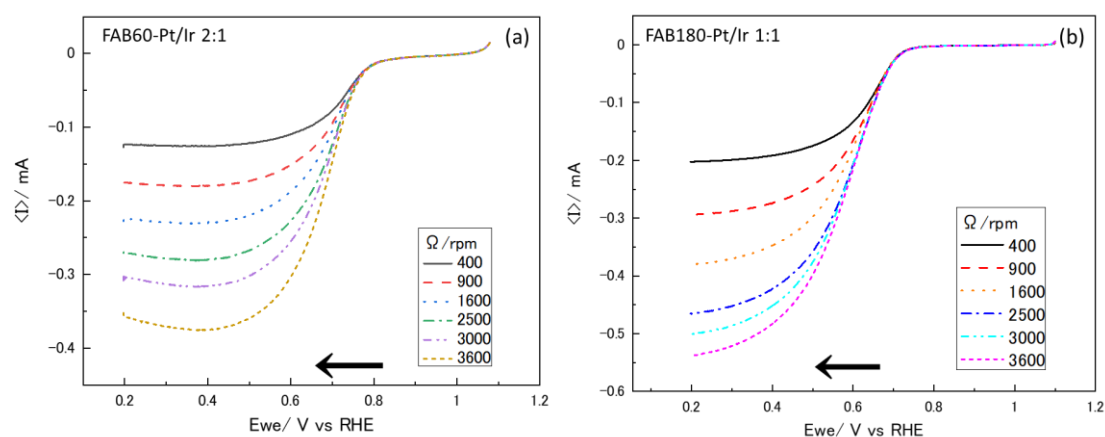
(Reference Electrode: Ag/AgCl   Counter Electrode: Pt   Scan speed: 50 mV/sec   Gas: Oxygen)

ORR results in 0.1M perchloric acid
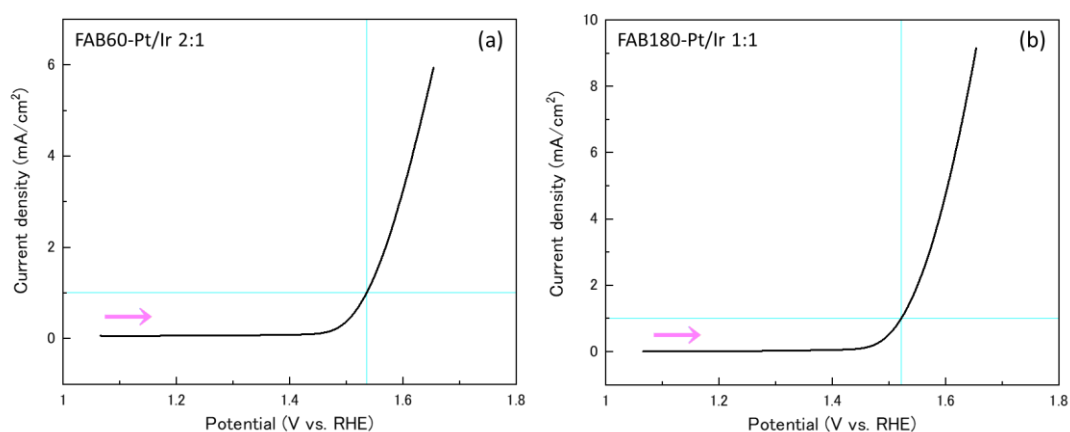
(Reference Electrode: Ag/AgCl   Counter Electrode: Pt   Scan speed: 50 mV/sec   Gas: Nitrogen)

OER results in 0.1M perchloric acid

Fig 3-4 LSV for catalyst

LSV analysis was performed to determine the onset potential and maximum current of the ORR for the FAB(x)-Pt/Ir catalysts. The FAB60-Pt/Ir 2:1 catalyst showed an onset potential of approximately 0.61V, while the FAB180-Pt/Ir 1:1 catalyst exhibited an onset potential of around 0.54V. In terms of ORR activity, the FAB180-Pt/Ir 1:1 catalyst demonstrated better performance than the FAB60-Pt/Ir 2:1 catalyst based on the maximum current value. However, the FAB60-Pt/Ir 2:1 catalyst performed better than the FAB180-Pt/Ir 1:1 catalyst in terms of the onset potential of the ORR reaction.

From Table 3-2, it can be seen that the OER activity of the FAB180-Pt/Ir 1:1 catalyst (28.21 Ag^{-1}) is lower than that of the FAB60-Pt/Ir 2:1 catalyst (36.77 Ag^{-1}), respectively. Additionally, the overpotential for the FAB60-Pt/Ir 2:1 catalyst is larger (304 mV) compared to that for FAB180-Pt/Ir 1:1 catalyst (294 mV). While the FAB180-Pt/Ir 1:1 catalyst has lower mass activity compared to FAB60-Pt/Ir 2:1, it has a lower overpotential, making it easier for the OER reaction to occur, which is favourable for the discharge process in a Li-air battery.

Table 3-2   OER activity

Catalysts	Loading (mg cm^{-2})	Mass activity (A g^{-1})	Overpotential @ 10 mA cm^{-2}	Refence
FAB60-Pt/Ir 2:1	0.0061 (Ir)	36.77	304	This work
FAB180-Pt/Ir 1:1	0.0102 (Ir)	28.21	294	This work
IrO$_2$/CNT	0.076 (Ir)	88	270	[6]
Pt/IrO$_2$	0.3 (Ir)	5	330	[7]
IrO$_2$	0.38 (IrO2)	9.6	282	[8]
IrOx-Ir	0.13 (IrOx-Ir)	8	–	[9]
Ir/Ti$_4$O$_7$	0.033 (Ir)	4.2	-	[9]

Table 3-3 shows OER activity for Ir metal include system. One of important aspect on OER active is mass activity.

The even and discernible crystal phase of FAB180-Pt/Ir 1:1 is likely responsible for the lower

overpotential observed during OER activity. This may be due to the more uniform distribution of active sites on the catalyst surface, which can facilitate the transfer of reactants and products during the electrochemical reaction. As a result, FAB180-Pt/Ir 1:1 exhibits a more efficient and stable OER performance, making it a promising candidate for use in Li-air batteries.

3.4.2. CV

The electrochemical measurements were performed under aqueous electrolyte 0.1M HClO$_4$ aq. (perchloric acid), using a glassy carbon electrode loaded with 20 μg/cm^2 of the FAB(x)-Pt/Ir catalysts. The electrochemical active surface area (ECSA) of the Pt-based materials was determined from the cyclic voltammetry (CV) curves in Figure 3-5, using an Ag/AgCl reference electrode with 3 mol NaCl and a platinum counter electrode. The ECSA values were calculated and presented in Table 3-3. In comparison with Pt-C [10] and Pt-TiOx [11] catalysts, the FAB-based catalyst exhibits remarkably high ORR activity.

The ECSA of FAB60-Pt/Ir 2:1 was found to be higher than that of FAB180-Pt/Ir 1:1. A comprehensive analysis of the electrochemical measurements can provide insights into the activity and potential of the FAB(x)-Pt/Ir catalysts for use in Li-air batteries.
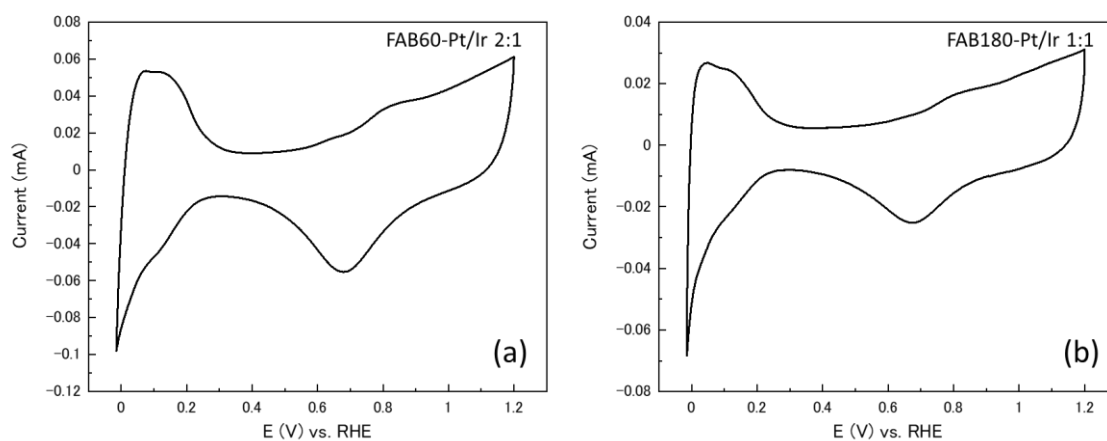
(Reference Electrode: Ag/AgCl   Counter Electrode: Pt   Scan speed: 50 mV/sec   Gas: Nitrogen)

*CV imagine with 0.1M perchloric acid*

Fig 3-5 CV

Table 3-3 ECSA from CV curve

Sample	ECSA/[m^2/g]
FAB60-Pt/Ir 1:1	38.8
FAB60-Pt/Ir 2:1	134.1
FAB180-Pt/Ir 1:1	37.4
FAB180-Pt/Ir 2:1	41.6
Pt-FAB [Rrf.10]	35
Pt-Vulcan XC-72 [Rrf.10]	31.5
Nb–Ti$_4$O$_7$ [Rrf.11]	45

The CV measurements in nonaqueous medium provided valuable information on the performance of the FAB180-Pt/Ir 1:1 sample, which is a promising candidate for use in Li-air batteries (Fig 3-7). The results showed that the oxidation peak occurred at 1.32 V, indicating the decomposition of Li$_2$O$_2$, while the reduction peak was observed at -1.53 V, which corresponds to the formation of Li$_2$O$_2$. Interestingly, after 50 cycles, the OER peak was not clearly visible, but after 100 cycles, a change was observed around the 1.32 V and -1.53 V peaks, and after 250 cycles, the OER peak appeared more clearly, also the peak area was changed less during cycles going large. This suggests that the OER activity of the FAB180-Pt/Ir 1:1 sample was improved during the cyclability studies, possibly due to the formation of more active IrO$_2$.

In the case of FAB180-Pt10% sample, on the other hand, lost its OER activity and even its ORR activity quickly, with a lower current density than the FAB180-Pt/Ir 1:1 sample in the OER peak. The results demonstrate the superior performance of the FAB180-Pt/Ir 1:1 sample over the FAB180-Pt10% sample (Fig 3-6).

In summary, the electrochemical properties of the FAB(x)-Pt/Ir catalysts were examined through CV testing under nonaqueous electrolyte, providing useful information on their ability of catalysts to maintain high activity during OER. These properties are essential for assessing their suitability for use in Li-air batteries. The research emphasizes the significance of considering factors such as metal composition and cycling stability when selecting catalyst materials for Li-air batteries.
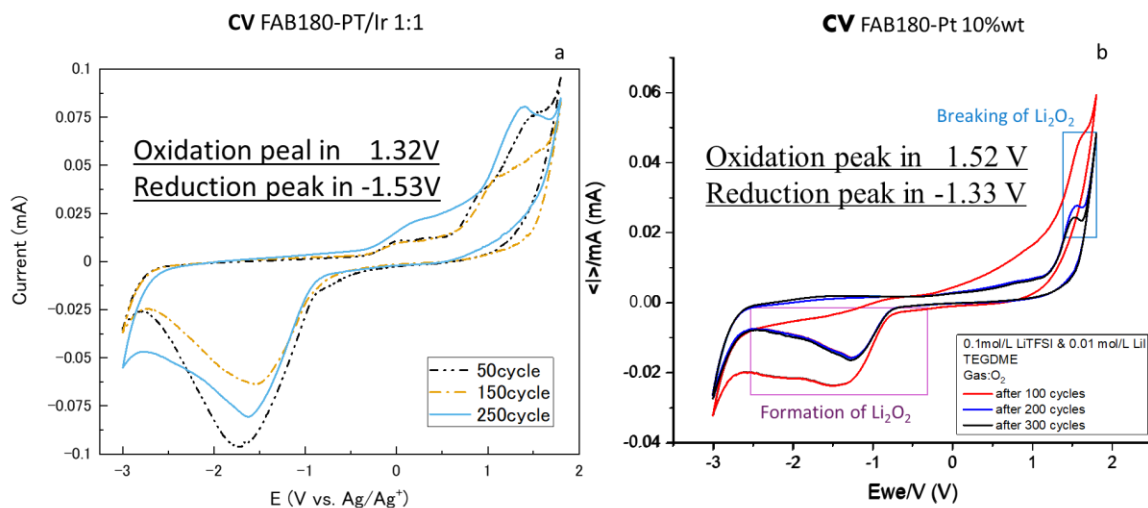
(Reference Electrode: Ag/Ag+   Counter Electrode: Pt   Scan speed: 50 mV/sec   Gas: Oxygen)

Fig 3-6 ORR results in 0.1M LiTFSI in TEGDME (a) with FAB180-Pt/Ir 1:1 (b) with FAB180-Pt10%

3.4.3. Charge-Discharge

In the series of the charge-discharge tests, the Li-air batteries were subjected to various measurement conditions. A current value of 0.0192 mA was applied, and the cutoff voltage was set at a potential (V) ≤ 2 V or ≥ 4.5 V. There was a pause time of 30 seconds between charging and discharging, and the O_2 pressure was set at 0.1 MPa. The charging and discharging time were set at 8 hours, ensuring that the battery was fully charged and discharged.

Table 3-6 compares performance of FAB-based electrocatalysts and highlights differences in overpotential between the 1st and 25th cycles (Fig-3-8). It is evident that both FAB180-Pt/Ir 1:1 and FAB180-Pt/Ir 2:1 exhibit overpotentials below 1V, with values of 0.38 V and 0.67 V, respectively. Table 3-6 compares the performance of FAB-based electrocatalysts and highlights the differences in overpotential between the first and 25th cycles. It is apparent that FAB180-Pt/Ir 1:1 and FAB180-Pt/Ir 2:1 exhibit overpotentials below 1V, with respective values of 0.38 V and 0.67 V. Figure 3-9 illustrates a gradual increase in overpotential from the first to the 25th cycle. All batteries were able to complete 25 cycles of charge-discharge at a capacity of 1000 mAh/g, as shown in Figure 3-10.

The data in Table 3-5 reveals that FAB-60 based catalysts, such as FAB60-Pt/Ir 2:1, exhibit an overpotential of up to 2.7V, which approaches the limit. Even FAB60-Pt/Ir 1:1 shows an overpotential of 1.7V.

When different composition of Pt:Ir (1:1 and 2:1) were compared in the FAB-60 catalysts, it is clear that the overpotential was much lower for the 1:1. This suggests that Ir is participating in the OER reaction and has an impact on the overpotential during charging. In contrast, FAB60-Pt/Ir 2:1 demonstrates that if Ir loses its OER activity or cannot control the charging process, the overpotential will become unmanageable.

Table 3-6 The overpotential of batteries

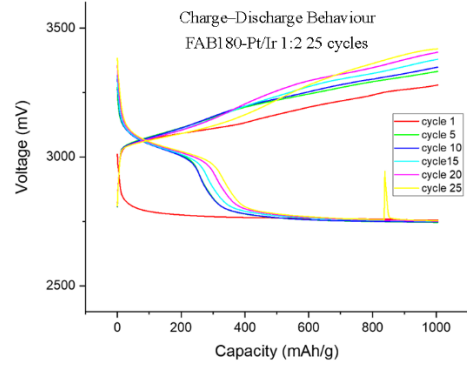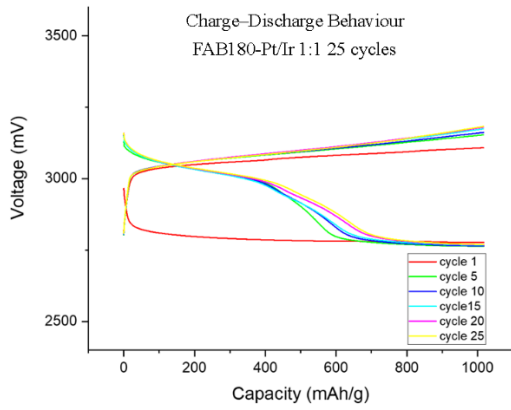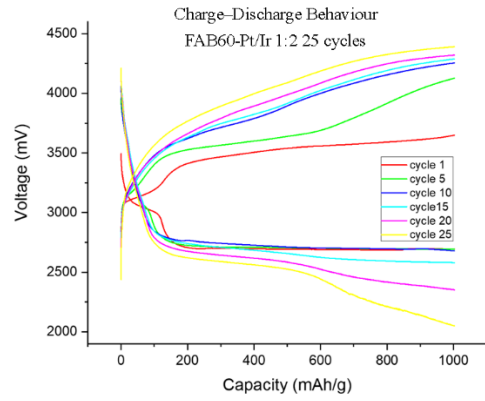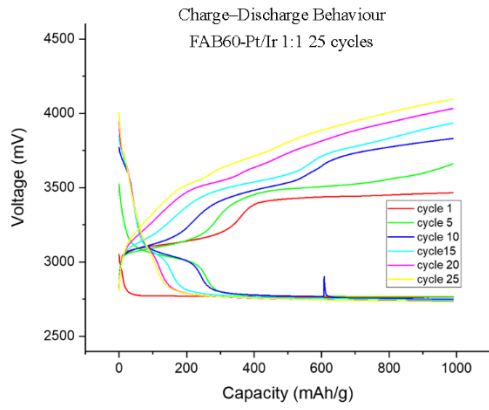|	FAB60-Pt/Ir 1:1	FAB60-Pt/Ir 2:1	FAB180-Pt/Ir 1:1	FAB180-Pt/Ir 2:1
Overpotential (V)	1.72	2.71	0.38	0.67
Discharge Capacity (mAh/g)	1000	1000	1000	1000
Columbic Effect %	100	100	100	100
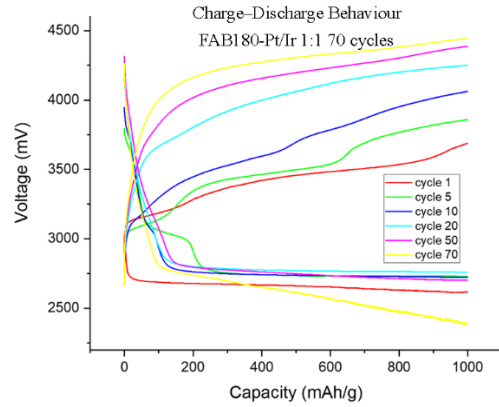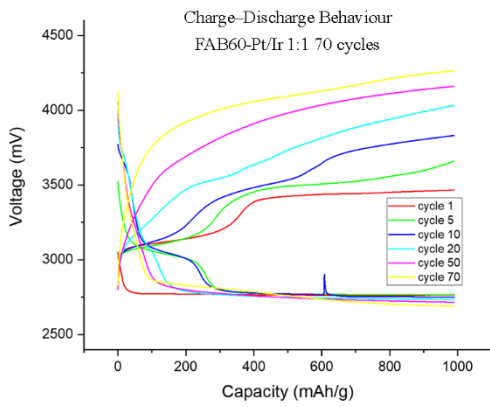
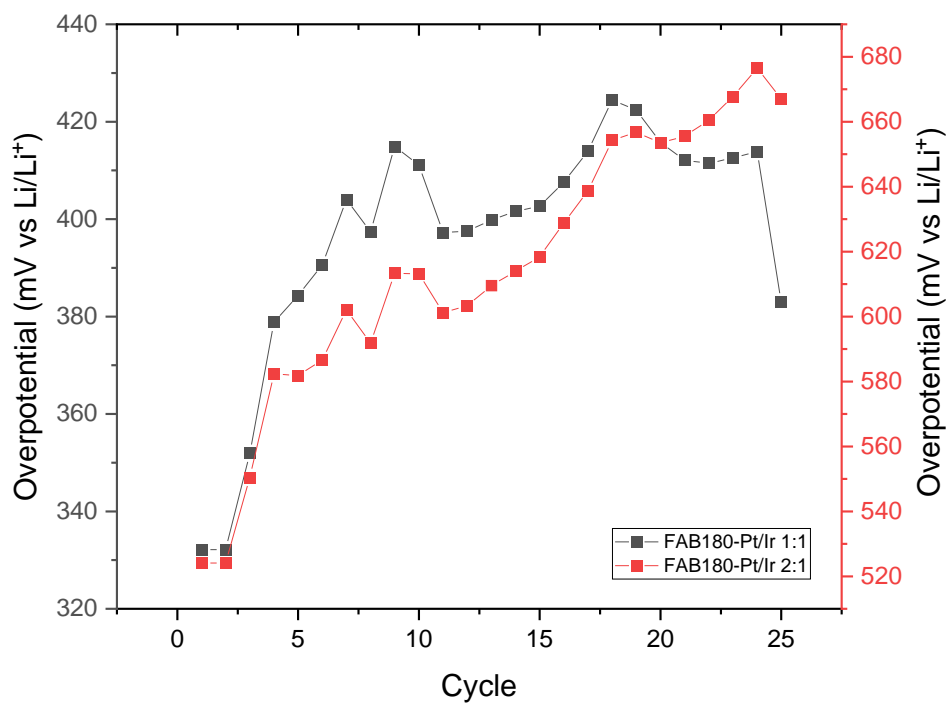Fig 3-8 Charge discharge behaviours of Li-air battery

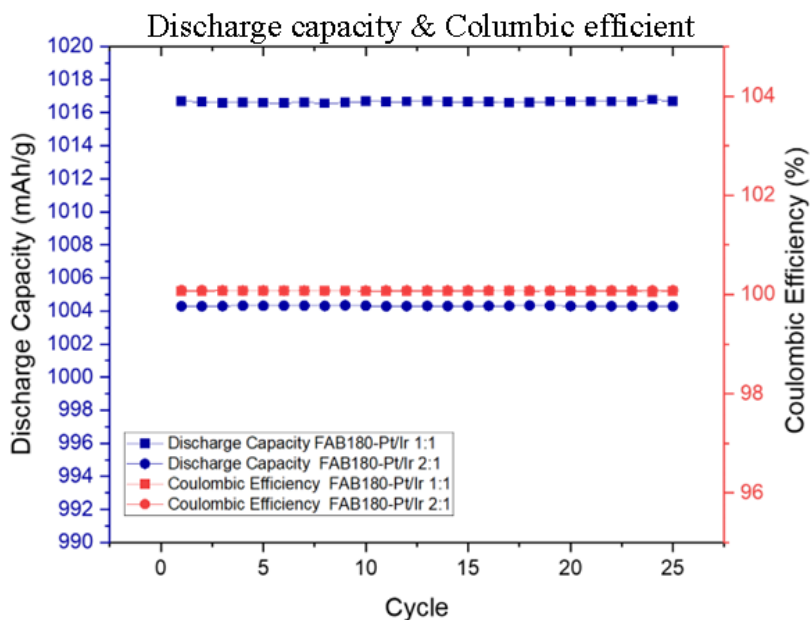Fig 3-9 Overpotential of FAB-180 type catalysts-based LAB during 25 cycles.

Fig 3-10 Discharge capacity and columbic efficiency of with FAB-180 type catalyst-based LAB during 25 cycles.

The Li-air battery with the FAB180-Pt/Ir 1:1 catalyst exhibited a discharge capacity of approximately 3000 mAh/g, as shown in Figure 3-11. Figure 3-12 displays the effect of different current rate during charge-discharge, with a capacity set at 500 mAh/g. It was observed that at higher current rates, several issues arose during discharge, such as rapid attainment of the voltage upper limit and a fast increase in overpotential. However, at or below 500 mA/g, the battery performed well during charge-discharge cycles. When the current exceeded 500mA/g during discharge, damage occurred, and the voltage upper limit was quickly reached. Therefore, it can be concluded that the Li-air battery in this study cannot handle high current rates of above 500 mA/during charge-discharge cycles.
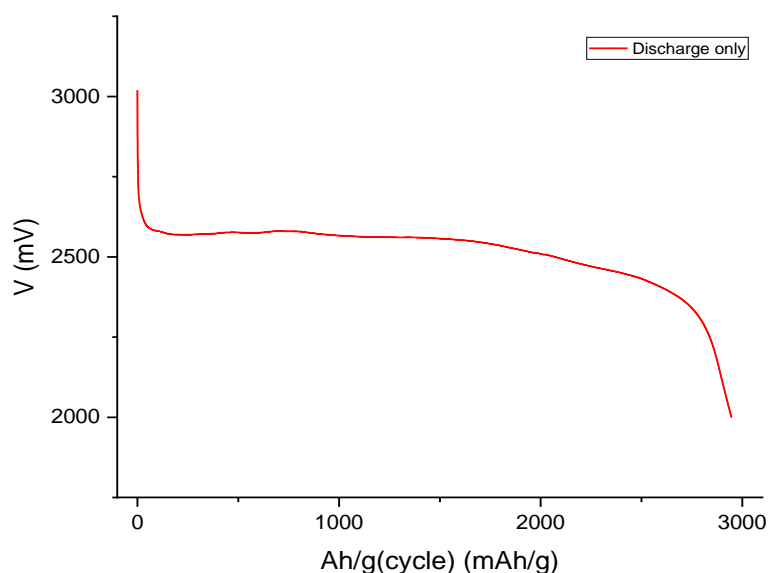
Electrolyte : 1.0 M LiTFSI with 0.1M LiI in TEGDME

Discharge current rate : 200mA/g.

Fig 3-11 FAB180-PT/Ir 1:1 with discharge only.
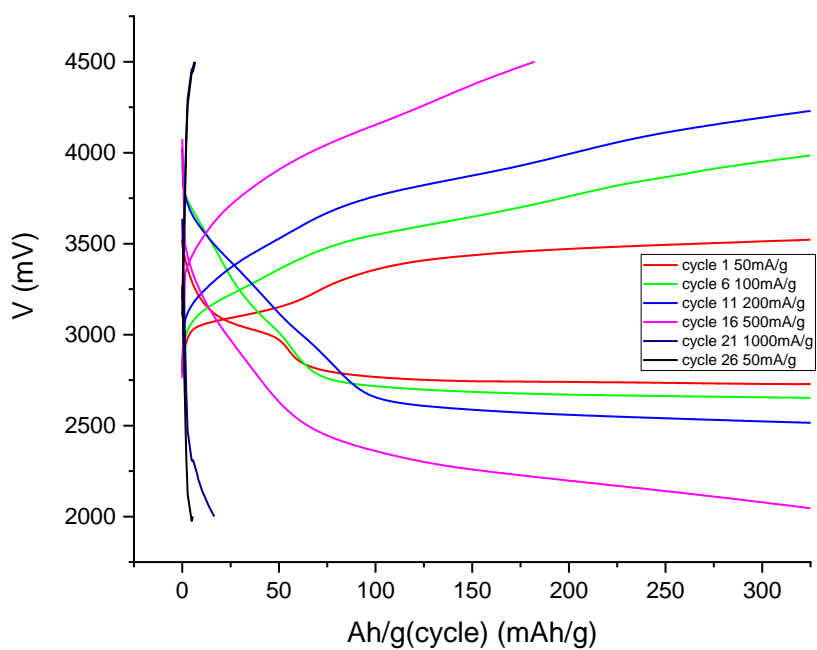
Electrolyte: 1.0 M LiTFSI with 0.1M LiI in TEGDME

Target capacity: 500mAh/g $_{catalyst}$

Fig 3-12 Chagre-discharge with FAB180-Pt/Ir 1:1 with change current rate

3.5. Conclusion

The FAB(x)-Pt/Ir catalysts demonstrated exceptional activity in both ORR and OER, which is attributed to the unique properties of the carbon support material and Pt/Ir nanoparticles structure. These results offer a promising pathway for developing high-performance Li-air batteries with FAB(x)-Pt/Ir catalysts. With such promising findings, further research is needed to explore the full potential of these catalysts in Li-air battery technology. The insights gained from this study will be valuable in the development of future catalyst materials and Li-air battery systems.

References

[1] Vicente, J. R., Kordesch, M. E., & Chen, J. (2021). Stabilization of mixed-halide lead perovskites under light by photothermal effects. *Journal of Energy Chemistry*, *63*, 8-11

[2] Girishkumar, G., McCloskey, B., Luntz, A. C., Swanson, S., & Wilcke, W. (2010). Lithium− air battery: promise and challenges. *The Journal of Physical Chemistry Letters*, *1*(14), 2193-2203.

[3] Christensen, L., Fischer, N., Kroffke, S., Lemburg, J., & Ahlers, R. (2011). Cost-effective autonomous robots for ballast water tank inspection. Journal of ship production and design, 27(3), 127.

[4] NASA GISS Surface Temperature Analysis (v4), <https://data.giss.nasa.gov/gistemp/graphs_v4/>, (2019).

[5] Ghosh, S. K., & Rahaman, H. (2019). Noble metal–manganese oxide hybrid nanocatalysts. In *Noble Metal-Metal Oxide Hybrid Nanoparticles* (pp. 313-340). Woodhead Publishing.

[6] Badam, R., Vedarajan, R., Okaya, K., Matsutani, K., & Matsumi, N. (2016). Sacrificial reducing agent free photo-generation of platinum nano particle over carbon/TiO2 for highly efficient oxygen reduction reaction. Scientific Reports, 6(1), 1-7.

[7] da Silva, G. C., Fernandes, M. R., & Ticianelli, E. A. (2018). Activity and stability of Pt/IrO2 bifunctional materials as catalysts for the oxygen evolution/reduction reactions. ACS Catalysis, 8(3), 2081-2092.

[8] Zhang, Z., Zhang, Y., Fan, H., Wang, Y., Zhou, C., Ren, F., ... & Chu, J. (2017). A Janus oil barrel with tapered microhole arrays for spontaneous high-flux spilled oil absorption and storage. Nanoscale, 9(41), 15796-15803.

[9] Lettenmeier, P., Wang, L., Golla‑Schindler, U., Gazdzicki, P., Cañas, N. A., Handl, M., ... & Friedrich, K. A. (2016). Nanosized IrOx–Ir catalyst with relevant activity for anodes of proton exchange membrane electrolysis produced by a cost‑effective procedure. Angewandte Chemie International Edition, 55(2), 742-746.

[10] Badam, R., Vedarajan, R., & Matsumi, N. (2015). Platinum decorated functionalized defective acetylene black; a promising cathode material for the oxygen reduction reaction. *Chemical Communications*, 51(48), 9841-9844.

[11] Ma, Y., Kajima, H., Shimasaki, Y., Nagai, T., Napporn, T. W., Wada, H., ... & Mitsushima, S. (2022). Degradation Analysis of Pt/Nb–Ti4O7 as PEFC Cathode Catalysts with Controlled Arc Plasma-deposited Platinum Content. *Electrochemistry*, *90*(5), 057004-057004.

4. Chapter 4

Total Conclusion

4.1. Conclusion of This Work

As we move into the new century, finding sustainable energy sources has become more urgent due to the challenges posed by global warming. Green energy has become a key focus in the 21st century, and renewable energies are cleanest sources of energy. However, the challenge lies now to store such energies.

One of the most promising technologies is the metal-air battery, which has been around since 1868 when the basic model was first proposed by Leclanche. In ideal conditions, Li-air batteries have been found to show very high energy density values, even comparable to gasoline at 11680 Wh/Kg, and approximately 10 times higher than Li-ion batteries. This represents a significant breakthrough in energy technology.

In chapter 1, it is crucial to have effective electrocatalysts to aid in the Oxygen Reduction Reaction (ORR) and Oxygen Evolution Reaction (OER) in the Li-air battery. Carbon-based materials are commonly used for this purpose due to their ability to maintain a large specific surface area and conductivity. The ORR and OER are two types of metal-catalysed reactions, and their activity under Li-air battery conditions is key to the battery's performance.

To promote the widespread application of all types of metal-air batteries, the catalyst is an important factor in their charge and discharge performance. For example, in Figure 4-1, the relationship between the electrolyte and oxygen on the surface of the Li-air battery cathode using catalysts is shown. Discussions revolving around the cathode materials and catalysts for metal-air batteries are hot topics in this area of research. With ongoing research and development, we are making strides towards more sustainable energy sources, and the Li-air battery, which offers high energy density values. This could help us reduce our reliance on fossil fuels in the years to come.
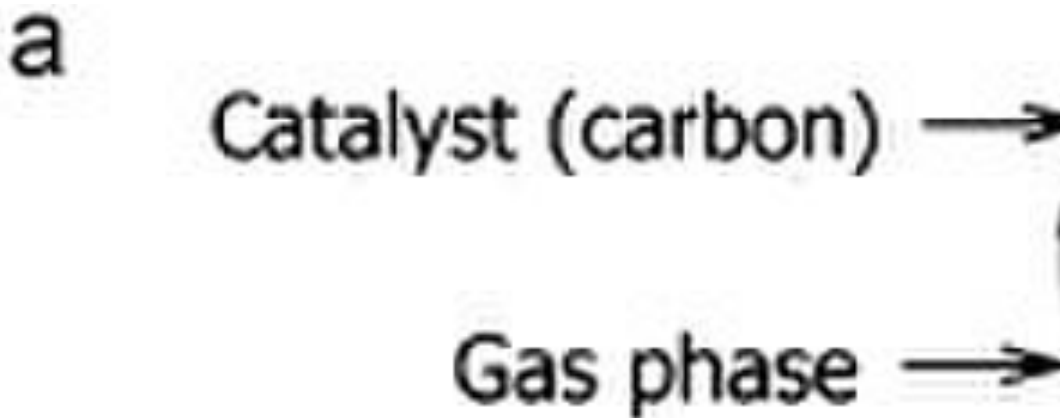
a

Catalyst (carbon) ⟶

Gas phase ⟶

Fig. 4-1 Models of the reaction zones for catalytic reduction of oxygen: (a) a "three- phase reaction zone" for aqueous electrolyte metal/air battery and (b) a "two-phase reaction zone" for non-aqueous electrolyte Li–air battery (the original figure is insignificantly modified)

Chapter 2 of this thesis focuses on synthesis of materials aimed at improving the performance of Li-air batteries, with a particular emphasis on dual catalyst design. Figure 4-2 shows the design of the catalyst and the basic synthetic route. In this study two carbon based bi-functionalized catalysts, FAB-60 and FAB-180, were obtained by varying the oxidation reaction time of AB carbon. These FABs have different oxygen contents and physical and chemical properties. Four types of electrochemical catalysts were designed, synthesized, and tested by controlling the weight percent of the metal loaded on the carbon. The microstructure of the FAB(x)-Pt/Ir family catalysts was influenced by the functional groups present in the carbon and the weight percent of the metal. The ideal effective area was observed to be larger when the weight or molar percent of Pt and Ir in the alloy was close to one another. If the carbon standard can support sufficient functional groups for metal bonding, the size of the nanoparticles can be uniformly controlled to be in the nanoscale range.

This research provides valuable insights into the development of high-performance Li-air batteries using FAB(x)-Pt/Ir catalysts. The FAB(x)-Pt/Ir catalysts demonstrated exceptional activity in both ORR and OER, which is attributed to the unique properties of the carbon support material and Pt/Ir nanoparticles structure. These results offer a promising pathway for developing high-performance Li-air batteries with FAB(x)-Pt/Ir catalysts. This is due to the unique properties of the carbon support material and the structure of the Pt/Ir nanoparticles.

Effective electrocatalysts are crucial for the charge and discharge performance of all types of metal-air batteries, including Li-air batteries. Carbon-based materials are commonly used due to their ability to maintain a large specific surface area and conductivity, making them the standard materials for this purpose. The ORR and OER are two types of metal-catalyzed reactions, and their activity under Li-air battery conditions is key to the battery's performance.

TEM analysis of the electrocatalyst revealed that FAB-180-based catalysts had a fully formed lattice structure. However, obtaining accurate crystal phase information for FAB-60-based catalysts was difficult.
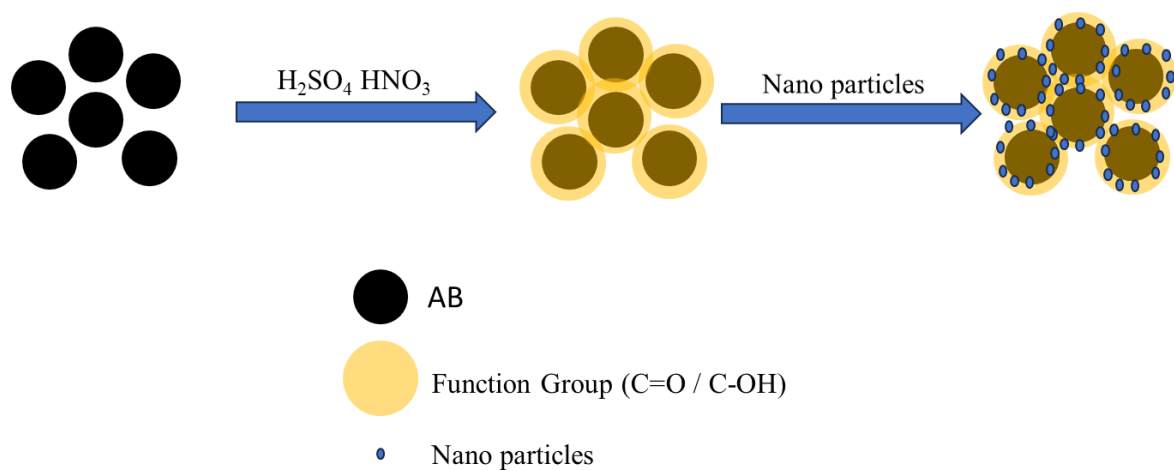

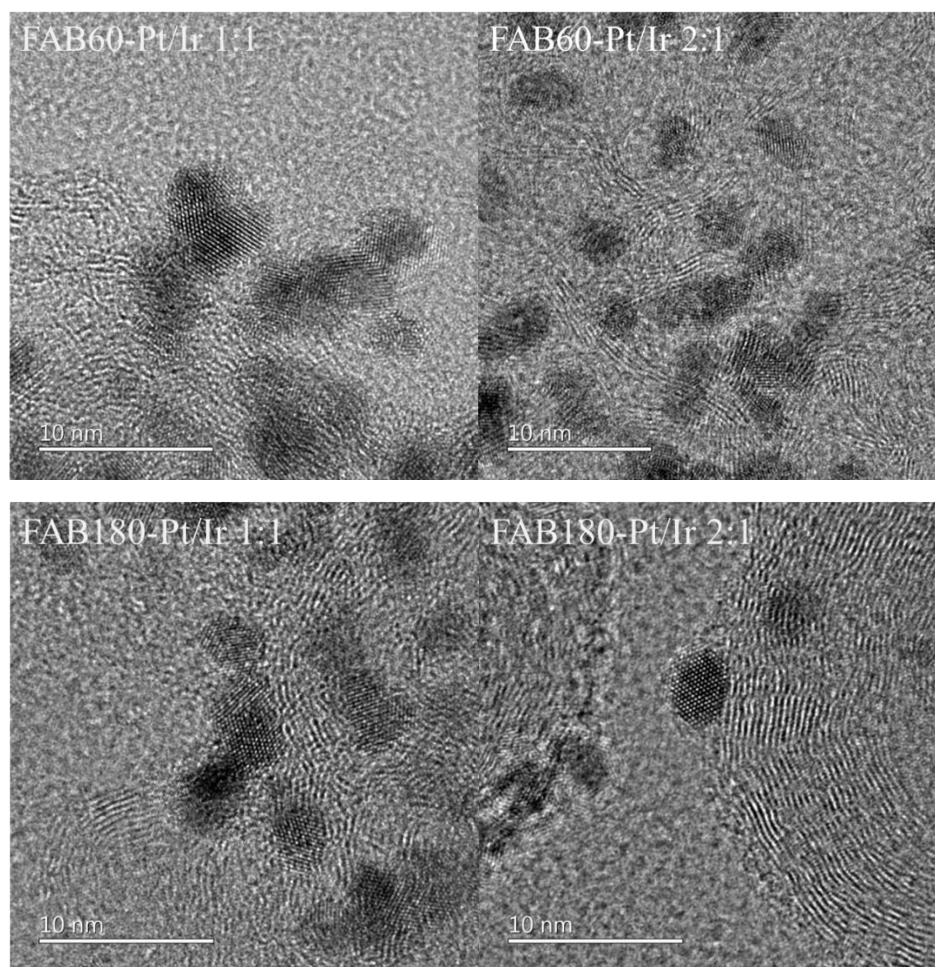Fig. 4-2 design and basic synthetic route

Fig4-3 TEM with catalyst.

In Chapter 3 of this thesis, the results of electrochemical measurements were discussed. The performance of cathode materials for Li-air batteries was evaluated. Among the various cathode materials studied, the FAB(x)-Pt/Ir catalyst family has exhibited better ORR (oxygen reduction reaction) and OER (oxygen evolution reaction) activity, surpassing that of other catalysts previously reported in the literature. The electrochemical characterization has enabled the determination of overpotentials and charge-transfer resistances, providing insight into the electrochemical behavior of the Li-air batteries. Moreover, the results of charge-discharge tests have shown the low over potential, and high discharge capacities and stable cycling of the FAB(x)-Pt/Ir catalysts as shown in Figure 4-4.

For example, the FAB180-Pt/Ir 1:1 catalyst based cell exhibited a discharge capacity of approximately 3000 mAh/g, overpotential with values of 0.38V after 25 cycles. Total charge-discharge cycles up to 200 cycles were performed.
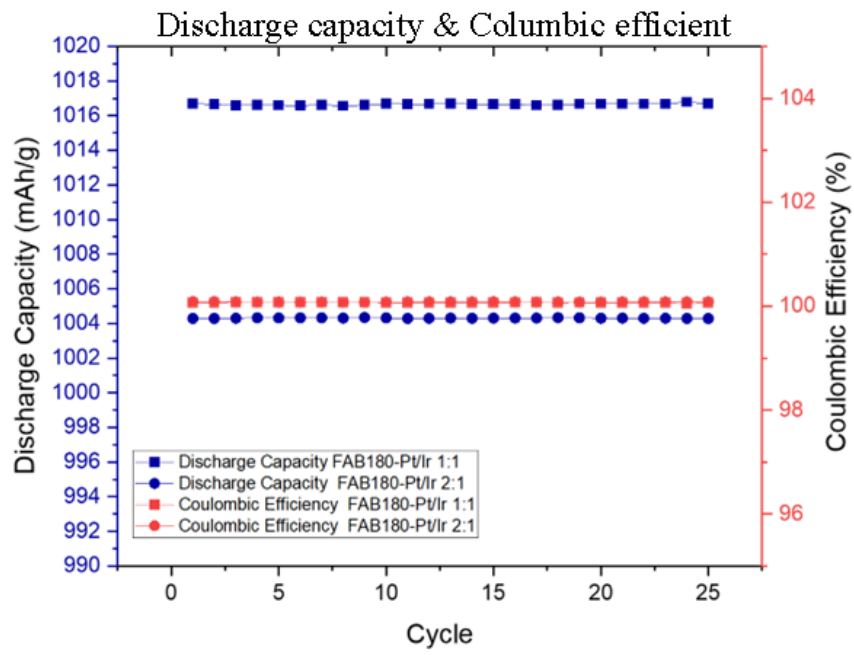
Fig 4-4. discharge capacity and columbic effect with FAB-180 carbon based catalyst during 25 cycles

4.2.   Future Scope of This Work

This work has promising implications for future research and materials design in the field of Li-air batteries. The high-performance activity demonstrated in this study for ORR and OER suggests potential for the development of related materials and new designs.

There are some possible outgrowths and ideas that can be explored based on the findings of this study, including:

(a) Pt alloy based high performance OER catalyst, such as Pt/Ni, Pt/Fe, Pt/Fe/Ir.

(b) FAB(x)-Pt/Ir catalyst family-based cathode in PEMFC.